2005
Annual Progress Report

ENERGY STORAGE RESEARCH AND DEVELOPMENT

Less dependence on foreign oil, and eventual transition to an emissions-free, petroleum-free vehicle

FREEDOMCAR AND VEHICLE TECHNOLOGIES PROGRAM

U.S. Department of Energy
Energy Efficiency and Renewable Energy
Bringing you a prosperous future where energy is clean, abundant, reliable, and affordable

FreedomCAR & Fuel Partnership

21st CENTURY TRUCK PARTNERSHIP

U.S. Department of Energy
Office of FreedomCAR and Vehicle Technologies
1000 Independence Avenue S.W.
Washington, D.C. 20585-0121

FY 2005

Progress Report for Energy Storage Research and Development

Energy Efficiency and Renewable Energy
FreedomCAR and Vehicle Technologies

David Howell
Manager, Energy Storage R&D

January 2006

Contents

Contents (Cont.)

I. INTRODUCTION

Our nation's energy security depends significantly on the efficiency of our transportation system and on which fuels we use. Transportation in the United States already consumes much more oil than we produce here at home. Domestic oil production has been dropping steadily for over 20 years, and by 2025 it is predicted that about 70% of our oil will be imported. Reducing our dependence on fossil fuels could also alleviate the currently tight supply as evidenced by the increase in gasoline prices following the 2005 hurricanes which hit our southern coast. Another issue is the rapidly increasing demand for oil, especially in countries such as China and India, where the number of motor vehicles in use is growing much more quickly than in the United States.

I.A FreedomCAR and Vehicle Technologies Program Overview

The United States Department of Energy (DOE) FreedomCAR & Vehicle Technologies (FCVT) Program office[1] works with industry to develop advanced transportation technologies that reduce the nation's use of imported oil. The program maintains a diverse set of R&D activities in vehicle technologies. Some of the technologies being supported by FCVT include hybrid drive system technologies, advance energy storage devices, power electronics, and motors, advanced structural materials, and advanced combustion engines and fuels.

Collaboration with automakers enhances the potential for success and the relevance of these programs. With this in mind, on January 9, 2002 the DOE and the United States Council for Automotive Research (USCAR)—representing DaimlerChrysler Corporation, Ford Motor Company, and General Motors Corporation—announced the creation of the FreedomCAR and Fuels Partnership[2]. This partnership is focused on funding high-reward/high-risk research that promises improvements in critical components needed for more fuel efficient, cleaner vehicles and provides ongoing guidance and expertise to FCVT activities.

I.B Energy Storage Research & Development Overview

Energy storage technologies, including batteries as well as ultracapacitors, have been identified as critical enabling technologies for advanced, fuel-efficient, light and heavy duty vehicles. The Energy Storage Research and Development effort within the FCVT Program is responsible for researching and improving advanced batteries for a wide range of vehicle applications, including hybrid electric vehicles (HEVs), battery electric vehicles (EVs), as well as fuel cell vehicles (FCVs). The office is working in close partnership with the automotive industry, represented by the United States Advanced Battery Consortium (USABC)[3].

---

[1] See http://www.eere.energy.gov/vehiclesandfuels/.

[2] For more information, please see http://www.uscar.org/Media/2002issue1/p1_freedomcar.htm, or www.eere.energy.gov/vehiclesandfuels/about/partnerships/freedomcar/index.shtml.

[3] The USABC partnership was formed in 1991 between DaimlerChrysler, Ford, and General Motors, see http://www.uscar.org/consortia&teams/consortiahomepages/con-usabc.htm.

The current effort is comprised of three major activities, battery technology development, applied battery research, and long-term exploratory research. A summary of the work done in each of these areas is presented below:

Battery Technology Development is subdivided into three closely related sets of activities: full system development, technology assessment, and benchmark testing.

- *Full System Development* - In cooperation with the USABC, efforts are focused on developing and evaluating lithium-battery and ultracapacitor technologies and designs for advanced vehicles. Specifically, this work is focused on the development of batteries for HEVs, 42 Volt vehicle systems, and FCVs; and on the development of ultracapacitor technologies for the 42 Volt start/stop application.

- *Technology Assessment* - Technology assessments are conducted on newly emerging technologies prior to full system development. These 12-month projects assess a developer's overall capabilities and validate technical claims through independent testing.

- *Benchmark Testing* - Benchmark testing of emerging technologies is important for remaining abreast of the latest industry developments. Working with the national laboratories, FCVT purchases and independently tests hardware against the manufacturer's specifications and the most applicable technical targets.

Applied Battery Research is focused on addressing the cross-cutting barriers that face lithium-ion systems which are closest to meeting all of the energy and power requirements for vehicle applications. Five national laboratories participate in this activity, each bringing its own expertise to remaining critical barrier areas: life, abuse tolerance, low temperature performance, and cost.

Focused Long-term Battery Research addresses fundamental problems of chemical instabilities that impede the development of advanced batteries. This research provides a better understanding of why systems fail, develops models that predict system failure and permit system optimization, and investigates new and promising materials. The work presently concentrates on research into several promising systems, including $LiNiCoMnO_2$, $LiFePO_4$, Li/Polymer, and new materials such as composite cathodes and non graphitic anodes.

This report highlights the activities and progress achieved in the Energy Storage Research and Development Effort during FY 2005. We are pleased with the progress made during the year and look forward to continued work with our industrial, government, and scientific partners to overcome the challenges that remain to delivering advanced energy storage systems for vehicle applications.

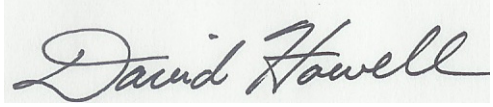

David Howell
Manager, Energy Storage Research and Development
FreedomCAR and Vehicle Technologies Program

II. BATTERY TECHNOLOGY DEVELOPMENT

Introduction

One of the primary objectives of the Energy Storage effort is the development of durable and affordable advanced batteries and ultracapacitors for use in a full range of vehicle applications, from start/stop to full-power hybrid-electric, electric, and fuel cell vehicles. This activity is subdivided into four mission areas: *system development*, focused on developing advanced battery systems for a wide range of vehicle applications; *technology assessment*, to evaluate developers' current capabilities and validate technical claims*; benchmark testing* of emerging technologies in order to remain abreast of the latest industry developments; and *Small Business Innovative Research (SBIR),* that provides funding for early-stage R&D to small technology companies or individual entrepreneurs.

II.A System Development

System Development is divided into two programmatic areas: *Vehicle High-Power Energy Storage*, focusing on the development of batteries and ultracapacitors for HEVs, 42 Volt vehicle systems, and FCVs; and *Electric Vehicle Battery Research and Development,* that supports the development of battery technologies to enable commercially competitive, full-function EVs. All battery system development for light duty vehicles is conducted in collaboration with industry through the USABC. All of the USABC subcontracts to develop advanced batteries are awarded competitively and are cost-shared.

II.A.1 Vehicle High-Power Energy Storage

Introduction

Vehicle High-Power Energy Storage is part of a multifaceted effort within FCVT to develop the technologies needed to encourage the adoption of advanced, cleaner, more fuel-efficient light-duty vehicles in the commercial marketplace. High-power energy storage devices are among the critical technologies essential for the continuing development of HEV, 42V vehicle systems, and FCVs.

Vehicle High-Power Energy Storage is focused on overcoming the main technical barriers associated with commercialization of high-power batteries, namely:

Cost - The current cost of Li-based batteries (the most promising high-power battery chemistry) is prohibitively high on either a kW or kWh basis. The main cost drivers being addressed are the high cost of raw materials and materials processing, and the cost of cell and module packaging.

Performance - The barriers related to battery performance are the reduced discharge pulse power that is available at low temperatures and the loss of available power over time due to use and aging.

Abuse Tolerance - High-power batteries are not intrinsically tolerant to abusive conditions such as short circuits, overcharge, over-discharge, crush, or exposure to fire and/or other high temperature environments.

Life - Hybrid systems with conventional engines have a life target of 15 years, and battery life goals have been set to meet these targets. The cycle life goal of 300,000 cycles has been attained in laboratory tests but the 15-year calendar life has not yet been demonstrated.

The Vehicle High-Power Energy Storage activity was created to develop solutions to these challenges. Battery requirements for HEVs and 42V vehicle systems, and FCVs were developed in close coordination with industry through the USABC technical teams and are shown in Table II-1 through Table II-3. (Also, see http://www.uscar.org/consortia&teams/consortiahomepages/con-usabc.htm.)

Table II-1. Energy Storage Targets for High Voltage, Power Assist Hybrid Electric Vehicles

Characteristics	Minimum value	Maximum value
Pulse discharge power (10s; kW)	25	40
Maximum regenerating pulse (10s; kW)	20 (55 Wh pulse)	35 (97 Wh pulse)
Total available energy (kWh at C/1)	0.3	0.5
Round trip efficiency (%)	>90–25 Wh cycle	>90–50 Wh cycle
Cycle life for specified SOC increments (cycles)	300k, 25-Wh cycle (7.5 MWh)	300k, 50-Wh cycle (15 MWh)
Cold-cranking power at −30ºC (three 2-sec pulses, 10-s rests between; kW)	5	7
Calendar life (years)	15	15
Maximum weight (kg)	40	60
Maximum volume (liters)	32	45
Production price @ 100k units/year ($)	500	800
Maximum operating voltage (Vdc)	<400 maximum	<400 maximum
Minimum operating voltage (Vdc)	>0.55 × V_{max}	>0.55 × V_{max}
Maximum self-discharge (Wh/d)	50	50
Operating temperature (ºC)	−30 to +52	−30 to +52
Survival temperature (ºC)	−46 to +66	−46 to +66

Table II-2. Energy Storage Targets for 42V Systems: M-HEV and P-HEV.

Characteristics	M-HEV Commercialization Goals	P-HEV Commercialization Goals
Discharge pulse power (kW)	13 (for 2 seconds)	18 (for 10 seconds)
Regenerative pulse power (kW)	8 (for 2 seconds)	18 (for 2 seconds)
Engine-off accessory load (kW)	3 for 5 minutes	3 for 5 minutes
Available energy (Wh @ 3 kW)	300	700
Recharge rate (kW)	2.6 kW	4.5 kW
Energy efficiency on load profile (%)	90	90

Characteristics	M-HEV Commercialization Goals	P-HEV Commercialization Goals
Cycle life, profiles	150 k	150 k
Cycle life and efficiency load profile	Partial power assist (PPA)	Full power assist (FPA)
Cold cranking power @ −30°C (kW)	8 (21 V minimum)	8 (21 V minimum)
Calendar life (years)	15	15
Maximum system weight (kg)	25	35
Maximum system volume (liters)	20	28
Self discharge (Wh/day)	< 20	< 20
Maximum operating voltage (Vdc)	48	48
Maximum open circuit voltage (Vdc)	48 (after 1 sec.)	48 (after 1 sec.)
Minimum operating voltage (Vdc)	27	27
Operating temperature range (ºC)	−30 to 52	−30 to 52
Selling price ($/system @ 100-k units)	260	360

Table II-3. Draft Energy Storage Targets for Fuel Cell Vehicle (FCVs)

Characteristics	Minimum	Maximum
Pulse discharge power (kW)	25 (for 18 s)	75 (for 18 s)
Maximum regeneration pulse (kW)	22 (for 10 s)	65 (for 10 s)
Total available energy (kWh)	1.5	5
Round trip efficiency (%)	>90	>90
Cycle life (cycles)	TBD (15 year life equivalent)	TBD (15 year life equivalent)
Cold-start at −30ºC (TBD kW for Tmin.; kW)	5	5
Calendar life (years)	15	15
Maximum weight (kg)	40	100
Maximum volume (liters)	30	75
Production price @ 100k units/year	500	1,500
Maximum operating voltage (Vdc)	≤ 440 maximum	≤ 440 maximum
Minimum operating voltage (Vdc)	$\geq 0.5 \times V_{max}$	≥ 0.5 × Vmax
Maximum self-discharge (Wh/d)	50	50
Operating temperature (ºC)	−30 to +52	−30 to +52
Survival temperature (ºC)	−46 to +66	−46 to +66

Specific objectives of the Vehicle High-Power Energy Storage activity include:

- By 2010, develop an electric drive train energy storage device with a 15-year life at 300Wh with a discharge power of 25 kW for 18 seconds and a cost of $20/kW.
- Reduce the production cost of a high-power 25-kW battery (for light-duty vehicle) from $3000 to $750 in 2006 and to $500 in 2010 (priority FCVT goal).
- Develop hardware for specific applications that can be tested against respective performance targets and used for subsystem benchmarking.

In the past, two candidate battery chemistries were identified as the most likely to meet the performance and cost targets: NiMH and lithium-based technology. NiMH batteries offer relatively good power capability as a result of the good ionic conductivity of the electrolyte. Lithium-based batteries offer excellent energy density that can be traded for higher power.

The USABC has supported development of these two technologies since the program's inception in 1997 by awarding subcontracts to a number of developers. Significant progress has been made in the development of the Li-ion technology as summarized in the graph shown in Figure II-1[4]. The USABC is continuing to support the development of Li-ion technology through contracts with Saft America (Li-ion), Johnson Controls, Inc**.** (Li-ion), and CPI/LG Chem (Li-ion polymer).

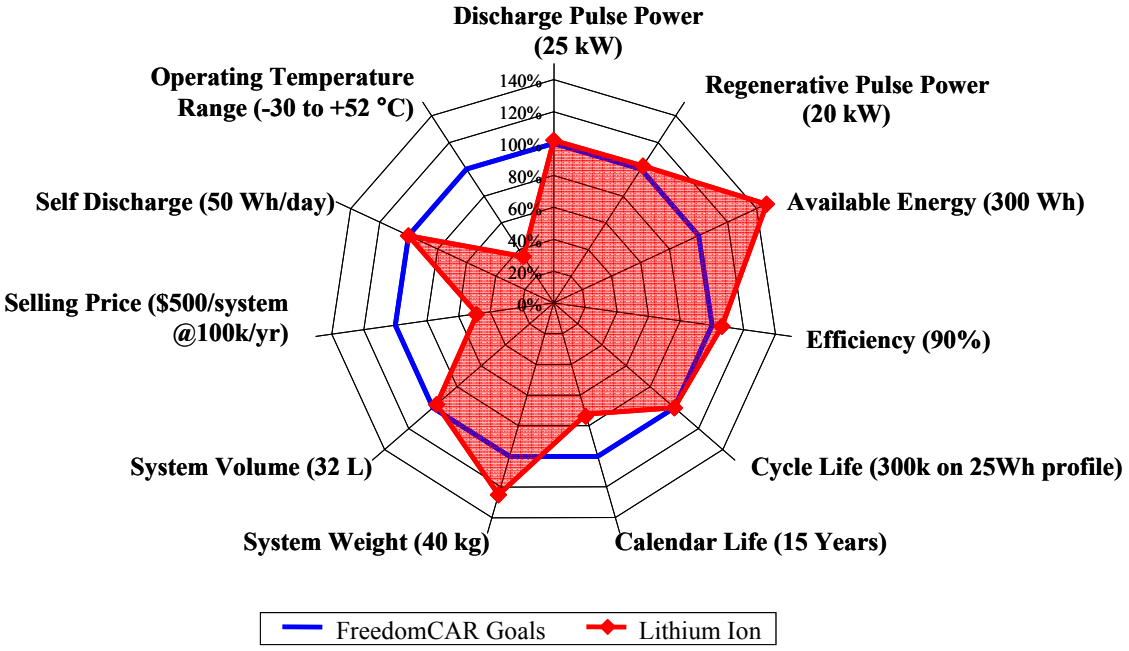

Figure II-1. Lithium ion Status versus Goals for Power Assist HEV

Li-ion Battery Development (42V Systems)

Saft continued the development of an inherently safe and affordable high-power 42V automotive battery. To carry out this work, Saft added capabilities in the areas of fundamental electrochemical materials, cell and module development, testing, modeling, and module design. Work focused on cells with an improved, low-cost cathode material, an improved negative material selected for better charge acceptance and power, and a promising new cell design.

The main objective was to verify that cells with this new material could meet the USABC cycle and calendar life goals. Tests to be run include:

- Static Energy
- Hybrid Pulse Power Characterization
- Self Discharge
- Cold Cranking
- Cycle Life at 30°C

[4] Barnes, James A., *Overview of Selected Battery and Fuel Cell Programs of the U.S. Department of Energy,* 2004 Taipei International Power Forum, Taipei, Taiwan, December 1, 2004.

Li-ion Battery Development (Full HEV)

In May of 2004, the USABC awarded a contract to Johnson Controls, Inc. (JCI), for development of an abuse-tolerant 40 kW Li-ion battery with significantly improved power-to-weight performance. The contract called for the delivery of modules of 10 Ahr cells to be tested for abuse tolerance, capacity, pulse power, calendar life, and cycle life. The development effort is being led by the advanced battery systems team at JCI headquarters in Milwaukee, WI.

JCI delivered 14 10-Ah cells to Argonne National Laboratory for evaluation. All cells were characterized according to the procedures outlined in the FreedomCAR Battery Test Manual for Power-Assist Hybrid Electric Vehicles.[5] The cells were evaluated against the power-assist maximum goals (40 kW and 500 Wh). After characterization, three cells were tested for calendar life at 45°C and 50% SOC; and three were tested for cycle life at 30°C and 60% SOC. The cycle life tests used the baseline (80th percentile), 50-Wh profile and a battery size factor (BSF) of 49. Testing started in January 2005 and was completed in July 2005.

Li-ion Polymer Battery Development (Full HEV)

In February 2004, Compact Power/LG Chem was awarded a contract to develop Li-ion polymer cell technology for HEV applications using a $LiMn_2O_4$ spinel-based cathode. $LiMn_2O_4$ spinel is an attractive cathode for HEV batteries due to the fact that Mn is abundant, environmentally benign, potentially abuse-tolerant, and capable of high-rates of discharge. Major problems to be overcome in this effort are the relative instability of the spinel cathode material at elevated temperatures and the comparatively poor cold cranking and low-temperature charging characteristics normally exhibited by Li-ion batteries.

A combination of approaches, including doping, coating, and the use of additives, was taken in order to enhance the calendar-life of the spinel cells. Experimental results indicate that a number of these approaches are yielding results which may significantly improve their calendar life.

In regard to low-temperature performance, modeling and initial laboratory results show that electrolyte conductivity plays only a minor role, while the cathode and anode properties (both interfacial and bulk) dictate the cold-cranking power of HEV cells (see section III).

Low-cost Separator Development

Studies at the national laboratories have shown that the cost of the separator dominates the cost of the non-active materials in a high-power Li-ion battery. To reduce this cost, the DOE, in conjunction with the USABC, is supporting research and development efforts to create novel, low-cost materials and to improve processing techniques so that currently available materials may be produced in a less costly manner. The goal is to develop a replacement separator (which costs $\$1/m^2$ or less) for current materials (which cost more than $\$2/m^2$) having the following properties:

- Thickness: < 25 μm
- Wettability: Complete Wet Out in Electrolytes
- Puncture Strength: > 300g/25.4 μm
- Permeability: MacMullin Number of < 11

[5] FreedomCAR Battery Test Manual for Power-Assist Hybrid Electric Vehicles, DOE/ID-11069, October 2003.

- Pore Size: < 1 μm
- Moisture Content: < 50 ppm
- Chemical Stability: Stable in Battery for 10 Years

Support is being provided to the development of a low-cost polypropylene (PP)-based separator using a wet process, an established dry production process applied to PP-based separators, and a nylon-based high-strength, low-cost separator. Contractors engaged in this activity during 2005 include Celgard, Inc., Advanced Membrane Systems (AMS), and Ultimate Membrane Technologies (UMT). Some highlights of the FY 2005 activities are presented below.

- **Celgard, Inc.** reported significant progress with its new approach, and completed initial lab-scale experiments. Initial screening trials were also completed on new resin selections. Lab-scale trials with alternative resins that may provide films with higher tensile strength and better process reproducibility were started. Studies of shut-down/melt integrity using alternative resins and hand-stretch samples were also undertaken.

- **AMS** signed a Phase II, 18-month, 50/50 cost-shared contract with the USABC. The objective of this new contract is to build on the success of the Phase I effort by fine tuning the formula in order to meet: the 100°C shutdown and 200°C melt integrity requirements. Modifications to the resin formula and processing conditions will be evaluated in order to meet the tensile strength, shrinkage, and puncture strength requirements.

- **UMT** is focused on demonstrating process uniformity and reproducibility of 135°C shut-down/165°C melt material. Work has shown that puncture strength, pore size, and tensile targets are achievable with polyolefin films. Shut-down/melt integrity development is proceeding with initial lab-scale development using alternative resins, including polyolefins with different melt flow indices. Top-to-bottom uniformity of stretched samples has been characterized and demonstrated, but work still needs to done to characterize the left-to-right uniformity across the film.

Ultracapacitor Research and Development

Ultracapacitors (symmetric carbon-carbon double layer type) have been extensively tested at the Idaho National Laboratory and appear capable of attaining about 50% of the energy density requirements for HEVs in power-assist mode. Full requirements are shown in Table II-4. However, their very high-power capability makes them a candidate technology for the 42V start-stop applications. To this end, the USABC has contracted with two developers, Maxwell Technologies and NESSCAP, to develop ultracapacitors for the 42 volt start-stop architecture. Some highlights of the FY 2005 activities are presented below.

Table II-4. Ultracapacitor Requirements

System Attributes	12V Start-Stop (TSS)		42V Start-Stop (FSS)		42V Transient Power Assist (TPA)	
Discharge Pulse	4.2 kW	2s	6 kW	2s	13 kW	2s
Regenerative Pulse	N/A		N/A		8 kW	2s
Cold Cranking Pulse @ -30°C	4.2 kW	7 V Min.	8 kW	21 V Min.	8 kW	21 V Min.
Available Energy (CP @1kW)	15 Wh		30 Wh		60 Wh	
Recharge Rate (kW)	0.4 kW		2.4 kW		2.6 kW	
Cycle Life / Equiv. Road Miles	750k / 150,000 miles		750k / 150,000 miles		750k / 150,000 miles	
Cycle Life and Efficiency Load Profile	UC10		UC10		UC10	
Calendar Life (Yrs)	15		15		15	
Energy Efficiency on UC10 Load Profile (%)	95		95%		95%	
Self Discharge (72hr from Max. V)	<4%		<4%		<4%	
Maximum Operating Voltage (Vdc)	17		48		48	
Minimum Operating Voltage (Vdc)	9		27		27	
Operating Temperature Range (°C)	-30 to +52		-30 to +52		-30 to +52	
Survival Temperature Range (°C)	-46 to +66		-46 to +66		-46 to +66	
Maximum System Weight (kg)	5		10		20	
Maximum System Volume (Liters)	4		8		16	
Selling Price ($/system @ 100k/yr)	40		80		130	

- **Maxwell Technologies, Inc.** has successfully completed design validation testing of 2.7V, 2600F cells and delivered samples to INL for evaluation. Continuing module design and development involves use of new low cost package design and an improved thermal design. Increasing the energy density involves improving the electrodes as well as optimizing the cell and module form factors. Maxwell is also benchmarking multiple carbon suppliers to find the proper cost-to-performance merit figure. Coin cells are used initially to allow fast screening. Carbons with parameters in line with baseline control carbon are then tested in larger-format cells.

- **NESSCAP, Co., Ltd**., is developing ultracapacitors for 42V start-stop applications by enhancing existing products and by formulating new electrode materials. The tasks include materials and electrode formulation, production verification, and module design. Major components that will be evaluated include the carbon, the electrolyte, and the binder. Carbons are characterized by particle size, surface area, pore size, pore size distribution, and impurities; electrolytes by viscosity and conductivity; and binders by morphology and electrode strength. Key cell parameters evaluated in the cell fabrication tasks include resistance**,** capacitance, leakage current, self discharge, low temperature performance, and cycle and calendar life. Cell and module design efforts will involve minimizing packaging

factors, minimizing leakage current, ensuring physical integrity, and minimizing cell-to-cell variability.

Thermal Management and Simulation

Improved Thermal Designs for Johnson Control Cells/Modules - Researchers performed electro-thermal analysis of JCI Li-ion cells and computational fluid dynamic analysis on its multi-cell module. They recommended design changes to improve the thermal performance, critical in achieving the performance and calendar life targets. The analysis showed that terminal cooling only (the design originally proposed) was not sufficient to keep the cells cool. Analysis showed that terminal cooling plus sidewall (exterior surfaces) cooling was needed. Cells with both oval and round cross sections were analyzed and the conclusions were the same. JCI incorporated the recommended side cooling design into their module design. In addition, the analysis suggested reducing the air gap around each cell to promote higher heat transfer and lower cell temperature, which was also incorporated.

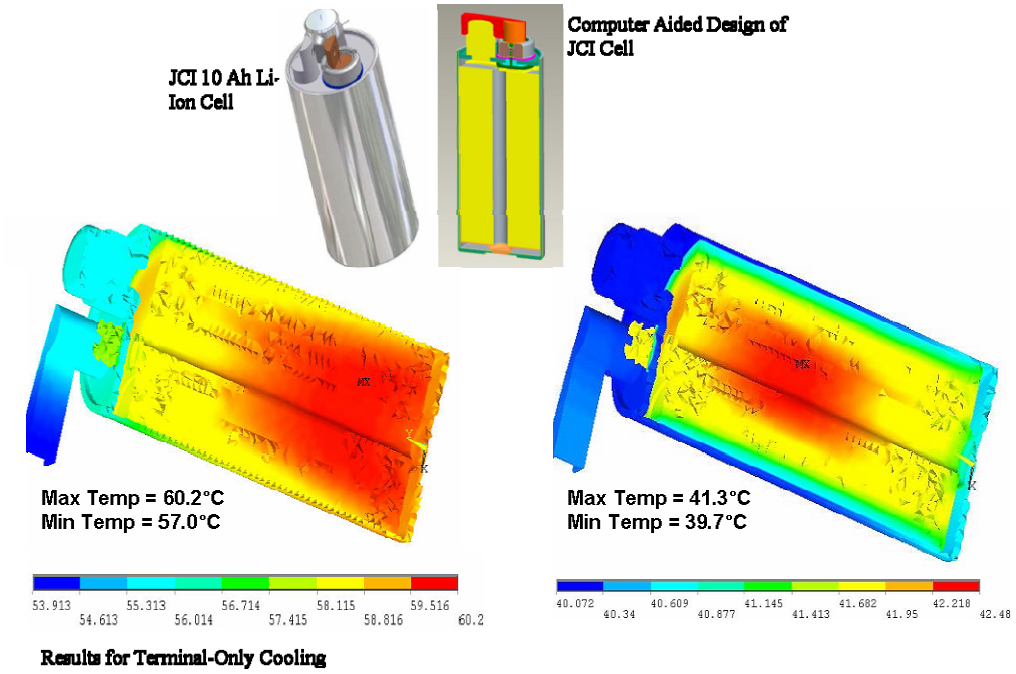

Figure II-2. Electro-Thermal Analysis of a JCI Li-Ion Cell with 4.1 W/cell of Heating at 35°C

Additional thermal and electrical characterization was performed on a JCI/Varta Li-ion battery, Figure II-3. The goal was to assess the thermal and electrical performance of the cell through laboratory testing and also to generate data for finite element thermal modeling. The heat generated from the cells under different charge/discharge cycles was measured in a calorimeter, and thermal images of the cells were obtained with infrared cameras. The experimental data were combined with finite element electro-thermal analysis to design the next generation of the cell.

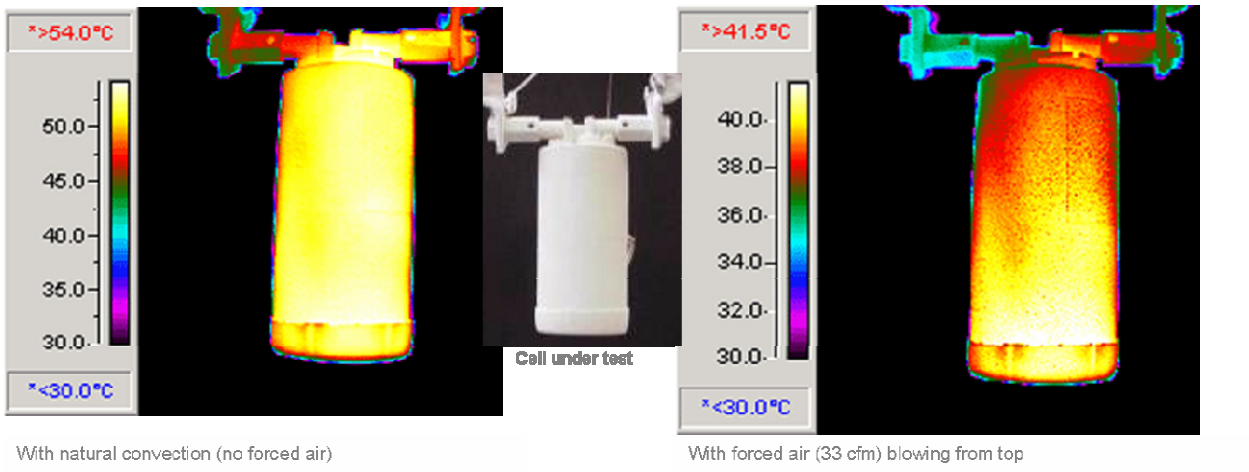

Figure II-3. Thermal Images of a 10 Ah JCI Li-Ion Cell under Continuous 100 A Charge & Discharge Pulses (2.1 sec charge, 2.0 sec discharge)

Modeling and Requirement Analysis

Process/Code for Generating Ultracapacitor Models - In support of the USABC Ultracapacitor Task Force, engineers developed a program to perform reference capacity and constant current test analyses. With this code, test data are processed to generate parameters for an ultracapacitor equivalent circuit model. The model may then be used in vehicle simulation tools such as ADVISOR for assessing the potential use and impact of a particular ultracapacitor. The process/code was presented at USABC Task Force meetings and at the 14th International Seminar on Double Layer Capacitors and Hybrid Energy Storage Devices, in Fort Lauderdale, FL, in December 2004. The code will be distributed with the modeling appendix in the next release of the *FreedomCAR Ultracapacitor Test Manual*.

Ultracapacitors in Start/Stop and Mild Hybrid Vehicles - In support of the FreedomCAR Energy Storage Technical Team, engineers performed analyses on the impact of using ultracapacitors in start-stop vehicles and power-assist mild hybrids. The analyses showed two findings for the standard urban/city driving cycle (both UDDS and US06): (1) the start-stop operation with a low-voltage energy storage system could improve the fuel economy of a mid-size car by as much as 7% to 15%; and (2) using a high-voltage ultracapacitor pack in a mid-size mild hybrid car with power-assist strategy but limited engine downsizing, the city fuel economy could be improved more than 50%. The results are being used by the USABC to determine a strategy for extending potential applications of ultracapacitors in the FreedomCAR Program.

Updated Simulation Models for the Latest Energy Storage Devices - For simulation of advanced vehicles using the latest energy storage devices, new hybrid pulse power characterization (HPPC) data was collected either through testing or from manufacturers and others. The latest devices include the Panasonic Gen II prismatic NiMH module, Saft VPL20 Li-ion cell, Kokam Li- polymer cells, COBASYS NiMH module, and Maxwell MC2600 ultracapacitor. These new devices perform

better than current energy storage models in vehicle simulation tools such as ADVISOR and PSAT. Updating the models will assist in performing vehicle simulations with the latest technologies and forming conclusions that are consistent with the state-of-the-art.

Impacts of Auxiliary Loads on Energy Storage of Start-Stop Vehicles - In support of the USABC, researchers completed an analysis on the impact of air conditioning (AC) on the ultracapacitor-powered vehicle's ability to conduct start-stop operation for a mid-size car and a full-size truck. The study indicated that ultracapacitor systems can sustain auxiliary loads with AC for about 30 seconds, and restarting the engine during longer stops would have less than 1% impact on fuel economy over the federal test procedure (FTP)-urban driving cycle. This minimal impact on the worst-cases of AC operation during long idle-off stops may constitute an attractive trade-off enabling the use of ultracapacitors.

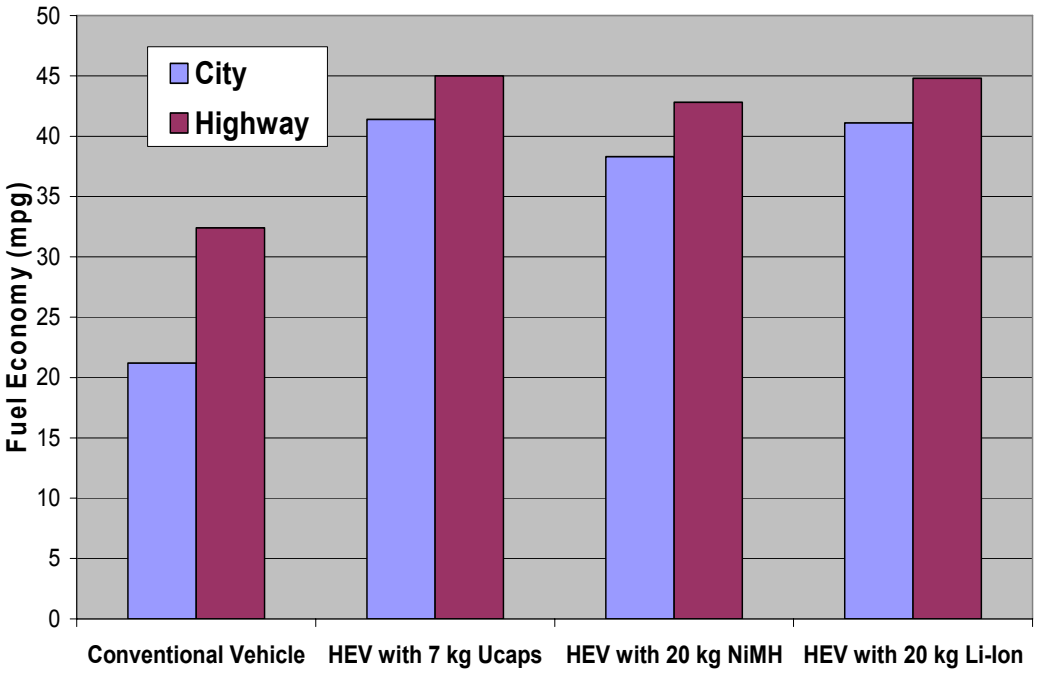

Figure II-4. Comparison of Fuel Economy of a Slightly Downsized Mild Hybrid Midsize Car Using Various Energy Storage Options for Two Standard Driving Cycles

Industry Support

Collaboration with EPRI to Evaluate Advanced Batteries for Plug-in HEVs - After several months of negotiations, the Electric Power Research Institute (EPRI) and NREL entered into an agreement on the evaluation of the performance and cycle life of batteries used for a commercial plug-in hybrid vehicle, the Daimler-Chrysler Sprinter van. The funding is cost-shared with EPRI at 20%. The objective is for EPRI to collect use-pattern data from driving plug-in hybrids, and then use it to obtain performance and cycle life data on Li-ion and NiMH batteries. Researchers will use the data for developing electrical and thermal models for plug-in batteries and also for the trade-off

analysis between vehicle fuel economy and battery cycle life of plug-in HEVs. The information is important for defining the future research and development needs of batteries for plug-in HEVs.

Energy Storage Analysis for Fuel Cell Vehicles – Analysis of energy storage requirements for FCVs continued for a newly formed USABC/FreedomCAR Energy Storage Fuel Cell Vehicle Working Group. The purpose was to finalize the energy storage requirements for fuel cell vehicles based on various control strategies. It appears that the existing high-power batteries for gasoline engine hybrids will be sufficient for fuel cell hybrids.

Collaboration with a South Korean Automotive Research Organization - As part of a work for others agreement with the Korea Automotive Technology Institute (KATECH), researchers performed the thermal and electrical characterizations of Li-ion polymer batteries produced by Kokam Engineering Co. of Korea. The cells were subjected to the HPPC profile to assess their electrical performance and the data was used to generate a battery model that was integrated into the ADVISOR vehicle simulator. Heat generation and thermal images of 2 Ah and 11 Ah cells were also obtained. Although this work was sponsored by KATECH, the battery results were shared with the DOE Energy Storage Program.

Publications and Presentations - Included the following:

- "*Ultracapacitor Modeling*" at the 14th International Seminar on Double Layer Capacitors
- "*Energy Storage Analysis for Fuel Cell Vehicle*," and "*Improving Battery Design using Electro-Thermal Modeling*," at the 21st Electric Vehicle Symposium
- "*Analysis of Ultracapacitor-VRLA Energy Storage System for Mild Hybrids*" at the 5th Advanced Automotive Battery Conference
- "*Ultracapacitors and Batteries in Hybrid Vehicles*," at the 2nd Advanced Capacitor Summit
- "*Electro-Thermal Modeling for Improving Battery Design*," at the IEEE Vehicle Power and Propulsion Conference.

Milestone Reports – As part of this thermal modeling work, researchers prepared and delivered the following milestone reports: (1) May Milestone, *Electro-Thermal Analysis of High-Power Batteries*; (2) June Progress Report to JCI, *Thermal Characterization of JCI Round Li-Ion Cell*; (3) September Milestone Report, *Paper on Technical Targets Energy Storage Systems for HEV and FCV;* and (4) September Letter Report, *Initial Report on Battery Profile in Plug-In Hybrid*.

Future Directions

In the future, the Vehicle High-Power Battery activity will continue to research lower cost separators, will define energy storage requirements for heavy hybrids, will ensure that new materials are made available to manufacturers, and will promote information exchange among the various participants in the program.

II.A.2 Electric Vehicle Battery Research and Development

Introduction

Electric Vehicle Battery Research and Development supports the development of battery technologies that would enable commercially competitive, full-function, EVs. EVs use no petroleum fuels and produce no vehicle emissions, thereby offering more significant petroleum saving and emission reduction potential than even HEVs. The activity conducts extensive benchmarking studies of advanced batteries from the U.S. and abroad to determine whether any can meet the technical requirements for the application, as defined in Table II-5.

Table II-5. U.S. Advanced Battery Consortium Goals for Electric Vehicle Batteries

Primary Criterion	**Long-term goals[6] (2005-2008)**
Power Density, W/L	460
Specific Power, W/kg (80% DOD/30 sec)	300
Energy Density, Wh/L (C/3 discharge rate)	230
Specific Energy, Wh/kg (C/3 discharge rate)	150
Life, years	10
Cycle life (cycles)	1000 (80% DOD) 1,600 (50% DOD) 2670 (30% DOD)
Power and capacity degradation[7] (% of rated spec)	20%
Ultimate price[8], $/kWh (10,000 units @ 40 kWh)	<$150 (desired to 75)
Operating environment	-30C to 65 C
Recharge time	< 6 hours
Continuous discharge in 1 hour (no failure)	75% (of rated energy capacity)
Secondary Criteria	**Long-term goals (2005-2008)**
Efficiency (C/3 discharge and C/6 charge[9])	80%
Self-discharge	<20% in 12 days
Maintenance	No maintenance. Service by qualified personnel only.
Thermal loss	Covered by self-discharge
Abuse resistance	Tolerant. Minimized by on-board controls.
Specified by contractor: Packaging constraints, Environmental impact, Safety, Recyclability, Reliability, Overcharge/over-discharge tolerance	

[6] For interim commercialization (reflects USABC revisions of September 1996).
[7] Specifics on criteria can be found in *USABC Electric Vehicle Battery Test Procedures Manual, Rev. 2,* DOE/ID 10479, January 1996.
[8] Cost to the original equipment manufacturer.
[9] Roundtrip charge/discharge efficiency.

Lithium/Sulphur Battery Development

Lithium/sulfur rechargeable batteries offer the possibility of several advantages over the current Li-ion rechargeable cells. Since sulfur is less expensive than lithiated metal oxides used for the cathodes in Li-ion systems, the lithium/sulfur system has the promise of significantly lower cost per kWh of stored energy. In addition, the use of a metallic lithium anode in these cells may allow for improved specific energy and energy density relative to the Li-ion system. In addition, the chemistry of the lithium/sulfur cell may also provide a "shuttle mechanism" that would allow the cell to be overcharged without significant safety problems or other adverse effects.

Unfortunately, the development activities on this system did not demonstrate the attainment of these potential advantages in prototype cells. As a consequence, no further development of this system is being undertaken following the completion of this project in 2005. However, a new high-energy RFPI has been posted to the USCAR web site and interested companies will be encouraged to participate.

II.B Technology Assessment

Technology assessments are conducted in order to validate a developer's technical claims by means of independent testing and to gauge the developer's ability to deliver a full-scale, fully packaged battery. The tests are performed both at the developer's facilities and at the DOE national laboratories in order to familiarize the developer with vehicular requirements and USABC testing procedures. The companies also share in the cost of the testing.

II.C Benchmark Testing

Benchmark testing of emerging technologies is important for remaining abreast of the latest industry developments. Working with the national laboratories, FCVT purchases and independently tests hardware against the manufacturer's specifications and the most applicable technical targets. Some products that were tested in 2005 include:

- Lead acid battery modules from EffPower and Japan Storage Battery,
- NiMH cells and modules from Cobasys,
- Li-Polymer batteries from Gaia and CPI,
- Li-ion cells from Hitachi, A123, Kokam, and GSY,
- Mg-Sulfur cells from Idea One, and
- Ultracapacitors from NessCAP.

II.D Small Business Innovative Research (SBIR)

The SBIR program was created by the Small Business Innovation Development Act of 1982 (P.L. 97-219) and has been reauthorized again until September 30, 2008. The SBIR program was designed to stimulate technological innovation, strengthen the technological competitiveness of small businesses, and use small businesses to meet Federal research and development needs. DOE's SBIR program budget for FY 2005 was approximately $102 million, based on a set-aside of 2.5% of the department's extramural R&D budget. These funds were used to support 291 Phase I and 120 Phase II projects. Phase I awards of up to $100,000 each for about 9 months are used to explore the

feasibility of innovative concepts. Phase II is the principal research or R&D effort, with awards up to $750,000 over a two-year period.

Over the past several years, SBIR/STTR contracts have provided valuable support to EV and HEV battery development efforts. There are currently over $4 million in Phase I and Phase II contracts focused on development of new anodes, cathodes, electrolytes, separators, salts, or assembly components.

Phase II contracts (~$750K ea.) active in FY 2005 are listed below:

- ***A123 Systems, Inc.*** **–** An Advanced Cathode Material for Li-Ion Batteries
- ***Farasis, Inc.*** *(Previously Called Redox Control)* **–** Stabilized Lithium Manganese Oxide Spinel Cathode for High-Power Li-Ion Batteries
- ***MER Corp.*** **–** Low Cost Carbon Anodes for Lithium-Ion Batteries
- ***Optodot Corp.*** **–** Low-Cost Nanoporous Sol Gel Separators for Lithium-Based Batteries
- ***T/J Technologies, Inc.*** **–** A Novel Cathode Material for High-Power Lithium Rechargeable Batteries
- ***TIAX, LLC*****,** *Cambridge, MA* – $LiFePO_4$ Cathode Material Designed for Use in Lithium-Ion Batteries

The following Phase I Proposals were funded in FY 2005:

- ***ADA Technologies, Inc.*** – High Performance Electrolyte for Electrochemical Capacitors
- ***Eltron Research, Inc.*** **–** Low Cost Synthesis of High Surface Area, Thermally Stable Lithium-Ion Battery
- ***Farasis Energy, Inc.*** **–** Abuse Tolerant, Voltage Stabilized Li-Ion Cell, and Accelerated Calendar Life Prediction for Li-Ion Cells
- ***Lithium Power Technologies*** **–** Organic Additives as Redox Shuttles for Overcharge Protection of Lithium-Ion Batteries
- ***MER Corp*** **–** Improved Performance of Lithium-Ion Cells at Low Temperature (STTR award in conjunction with Brookhaven Nat. Lab.)
- ***Optodot Corp*** **-** Shutdown Separators for Protection of Lithium-Ion Batteries Against Thermal Runaway
- ***Physical Sciences, Inc.*** **–** Electroactive Polymer Separator to Protect from Overcharging in Lithium-Ion Batteries
- ***TIAX, LLC*** **–** Improved Low-Temperature Performance of Safer, Low-Cost Lithium Iron Phosphate Cathodes for Lithium-Ion Batteries
- ***TOXCO, Inc.*** **-** Safer, Non-Toxic, Alternative Electrolyte
- ***Yardney Technical Products*** **–** Program to Address the Low Temperature Performance of Li-Ion Batteries

An SBIR Success Story - Black and Decker recently announced that it will use a new generation battery system developed by A123 Systems in a new line of heavy-duty power tools from it's DeWalt brand. The A123 battery, partially developed with support from the SBIR program, is a Li-ion/iron phosphate system using proprietary, nano-size materials that allow high rate discharge and charge.

III. APPLIED BATTERY RESEARCH

III.A Introduction

The applied battery research program is being conducted in support of the FreedomCAR and Fuel Partnership, which is targeting more fuel efficient light duty vehicles that can reduce U.S. dependence on foreign petroleum and reduce emissions, without sacrificing performance across a broad range of vehicles. There is an emphasis on developing and improving critical component technologies needed for more fuel efficient and cleaner vehicles. Advanced energy storage technologies are one of these critical components. Energy storage devices help to level the load on the prime power source in HEVs, thereby enhancing the efficiency of the prime power source, and they capture regenerative braking energy to produce more fuel efficient and cleaner vehicles. Better energy storage systems are needed to help expand the commercial markets for HEVs. This program focuses on assisting industrial developers of high-power Li-ion batteries to overcome key barriers to the commercialization of this promising energy storage technology for use in light-duty HEV applications.

The energy storage requirements for HEVs, 42-volt systems, and fuel cell electric vehicles are presented in Section II. For high-power Li-ion batteries, the key barriers are:

- 15-year calendar life
- Operation between -30^{o}C and +52^{o}C
- Selling price of $20/kW and
- Adequate abuse tolerance for use in on-road light-duty vehicles

This applied battery research program, denoted the Advanced Technology Development (ATD) program, focuses on these barriers for high-power Li-ion batteries. It was initiated to understand the factors that limit calendar life, abuse tolerance, and performance over the desired temperature range, so that improvements can be made in these three key areas. Also, it addresses the cost barrier at the cell level through the identification and development of lower-cost and more-stable cell materials and components. The program seeks to advance the development of more optimal cell chemistries for this application through the identification and development of cell materials that are more chemically, structurally, electrochemically, and thermally stable in the cell environment, as well as possessing a cost savings advantage over current state of the art (SOA) materials. Conventional high-energy Li-ion batteries, of the type used in consumer electronics, employ rather sophisticated electronic control systems that limit their exposure to abusive conditions. This program focuses on enhancing the inherent abuse tolerance of the cell chemistry, which will help reduce the level of sophistication of the electronic control system and thereby realize additional cost savings.

This year the program had the four cell-level focus areas listed below, each addressing one of the key barriers:

- Understand life-limiting mechanisms and enhance life
- Understand and enhance low-temperature performance

- Understand and enhance inherent abuse tolerance
- Lower cell-level costs via lower cost materials, components, and technologies

The main activities associated with each of these four focus areas are shown in Figure III-1.

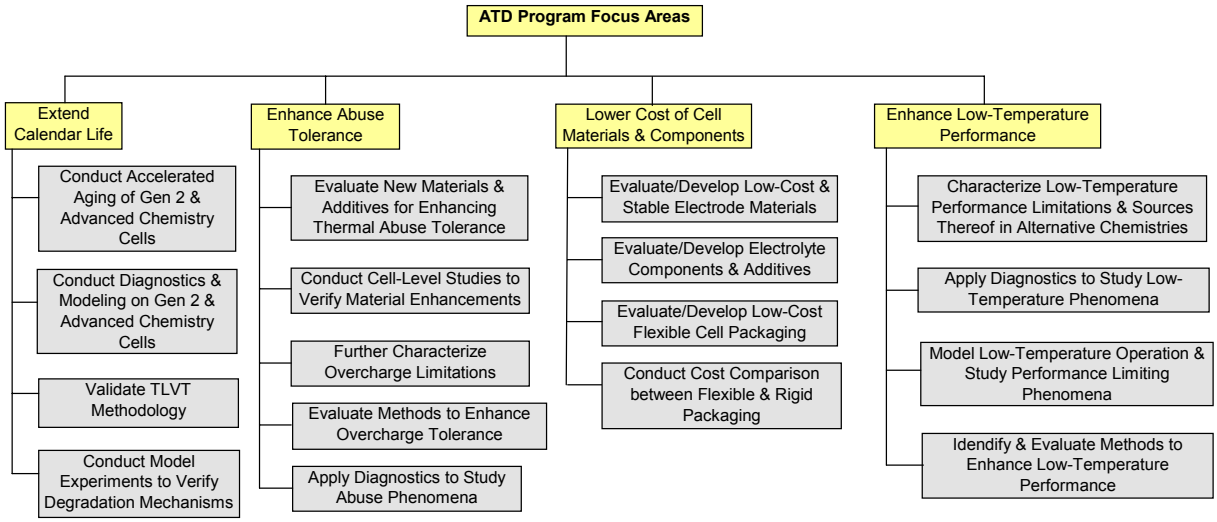

Figure III-1. Diagram of the activities conducted under the Applied Battery Research program.

Five DOE national laboratories collaborate in the program. Argonne National Laboratory (ANL) is the lead laboratory and provides coordination of the program activities for DOE. The other four participating DOE laboratories are Brookhaven National Laboratory (BNL), Idaho National Laboratory (INL), Lawrence Berkeley National Laboratory (LBNL), and Sandia National Laboratories (SNL). Also, the U.S. Army Research Laboratory (ARL) contributes in identifying and developing more optimal electrolyte systems, including for low-temperature operation. As part of this program, ANL researchers maintain close communications (and in some cases close collaborations) with a large number of international material supply companies, through which they gain access to the latest advanced electrode and electrolyte materials for evaluation.

In recent years, the program has thoroughly studied and characterized its own gen 2 cell chemistry and assessed two variations on it (one employing a modified cathode material and the other employing an alternative anode material). These cell chemistries were provided in last year's report. Studies on these gen 2 cell chemistries were completed during the last year and a new cell chemistry was selected for study. The new cell chemistry, denoted gen 3, employs a lithium-rich $LiNi_{1/3}Co_{1/3}Mn_{1/3}O_2$ layered cathode material and a synthetic graphite anode (MCMB 10-28). Results from gen1 and gen 2 cell chemistry studies showed that the cathode played a dominate role in both the calendar life and abuse tolerance limitations of the cells. Therefore, the goal in the study of the gen 3 cell chemistry is to thoroughly assess the impact of a more stable cathode material on both the life and inherent abuse tolerance of these cells. The conventional graphite anode material is being used to avoid possible complications associated with the use of a non-traditional material.

The following subsections provide technical highlights and progress on the Applied Battery Research program for FY 2005. The information provided is representative only and detailed information is available in the publications sited at the end of this section.

III.B Understand Life-Limiting Mechanisms and Enhance Life

Objectives

- Develop aging protocols and explore new tests, analyses, and modeling methodologies related to calendar and cycle life and provide results to battery developers and other laboratories.
- Develop enhanced understanding of life-limiting mechanisms.
- Select next generation chemistry for analysis by the program.
- Develop life models and correlations to gain understanding of fade mechanisms.
- Document and document methodology for the more accurate life prediction of Li-ion cells in TLVT manual.

Approach

- Continue diagnostic studies on gen 2 cell components from new and aged cells to understand material changes to make in gen 3 cell build.
- Perform accelerated aging tests and thoroughly analyze life test data on gen 2 cells.
- Refine and apply cell model to link diagnostic findings to observed performance degradation.
- Document Technology Life Verification Test (TLVT) methodology, tool, and manual. Establish the test protocols needed to validate the TLVT

Accomplishments/Findings

- Completed performance analysis of all available gen 2 characterization and life-testing data.
- Determined that impedance growth at the cathode is the greatest contributor to power fade, and lithium loss at the anode contributes to capacity fade.
- Finalized gen 3 chemistry and ordered high power cells for testing and analysis.
- Refined models to explain the impedance growth with time using new low temperature modeling results.
- Publish final TLVT manual and ordered cells to perform TLVT validation testing.

Future Studies

Power and Capacity Fade

- Begin life testing, data analyses, diagnostics, and modeling on the gen 3 cells.
- Conduct Phase I cell formation/SEI study to determine the key parameters of the formation process that produce more stable SEI layers on the positive and negative electrodes.
- Investigate SEI and its impact on life.

TLVT Manual

- Validate TLVT by performing life testing on sample developer cells.

Selected Publications

Please see list at the end of this chapter.

III.B.1 Introduction

This subsection provides highlights and progress on work focused on understanding the life-limiting mechanisms in high-power Li-ion cell chemistries and using this knowledge to develop more stable and lower cost cell materials and chemistries that should result in longer life cells. Since the beginning of this ATD program, it has been studying the aging characteristics of different cell materials and chemistries. This involves the accelerated aging of and diagnostic studies on high-power Li-ion cells, as well as electrochemical cell transport modeling to understand the factors that control the cycle and calendar life of cells that employ different materials and cell chemistries. This year these studies continued on gen 2 baseline, gen 2 variant C, and gen 2 GDR cells. These three variations on the gen 2 cell chemistry were described in last year's report.

Last year this program began work on developing more accurate life prediction methodologies. That work was continued this year, as well. The goal of this year's effort was to publish the methodology in a "Technology Life Verification Test" (TLVT) manual and then to initiate a study to assess the validity of the methodology using prototype HEV cells.

Figure III-2 provides a schematic diagram of how the activities in this focus area relate to each other, while Table III-1 summarizes how the five DOE laboratories contribute to the work.

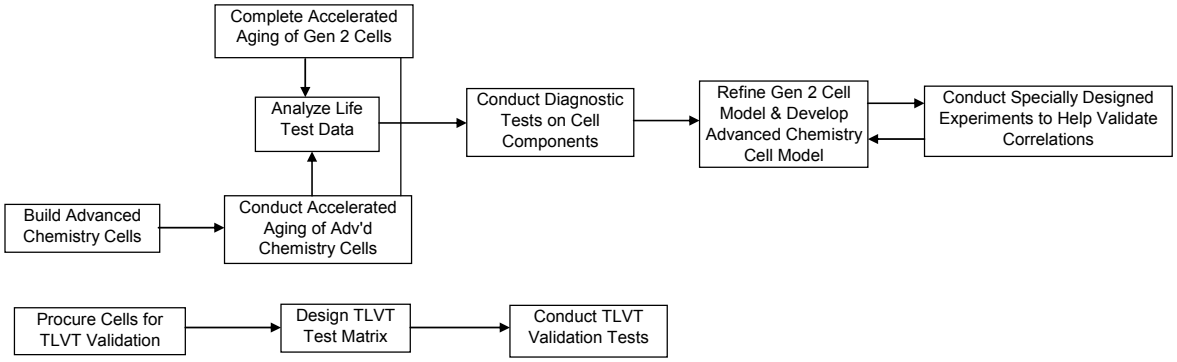

Figure III-2. Diagram of activities conducted in the "Life Enhancement" focus area.

Table III-1. Summary of DOE laboratory contributions to the "Life Enhancement" focus area.

	ANL	BNL	INL	LBNL	SNL
Accelerated Cell Aging and Data Analysis	X		X		
Cell Component Diagnostics	X	X		X	
Cell Transport Modeling	X				
Advanced Chemistry Cell Build	X				
Prototype HEV Cell Procurement	X				
TLVT Validation Testing and Data Analysis	X		X	X	X

III.B.2 Aging Characteristics of High-Power Cells

One of ATD's objectives is to understand the factors that limit life. High-quality cells with precisely defined histories/aging conditions (high quality testing) are needed in this process. Data analysis can give insights into the types of mechanisms in operation. A summary of the cell test matrix is given in Table III-2. There were two aging schemes used: life cycle and calendar aging. These testing protocols are described in the Partnership for a New Generation of Vehicles (PNGV) Test Procedures Manual[10]. The baseline cells were tested at 60% state-of-charge (SOC) and three temperatures, 25, 45, and 55°C. The Variant C cells were tested at the same SOC but at 45°C only.

Table III-2. Summary of Test Matrix

Cell Chemistry	Temperature		
	25°C	45°C	55°C
Baseline	15 cycle life	15 cycle life 2 calendar life	15 calendar
Variant C		14 cycle life 10 calendar life	

All of gen 2 cell aging is complete as of February 2005 and all cells were taken off test. They were sent to the diagnostics labs or put in cold storage pending diagnostic work. The results of the aging experiment are summarized in Table III-3.

Table III-3. Summary of aging results.

Chemistry		Temp., °C	Weeks on test	C/1 Fade, %	C/25 Fade, %	Power Fade at 300-Wh, %
Baseline	Cycle life	25	140	32.0	16.7	50.2*
		45	68	30.1	20.5	51.0*
	Calendar life	45	88	34.4	23.6	50.9**
		55	40	18.5	24.8	46.1
Variant C	Cycle life	45	124	16.9	16.9	49.6
	Calendar life	45	148	15.2	19.9	44.3**

* Average power fade is temperature compensated.
** Only one cell was aged to 50% power fade.

Sample Experimental Results. As the cells age, the area-specific impedance (ASI) increases. A plot showing the average change in ASI vs. time for all the cells tested is given in Figure III-3. From Figure III-3, the ASI data from the baseline cells display obvious changes. In the beginning, the ASI data follow a $t^{1/2}$ dependence and, later on, a dependence on t. These two dependencies have been ascribed to a change in the mechanism that is responsible for ASI increase. The $t^{1/2}$ dependence implies thin film growth, as in SEI formation. The linear dependence on t could be due to a physical separation of the particles or some other mechanism. From the plot, the time at which the change occurs depends on test temperature. It occurs later at lower temperatures. Also, the

[10] See http://www.uscar.org/consortia&teams/consortiahomepages/con-usabc.htm

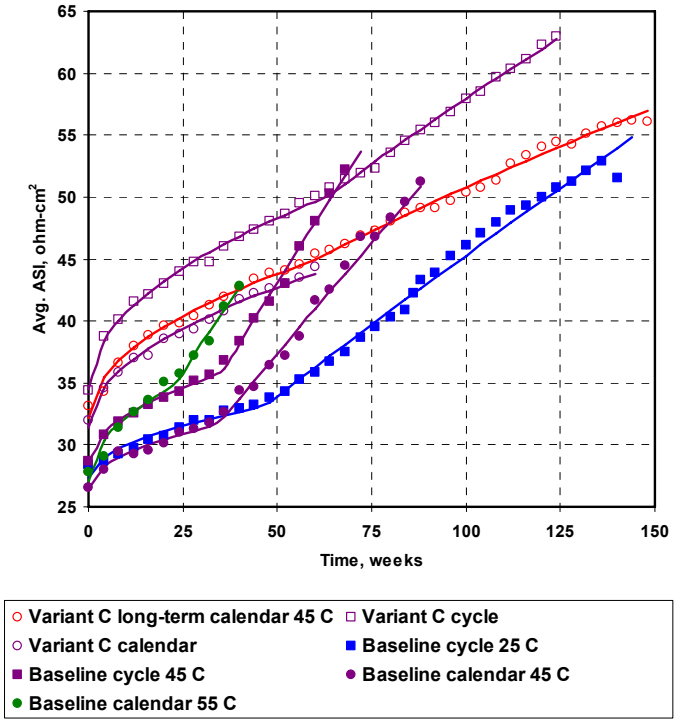

Figure III-3. Average ASI vs. test time for all cells in the aging experiment. The markers are the experimental points and the solid lines from the curve fitting work.

effect of cathode composition is seen. There is an obvious "break" in the baseline curves. The data from the Variant C cells also show a similar change in mechanism, but the change is more subtle. Since the only significant difference between the two cell chemistries is the composition of the cathode, this difference in aging behavior is most likely due to that electrode.

The change in mechanism in Variant C is more apparent when the C/1 data are included in the analyses (see Figure III-4 and Figure III-5). Figure III-4 shows that the C/1 data from the baseline cells follows the two-step mechanism exhibited by the ASI data.

Figure III-5 shows that the C/1 data from the Variant C cells also exhibits similar behavior with time. Curve fitting using the non-linear equation, $ASI = at^{1/2} + c(t-t_0) + ASI_0$, where t is time, ASI_0 is the ASI at t=0; a, c and t_0 are constants; and c=0 when $t < t_0$, was performed to gain some mechanistic insights. The regression coefficients (r^2) in all cases were 0.99 or greater. The fit data are given in Table III-4 and are shown as solid lines in Figure III-3. From the data in Table III-4 the effect of cathode composition, test type and temperature are clearly seen. For example, examining the data in the t_0 column shows that the value is 35 weeks for the baseline cells, but on the order of 60 weeks for the Variant C cells. This may be related to greater Al content in Variant C.

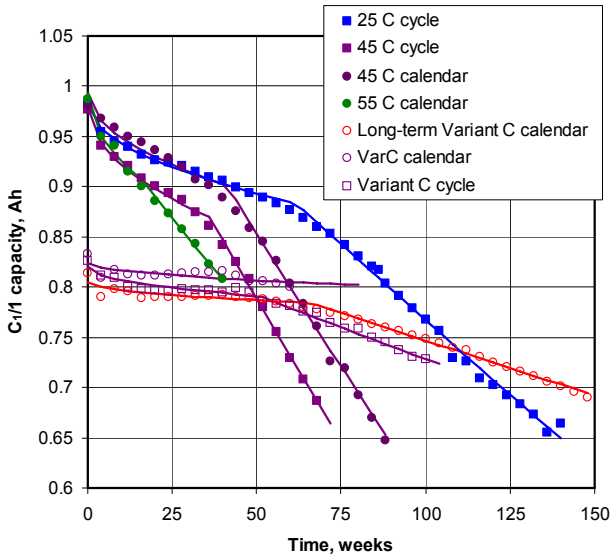

Figure III-4. C/1 capacity vs. time for all cells tested. The new data in this report start at 98 weeks for the Var C calendar cells, at 100 weeks for Var C cycle life cells and at 116 weeks for the 25°C baseline cycle life cells.

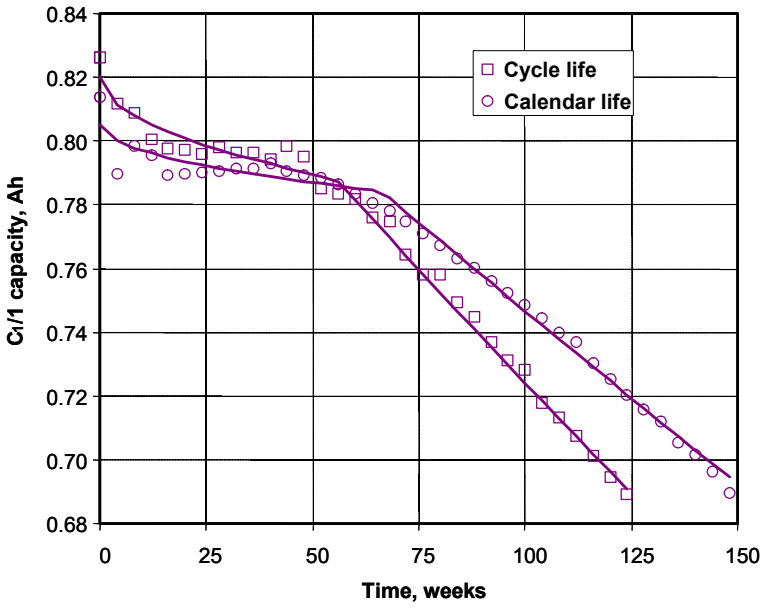

Figure III-5. C/1 capacity vs. time for the Variant C cells only. This is an enlargement of the plot in Figure III-4.

Table III-4. Results from curve fitting of the experimental data.

	ASI_0	a	c	t_0
Baseline cycle life 25°C	27.34	0.85	0.14	44.30
Baseline cycle life 45°C	28.46	1.23	0.40	35.15
Baseline calendar life 45°C	26.44	0.89	0.30	34.48
Baseline calendar life 55°C	27.04	1.63	0.31	22.78
Variant C cycle life 45°C	34.44	1.96	0.10	62.60
Variant C calendar life 45°C	23.16	1.64	0.05	59.70

From curve fitting, the C/25 capacity data from all cells follow $t^{1/2}$ rate laws (Figure III-6). C/25 capacity is not sensitive to cathode composition and may reflect anode chemistry.

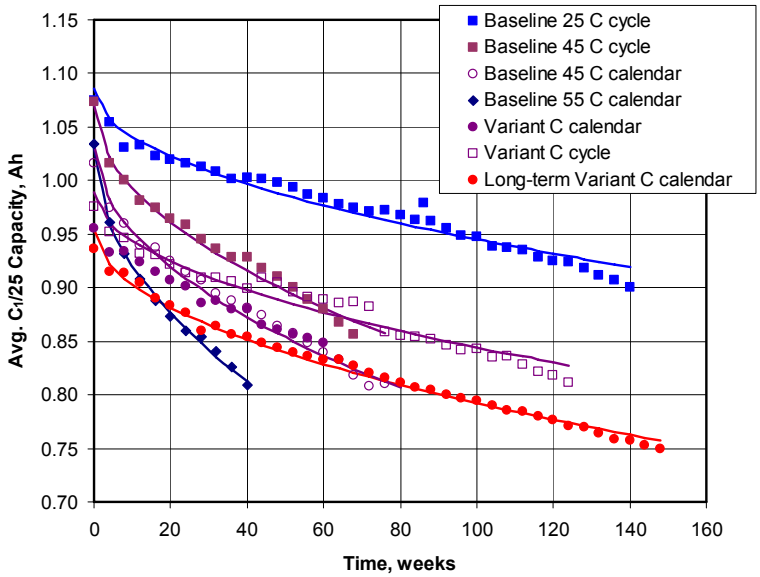

Figure III-6. Average C/25 capacity vs. time for all cells in the aging experiments

Another model has been developed to evaluate aging data for ATD cells. The Multiple Sigmoid Model (MSM) is a physics-based model that can project the effects of cumulative life on test on cell performance. The MSM asserts that a given time-dependent performance indicator Ψ (e.g., impedance rise, power fade, capacity fade, etc.) can be expressed as a summation of *n* sigmoid functions, wherein each function represents a major or net degradation mechanism, typically isolated at one or more of the major cell components (cathode, anode, separator, electrolyte, etc.):

$$\Psi(t) = \sum_{i=1}^{n} \Psi_i(t) = \sum_{i=1}^{n} \left\{ 2M_i \left[\frac{1}{1 + \exp\left(-\left(t^{b_i} / a_i \right) \right)} - \frac{1}{2} \right] \right\}$$

where $(a, b, M)_i$ are model parameters related to the rate constant, effective reaction order, and upper boundary for the i^{th} degradation mechanism. The MSM can be linked to physical parameters within

the cell, most notably the effective capacity or the net active surface of each electrode. If net degradation mechanisms are assumed to reside primarily at the electrodes, then a Double Sigmoid Model (DSM) is gotten from the above expression. Additional sigmoid terms can be added to the DSM to account for other factors such as the potential increase of electrolyte viscosity with aging. An example of DSM results is given in Figure III-7. Here, the DSM was fit to power fade data from the baseline and Variant C cycle-life cells through 68 weeks, and extrapolated thereafter. From this figure, the DSM fit is very good, and provides good predictions of when cells reach 50% power fade.

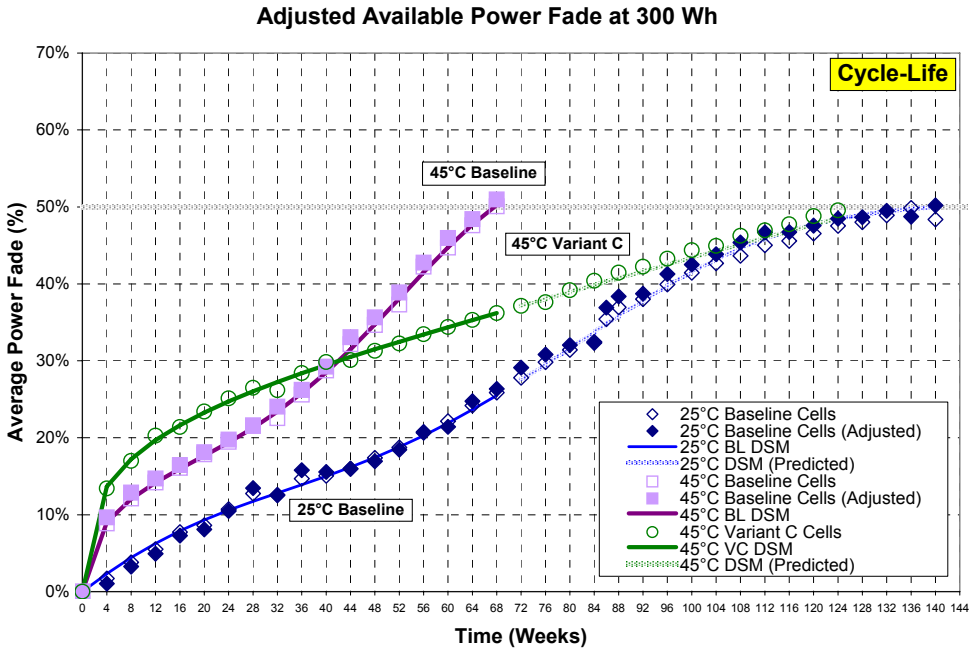

Figure III-7. Average power fade vs. time and the predictions made by the DSM model. The "adjusted" notation refers to data adjusted to true test temperature.

III.B.3 Diagnostic Results on Aged Cells

In FY05, the diagnostics team continued to examine the mechanisms that limit the performance of Gen 2 cells on accelerated aging. Experiments were conducted both on electrodes harvested from the aged Gen 2 cells and on "model" systems. Some of the results are described below; a comprehensive description is presented in "Diagnostic Examination of Generation 2 Lithium-Ion cells and Assessment of Performance Degradation Mechanisms" (ANL-05/21).

III.B.3.1 Effect of Testing Temperature on Cell Capacity and Impedance

Testing temperature has a significant effect on the capacity and impedance data of fresh and aged high-power Li-ion cells. Experiments conducted in reference electrode cells containing harvested 18650-cell electrodes showed that increasing the test temperature from 22° to 55°C reduced the width of the mid-frequency arc in the $LiNi_{0.8}Co_{0.15}Al_{0.05}O_2$-positive electrode EIS data but did not affect the low-frequency diffusion tail data, Figure III-8. The testing temperature effects were

reversible, i.e., the data depended only on the test temperature, and were independent of the process (cell heating, cooling) by which the temperature is attained. It is apparent that the interfacial feature (oxide particle surface films, etc.) responsible for the mid-frequency arc is sensitive to the testing temperature: higher the test temperature, lesser the effect of this interfacial feature. The relative insensitivity of the low-frequency impedance tail to temperature indicated that this feature is mainly associated with diffusion-limited processes into and through the oxide particles. Increasing test temperature also increased the capacity of electrodes, especially of aged electrodes that were cycled at higher rates. The capacity gains and the cycling hysteresis reductions in the higher temperature measurements result from impedance reductions arising from improved electrode interfacial kinetics.

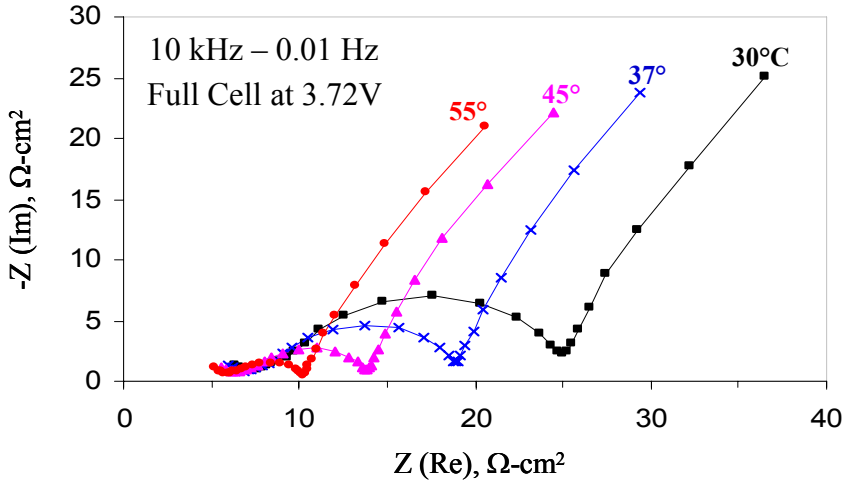

Figure III-8. Effect of testing temperature on positive electrode impedance.

III.B.3.2 TEM/EDX and SEM Studies of Positive Electrode Oxide Particles

A strong quantitative correlation has been established between oxygen loss (measured by Energy Dispersive Spectroscopy (EDS)) from cathode particle surfaces and cell power fade. SEM images revealed some disintegration of secondary oxide particles in Gen 2 cathodes. Further qualitative evidence for degradation of cathode active material was obtained from a TEM/EDX investigation of aged cathode material. The morphology and electron diffraction patterns (Figure III-9) of small particles show considerable disorder and polycrystallinity. Particles of this type are not observed in fresh electrodes. The structure and composition are close to those of the fresh cathode particles. Larger particles show much less disorder.

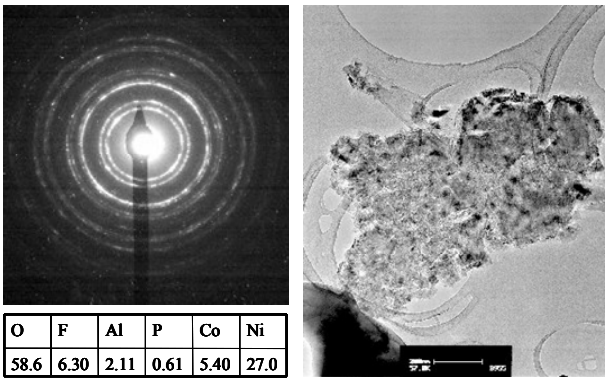

O	F	Al	P	Co	Ni
58.6	6.30	2.11	0.61	5.40	27.0

Figure III-9. TEM-EDX images of small, disordered particle from I138 cathode

III.B.3.3 XRD Studies of Positive Electrode Oxide Particle Isolation

Evidence for oxide particle isolation was found in all gen 2 positive electrodes studied from cycled or aged cells with significant power fade. High resolution XRD patterns (Figure III-10) obtained on aged electrodes that were rapidly charged to 4.1V showed a bimodal distribution of states of charge between well-connected and poorly-connected oxide particles.

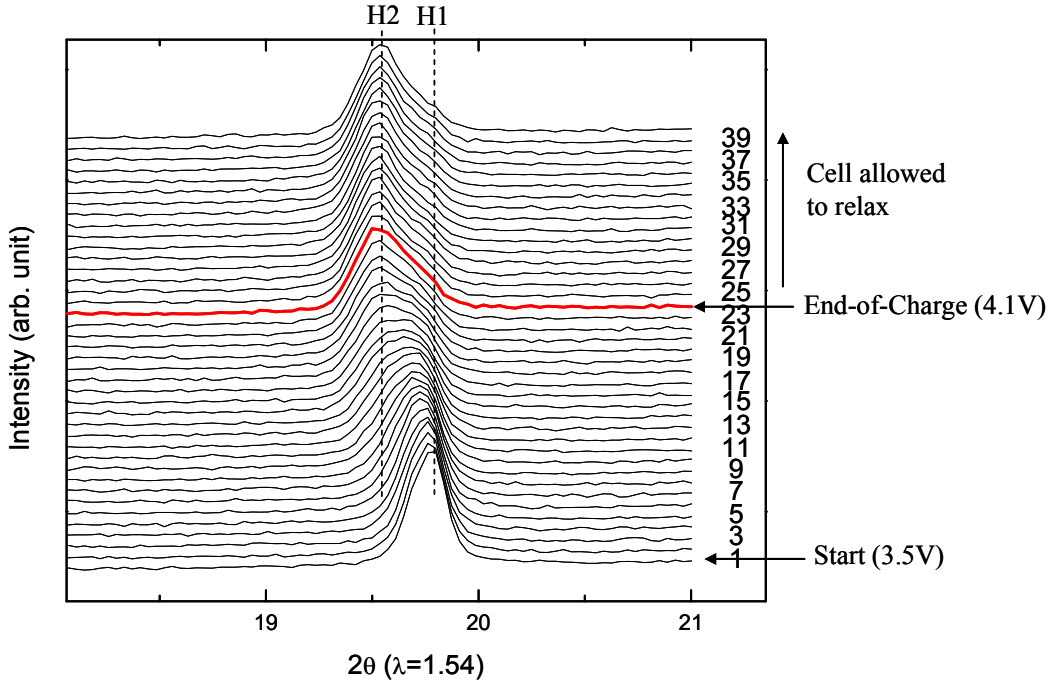

Figure III-10. In situ XRD spectra from highly aged positive electrode (>50% power fade cell).

In Figure III-10, on charging the cell from 3.5V to 4.1V, the oxide crystal structure changes from H1 to H2. For relatively-new electrodes at 4.1V the oxide displays the H1 structure. In contrast, the aged electrodes show the co-existence of H1 and H2 structures at 4.1 V. The H2 content increases

when the cell is allowed to relax, but the H1 residue remains in the patterns. These data indicate that a portion of the C/1 capacity fade arises from a loss of the dynamic response resulting from the positive electrode impedance increase. The H1 structure residue indicates that some oxide particles do not participate during cell charging, i.e., they appear to be isolated.

III.B.3.4 Studies of Carbon Additive Migration in Model Gen 2 Cells

Carbon retreat was observed and verified in the gen 2 cathodes and linked with other detrimental phenomena that led to cell degradation e.g., increased carbon disorder in tested graphite anodes, decrepitation of oxide agglomerates, poor electronic contact between primary particles, etc. A primary objective in FY05 was to design and carry out diagnostic studies of the carbon retreat mechanism in gen 2 cathodes and determine its impact on cathode and anode electrochemical performance.

^{13}C hard carbon powder from ISOTEC was used instead of standard acetylene black in gen 2 cathodes to study the retreat of carbon additive. ^{13}C-enriched cathodes displayed a fairly uniform distribution of electrode components. However, full surface carbon coverage could not be achieved in the model electrodes as it was observed in original gen 2 cathodes. The ^{13}C-enriched electrode displayed only 87% of its theoretical capacity (vs. Li metal anode) at C/20 and showed significant power loss at higher current rates. Electrochemical cycle life tests exhibited rapid capacity fading. It became clear that the structure and morphology of ^{13}C black powder and its distribution in the electrode require further optimization to achieve performance similar to the observed for the gen 2 cathode. Preliminary post-mortem diagnostic analysis of tested cells showed only minor changes in the surface composition of the cathode. SEM images showed no visible structural damage to the oxide. Qualitative analysis of the lithium anode revealed the presence of ^{12}C amorphous carbon but no trace of ^{13}C. The most likely source of amorphous ^{12}C is graphite, which is also present in the cathode. The absence of the ^{13}C isotope in the anode could be explained by significant differences in the hard carbon black morphology, particle size, structure and electrochemical properties compared to the standard carbon black additive. This group is currently carrying out another set of experiments with composite gen 2 cathodes enriched with ^{13}C soft carbon powder.

III.B.3.5 Electrolyte Studies

Wet chemical analysis studies on cell components have continued in an effort to eliminate some uncertainties with previous results on the apparent formation of higher molecular weight materials in the electrolytes. This has involved the development of extraction techniques that do not use water and the use of non-aqueous eluents to separate products. An example of the results of these efforts is shown in Figure III-11, which is a gas chromatogram of a DMC extract of a gen 2 cathode from a cell with 50% power fade. The cathode had been rigorously extracted with DMC using ultrasonication and the solvent was then concentrated and injected directly on the gas chromatograph (GC) and the GC/mass spectrometer. The inlets for these instruments are cooled to -15^{o}C for the injection so there are no thermal effects due to the injection process.

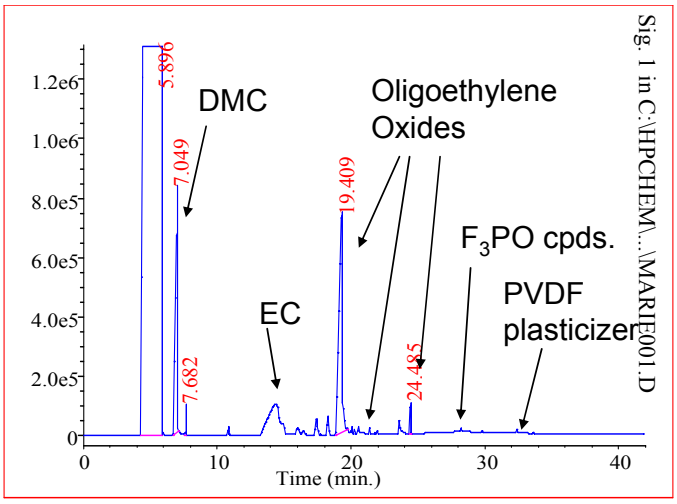

Figure III-11. Gas chromatogram of DMC extract of a cathode from A217 (50% PF)

It can be seen that a large peak is visible that corresponds to pentaethylene glycol and smaller peaks are visible that correspond to oligoethylene oxides. The spectral patterns show a very strong fit to standard spectra. However, it is noted that polyetherpolycarbonates also show similar spectra under electron impact ionization. Both types of compounds result from acid or basic ring-opening of EC. The analysis also detected the presence of PF_3=O which is known to be a product of reaction of PF_5 and water as well as PF_5 and ethers. Some evidence was obtained for the presence of an EC-PF_5 adduct in the mass spectra. Also visible in the extract was the phthalate ester plasticizer from the PVdF binder which is a reminder that small impurities may play a role in surface chemistry. These results indicate the formation of some compounds in the electrolyte that have a higher molecular weight and may be organofluorophosphates that easily decompose during the analysis. These higher molecular weight materials may play a role in affecting the interfacial impedance and exchange current densities.

The failure to detect PEO by vibrational spectroscopy may be because (a) PEO is not the end-product of cell reactions and (b) the products of PF_5 and PEO-type materials are very soluble in the electrolyte and washed off during sample preparation. The data strongly imply that prevention of the chemical reactions of PF_5 and other acid or basic species on the solvent components and the electrode surfaces will inhibit the growth in the cell impedance. The use of vinylene carbonate can be linked to this through generation of a better SEI layer which inhibits the irreversible reduction of CO_2. The complicated acid-base and hydrolytic chemistry of the $LiPF_6$ and electrolyte/electrode components involves many reactions that are reversible (e.g. hydrolysis to PF_3=O). Only when driven by an irreversible reaction such as CO_2 reduction to carbonate do the reactions damage the performance.

III.B.4 Electrochemical Modeling of Aged Cells

The electrochemical modeling effort is aimed at examining the impedance rise in gen 2 cells. The overall goal of this work is to associate changes seen in the post-test diagnostic studies with the loss of electrochemical performance, as measured by the HPPC tests. The approach taken is to develop a

model based on the diagnostic studies, establish the model parameters, and conduct parametric studies with the model. The parametric studies are conducted to gain confidence in the model, examine degradation mechanisms, and analyze cell limitations. To accomplish these tasks two versions of the model have been developed. One version simulates the cell response from AC impedance studies[11], and another version is utilized for examining HPPC tests. Both of these experimental techniques are extensively used in the program to quantify the cell's and its components' electrochemical performance. The underlying basis for both models is the same, as well as their parameter set. While both electrodes have been examined, the modeling effort has concentrated on the positive electrode because of its importance in the cell's overall impedance rise

The general methodology for the model follows the work of Professor Newman at Berkeley. Concentrated solution theory is used to describe the transport of salt in the electrolyte. Volume-averaged transport equations account for the composite electrode geometry. Electrode kinetics, thermodynamics, and diffusion of lithium in the oxide active particles are also included. The detailed theoretical description of the oxide active material/electrolyte interface, commonly referred to as the SEI, is based on post-test analytical diagnostic studies. The SEI region is assumed to be a film on the oxide and an oxide layer at the surface of the oxide. The film on the oxide is taken to be an ill-defined mixture of organic and inorganic material through which lithium ions from the electrolyte must diffuse and/or migrate to react electrochemically at the oxide surface. The lithium is then assumed to diffuse through the oxide surface layer and into the bulk oxide material. Capacitive effects are incorporated into the model at the electrochemical interfaces and a localized electronic resistance between the current carrying carbon and the oxide interface can also be included.

Besides the development of the electrochemical model and the determination of its parameters, previous years' highlights under this effort include: examination of the impedance rise of the positive electrode during aging, correlating AC impedance studies with HPPC tests, and positive electrode optimization studies. These accomplishments and others are discussed in Appendix H of the diagnostic report on gen 2 Li-ion cells, released this year[12].

Activities this year have been in three main areas. First, the low-temperature cell modeling studies indicated that early assumptions concerning gen 2 separator tortuosity and positive electrode electrochemical active area needed to be modified. Since the active area indirectly affects all the interfacial and oxide particle diffusional parameters, these parameters were refined based on the new data. The validity of the early conclusions was reevaluated and the results are discussed in the Low Temperature Cell Performance Modeling section (III.C.4). Second, an oxide particle electrochemical model was developed to examine lithium diffusion and electronic conduction through and between agglomerated primary particles. This work strongly suggests that loss of contact area between the carbon and the oxide active material particles does not have a major impact on the impedance. Finally, the electrochemical cell model was extended to two dimensions to examine current distribution issues, such as edge effects and reference electrode design and placement. The reference electrode placement is particularly important because of its use in the diagnostic studies. An internal

[11] D. Dees, et. al., "Alternating Current Impedance Electrochemical Modeling of Li-ion Positive Electrodes," *J. Electrochem. Soc.* **152** (7), A1409 (2005).

[12] "Diagnostic Examination of Generation 2 Li-ion Cells and Assessment of Performance Degradation Mechanisms," D. Abraham editor, **ANL-05/21**

reference electrode (i.e. placed inside the cell between separator layers) is more of a challenge to use, but has thus far has given the most consistent results.

As a first step to examining internal and external reference electrodes, a series of simulations of a cell with an edge in a pool of electrolyte undergoing an HPPC discharge pulse were conducted. It was assumed that the inside and outside reference electrodes were perfect (i.e. had infinitesimal size and were reversible). It was found that the internal and external reference electrodes gave essentially the same results provided the electrode layers were perfectly aligned. However, if the positive and negative electrodes were misaligned, even by a fraction of a millimeter, the results were dramatically different. Depending on which electrode overlaps the potential of the electrolyte pool is essentially that of the electrolyte in one of the electrodes near the edge. The variation in the outside reference electrode potential vs. the inside reference electrode potential with the extent of misalignment is given in Figure III-12. One can see that the ASI of the positive electrode is relatively constant when measured with the internal reference electrode, but varies significantly when using the outside reference.

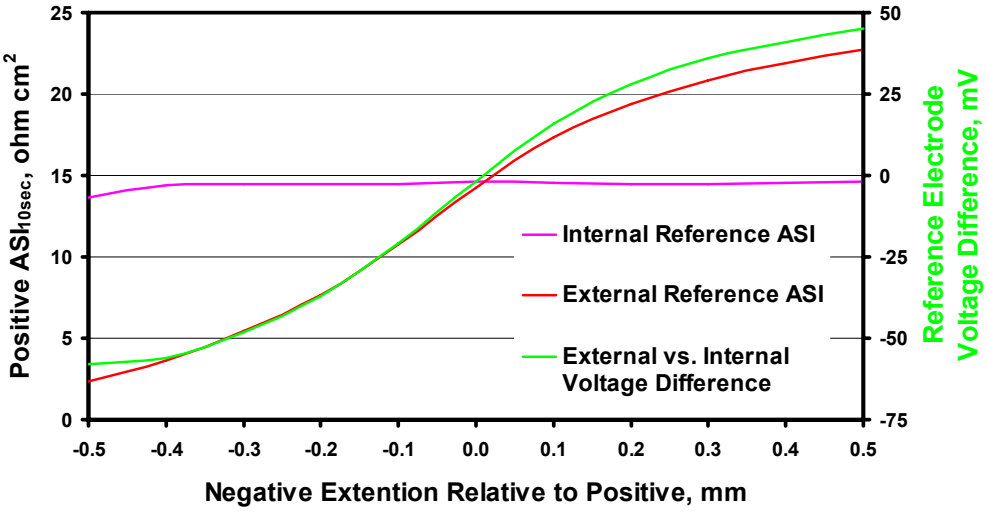

Figure III-12. ASI of the positive electrode at the end of a 5C 10 sec discharge pulse vs. the extent of electrode misalignment, as measured by ideal internal and external reference electrodes. Also shown is the variation in the outside vs. the inside reference electrode potential.

III.B.5 More Accurate Life Prediction Methodology Development

The Technology Life Verification Test (TLVT) manual was published and posted to the USCAR website on February 2005. The methodology presented in the test manual is being validated by carrying out the procedures and testing cells. For fiscal year 2005, efforts towards this included identifying a cell builder and chemistry, developing an aging model, and evaluating some of the assumptions made in the test manual, such as that the newly defined minimum pulse power characterization (MPPC) test provides the same results as the HPPC test.

Based on experience with Saft's technology, ATD decided to approach them as the supplier for TLVT testing. They accepted a purchase order for 55 cells in January, the expected delivery date is early FY06. It was agreed that they would use a cell chemistry similar to the one used in an earlier FreedomCAR program that demonstrates, on limited cell testing, 22 year life. Saft does not make 18650 size cells, so it was also agreed that they would supply 7 Ah cells for the analysis.

The decision to use 7 Ah cells for the analysis effectively reduced the available testing capability. In the ATD program, a large number of channels are available for testing ~1 Ah cells. These new cells from Saft require much larger test channels. To compensate for this, INL found that it could parallel smaller channels to perform, but this would limit the number of available channels. ANL preferred not to bundle channels, but had some higher power channels available.

To perform full methodology validation, both cycle and calendar life testing need to be performed. INL found that performing the MPPC at 3C was just as representative of cell impedance as the MPPC performed at 5C. Performing the MPPC at 3C allowed for calendar testing 30 cells at INL. Based on all of the above, the calendar and cycle life test matrix given in Table III-5 was developed. The calendar life test matrix represents a 3^2 full factorial response augmented with three cells aged at 30°C. The nature of the design allows for nonlinear effects of temperature and SOC to be observed. The cycle life test matrix represents a 2^2 full factorial interaction design augmented with three cells to be cycled at a different power rating. The design will allow main effects (and interaction) of throughput and temperature to be observed.

With this very limited calendar-life data supplied by Saft, a model was developed of the form $ASI(t) = ASI_0 \cdot \exp(k \cdot t)$ where $\ln|k| = \gamma_0 + \gamma_1 \cdot 1/T + \gamma_2 \cdot V + \gamma_3 \cdot V^2$. The data in provided were used to estimate the model parameters from which the set of results in Table III-6 (life on test and acceleration factors) were obtained.

Table III-5. Preliminary Cell Test Matrix (T-put = energy throughput per cycle, and the last two columns under Cycle Life stand for percent of rated power)

Calendar Life – 30 cells: calendar (10 experimental conditions – 3 cells per) @INL		
	30°C	@ 80% SOC (SOC based on voltage)
	45°C	@ 60% 70% 80% SOC
	52.5°C	@ 60% 70% 80% SOC
	60°C	@ 60% 70% 80% SOC
Cycle Life: 15 cells: cycle (5 experimental conditions – 3 cells per) @ ANL		
	45°C, 80% SOC, 20Wh T-put, 100% rated, 100% rated	
	45°C, 80% SOC, 25Wh T-put, 100%,	100%
	60°C, 80% SOC, 20Wh T-put, 100%,	100%
	60°C, 80% SOC, 25Wh T-put, 100%,	100%
	60°C, 80% SOC, 25Wh T-put, 80%,	80%

Table III-6. Calculated Acceleration Factors Based on Proposed Rate Equation

T **(°C)**	***V*** **(Volts)**	**Life-on-Test (years)**	**Acceleration Factor Reference: 30°C, 3.75V**
30	3.75	24.8	1
45	3.60	13.0	1.9
45	3.75	10.6	2.3
45	3.90	3.0	8.3
52.5	3.60	8.7	2.8
52.5	3.75	7.1	3.5
52.5	3.90	2.0	12.4
60	3.60	6.0	4.1
60	3.75	4.9	5.1
60	3.90	1.4	17.7

The results in Table III-6 reveal the strong dependence of life-on-test (and acceleration factor) on voltage and temperature. The apparent nonlinear effect of voltage warrants the three levels of SOC specified in Table III-5. The three temperatures (45°C, 52.5°C, 60°C) specified in Table III-5 will provide the ability to accurately assess the effects of temperature. Thus, for the limited channels available, the proposed calendar life test matrix (Table III-5) is efficient and will be informative. Unfortunately, preliminary experimental data regarding the effects of the cycling stress factors were not available to facilitate the design of the cycle life test matrix. Nevertheless, the proposed test matrix will allow the team to observe the main effects (and interactive effects) of throughput and temperature on cycle life.

Reference Performance Test Studies. The MPPC test is the new reference performance test (RPT) for the TLVT Manual. It consists of two HPPC profiles, one each at the voltages corresponding to SOC_{MAX} and SOC_{MIN} with a $C_1/1$ taper discharge in between (SOC_{MAX} and SOC_{MIN} are typically determined by the manufacturer). This sequence is performed first at life-test temperature (for temperature compensation), and then at a reference temperature (e.g., 30°C). The primary objective of the MPPC is to provide statistically similar results to the HPPC test while reducing irrelevant stresses induced by the RPT. Consequently, all full discharges and charges have been eliminated. The pulse power verification (PPV) test was also introduced in the TLVT Manual as a way to verify that the MPPC and HPPC tests were yielding the same results. The PPV test consists of a standard L-HPPC test (capacity-based) with an additional pulse profile at the voltages corresponding to SOC_{MAX} and SOC_{MIN}.

Four gen 2 baseline cells were used for a direct comparison between the MPPC and PPV tests. Two of these cells were fresh (i.e., low power fade), and the other two had been aged to approximately 50% power fade. These cells were subjected to a path dependence study using the sequence shown in Table III-7 at a test temperature of 25°C and a SOC_{MAX} and SOC_{MIN} of 90 and 50%, respectively. The purpose of this study was to determine if there was a difference between starting with an MPPC or PPV (i.e., Parts 1 and 2), and also to see the effect of starting the MPPC from a charged state (i.e., $MPPC_1$ and $MPPC_4$) or discharged state (i.e., $MPPC_2$ and $MPPC_3$). The TLVT Manual defines an MPPC test as starting from a discharged state.

Table III-7. Path dependence test sequence

Test	BOT Condition	Purpose
PPV_1	Full Charge	
$MPPC_1$	Full Charge	Path Dependence (Part 1)
PPV_2	Full Charge	PPV → MPPC
$MPPC_2$	~ Full Discharge	
L-HPPC	**Full Charge**	
$MPPC_3$	~ Full Discharge	
PPV_3	Full Charge	Path Dependence (Part 2)
$MPPC_4$	Full Charge	MPPC → PPV
PPV_4	Full Charge	

Figure III-13 shows the discharge ASI at SOC_{MAX} for all four cells. These data show that there is no apparent path dependence by having the PPV or MPPC test first. However, there is an effect on ASI from the beginning of test condition. Both the $MPPC_2$ and $MPPC_3$ tests were charged to the voltage corresponding to SOC_{MAX} and yielded lower ASIs, while the other MPPC tests were discharged to the same voltage. Interestingly, the percent-change in ASI is greater for the fresh cells than for the aged cells. This indicates that the MPPC test may also have a different aging effect than the HPPC test, which obviously has an impact on life predictions. At SOC_{MIN}, all ASIs from the MPPC or PPV tests are similar since all cells reached the target voltage by a discharge from SOC_{MAX}.

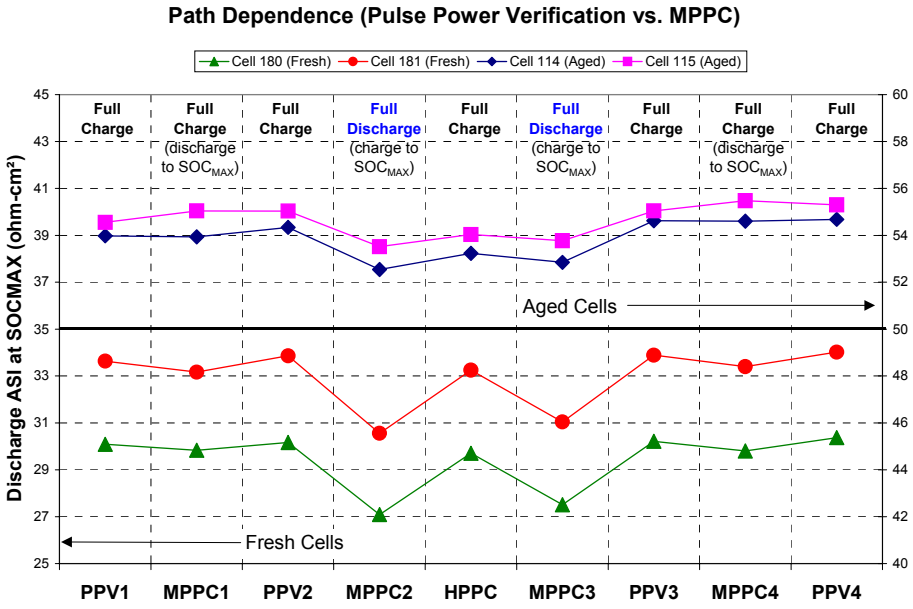

Figure III-13. Effects of ASI at SOC_{MAX} for the path dependence study

Therefore, although the MPPC is a valid reference performance test, it appears to affect cell behavior differently than an HPPC. Approaching a target SOC from a charge or discharge will have an impact on ASI and, thus, life prediction. As a result of this study, various modifications to the MPPC have been discussed, and an RPT screening test will be conducted.

III.C Understand and Enhance Low-Temperature Performance

Objectives

- Understand factors that limit low-temperature performance and identify approaches to enhance performance at low temperature.
- Develop a model of low temperature behavior of electrolytes specifically and Li-ion cells generally.
- Thoroughly characterize the gen 2 cell chemistry at low temperatures, including the dramatic power loss during high-current pulse discharge and plating of metallic lithium during high rate regenerative pulse charging.

Approach

- In order to characterize the gen 2 chemistry at low temperatures:
  - Use reference electrode cells to isolate problem as arising at the anode or cathode,
  - Use EIS to identify potential sources of the problems, and
  - Use diagnostics and modeling to aid in identifying sources of problem.
- Based on the above information, identify potential methods for enhancing low-temperature performance and evaluate them experimentally.

Accomplishments/Findings

- Determined that the positive and the negative electrode interface contribute nearly equally to the low-temperature impendence rise. The responsible phenomenon may be independent of active material.
- Determined that impedance growth of the electrolyte alone is not sufficient to explain the overall cell impedance rise. EIS data have shown that the impedance growth is interfacial and fairly evenly distributed between the positive and negative electrode interfaces.
- Modeled cell response at low temperature and adjusted model parameters based on experimental data.

Future Studies

- Develop in-situ diagnostics to investigate Li-ion cells and components at low temperatures.
- Investigate SEI and its impact on low temperature performance.
- Continue testing hard carbons, alternative cathode and electrolytes for use at low temperatures.

Selected Publications

Please see list at the end of this chapter.

III.C.1 Introduction

This subsection provides highlights and progress on understanding the factors that limit the low-temperature performance of high-power Li-ion cells and using this knowledge to identify methods of enhancing low-temperature performance, via cell material and component changes. The limitations include Li plating on the graphite negative electrode during low-temperature charging and a major loss of discharge power below -10°C. The later cannot be explained by the conductivity of the

electrolyte. Efforts this year involved further studies to thoroughly characterize these limitations in the gen 2 baseline cell chemistry, isolating the source(s) of these limitations, employing electrolyte modeling, evaluating alternative electrolyte salts and solvents, and developing a low-temperature cell transport model to study these phenomena.

Figure III-14 provides a schematic of how the activities in this focus area relate to each other, while Table III-8 provides a summary of how the participating DOE laboratories, together with the Army Research Laboratory, contribute to this focus area.

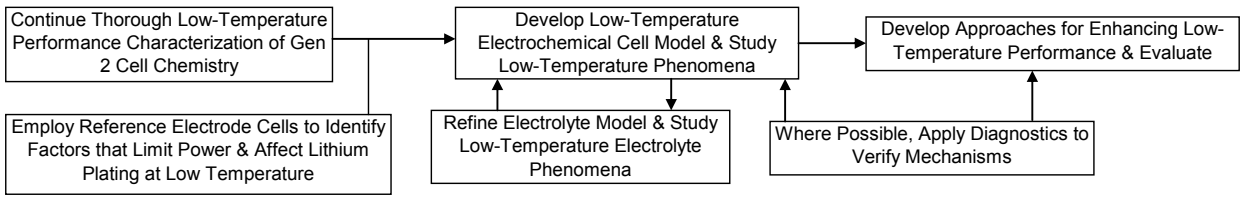

Figure III-14. Diagram of activities conducted under the "Low-Temperature Performance" focus area.

Table III-8. Summary of how the DOE laboratories and the Army Research Laboratory contribute to the "Low-Temperature Performance" focus area.

	ANL	ARL	BNL	INL	LBNL	SNL
Characterize gen 2 Cell Chemistry	X			X	X	
Reference Electrode Diagnostics	X					
Electrolyte Modeling				X		
Electrochemical Cell Modeling	X					
Evaluate Alternative Materials	X	X				

III.C.2 Low-Temperature Performance Characteristics

Lithium plating on the negative electrode during low temperature charge pulses creates serious limitations on the cycle life of Li-ion batteries. This deposited lithium reacts quickly with the electrolyte in an attempt to form a passivation layer (SEI). Unfortunately, this lithium consumption occurs on each cold cycle charge pulse, resulting in a steady capacity loss. One milestone this year was to investigate the propensity of various carbons/graphites to deposit lithium. Four carbon-based materials were selected that represent the major types used in the Li-ion industry: GMCF (a MELBLON milled fiber from pitch); MCMB-25 (a large spherical graphite bead); GDR-AA-3-3 (a carbon-coated natural graphite); and MAG-10 (a synthetic graphite – gen 2 negative). Hard carbon was investigated last year and was found to be unlikely to plate lithium because its potential is further from lithium potentials.

These four carbon electrodes were tested against the gen 2 positive electrode in gen 2 electrolyte at temperatures that varied between 30 and -30°C. The overall results were very similar for each cell system; the impedance increased significantly below 0°C and there is ample evidence to suggest that two Arrhenius regions exist over this wide temperature. One process dominates above 0°C and

another below 0°C. All four carbon electrodes exhibited possible lithium plating at -30°C not only during charge pulses, but also during the constant voltage charging. The MCMB-25 graphite cell did show greater impedance at low temperature as compared to the other carbon cells, probably due to its much smaller surface area.

Other types of materials were investigated for their low-T electrochemical performance, including a new class of copper-alloy anode material developed at ANL, namely, CuSn and CuSb. Several interesting observations were made from a comparison of the capacity data of these anode materials to that of the gen 2 Mag-10 graphite. Mag-10 graphite has higher lithium capacity than the copper-based alloys at 30°C, which is as expected based on a comparison of their theoretical capacity. However, below 0°C there is no advantage of one material over the other. This indicates that a mechanism that is more dominant than lithium diffusion in the active material is limiting the capacity (and power) at low temperature. Similar impedance rise at low temperature was found for another type of anode, $Li_4Ti_5O_{12}$. Even though these new types of anodes suffer at low temperature just like graphite systems, they are not as likely to plate lithium during charge because they operate at potentials further from lithium potentials. In addition, $Li_4Ti_5O_{12}$, CuSn and CuSb all exhibit strong voltage plateaus in their charge profiles, unlike hard carbon, which should prevent the positive electrode from drifting to higher potentials.

It has become fairly clear at this point that the choice of electrode material does not have a significant effect on the low temperature performance, although there is some evidence that particles with low surface area may suffer more at low temperature. The most likely reason for the poor low T performance is the interface between the electrode and electrolyte. (The reduced bulk ionic conductivity of the electrolyte at low temperature contributes to the power loss but is not as significant.) It is possible that the poor low T performance is inherent to the carbonate-based electrolyte system.

Efforts were directed to investigate other electrolyte properties such as viscosity and density at low temperature. These properties, shown in Figure III-15, were measured between 45 and -40°C. Density increased linearly from 45 and -40°C by only 8%. However, the viscosity increased by 1500% over this same temperature range. The influence of viscosity on electrochemical performance will be explored further in FY06.

Low temperature cell testing at INL included development of low-temperature testing protocols. Test cells included gen 2-based button cells (BC) and 18650-size cells. The aim of this work was to characterize low-T performance to gain insights into root-cause limitations and to quantify performance boundaries. INL focus areas for low-temperature testing included BC formation studies, differential capacity measurements, BC polarization studies, cold-crank studies, Special Reference Performance Test (SRPT), and an EIS-based study of interfacial phenomena. A summary of these efforts follows.

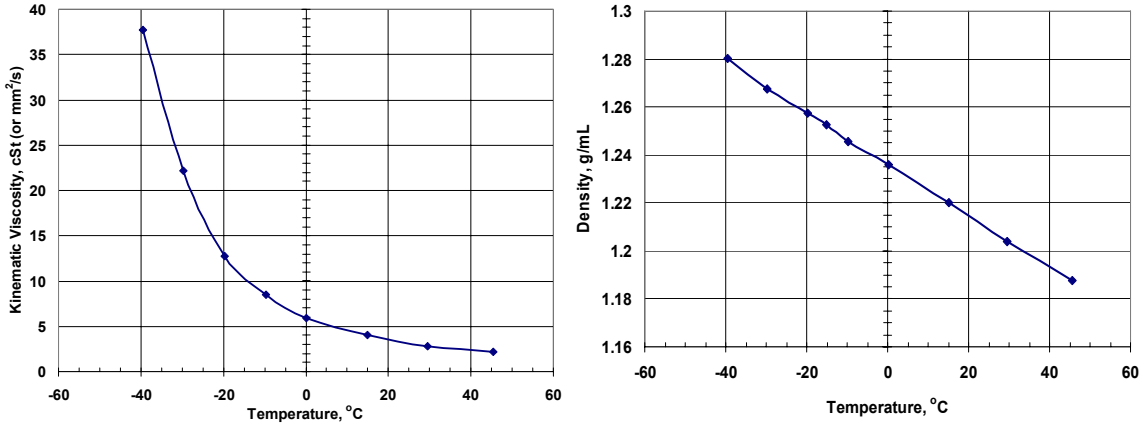

Figure III-15. Kinematic viscosity and density of 1.2M $LiPF_6$ in EC:EMC (3:7) over a wide range of temperature.

Some of the conclusions from recent studies on formation processing of button cells are that consistent formation methods produce good and consistent results but that quicker formation, which would greatly benefit large volume Li-ion battery manufacturers, can also work if well designed conditions are used; and finally that the choice of electrolyte chemistry is most important.

Differential capacity (Figure III-16) measurements have been used to show charge-limited behavior at colder temperatures. To investigate this further, BC polarization studies were performed on gen 2 chemistry which showed a considerable drop in capacity starting at –10°C for a C/1 rate and –20°C for C/3; below which charge-limited behavior is evident (Figure III-17).

An investigation into cold cranking has shown that fresh gen 2 cells meet the cold cranking power goal down to about –14°C, while aged cells can't meet goal below –4°C. A longer discharge pulse of 5-seconds causes an increase in R_O (yet a small decrease in R_P), and a net increase in cell impedance. Dropping V_{min} to 2.5V allows power goals to be met at slightly lower temperatures.

Finally, to investigate interfacial impedance, an EIS study of interfacial phenomena was undertaken. It has been found that interfacial impedance grows with aging, but the associated activation energy changes little with age or with SOC. One interpretation of this result is that the electrochemical nature of the SEI is largely unchanged with aging, but that it grows in thickness over time. A slight increase is seen in activation energies at colder temperatures (perhaps indicating an onset of phase transition). A plausible link has been established between lithium desolvation and the activation energy required for lithium transport through interfacial regions.

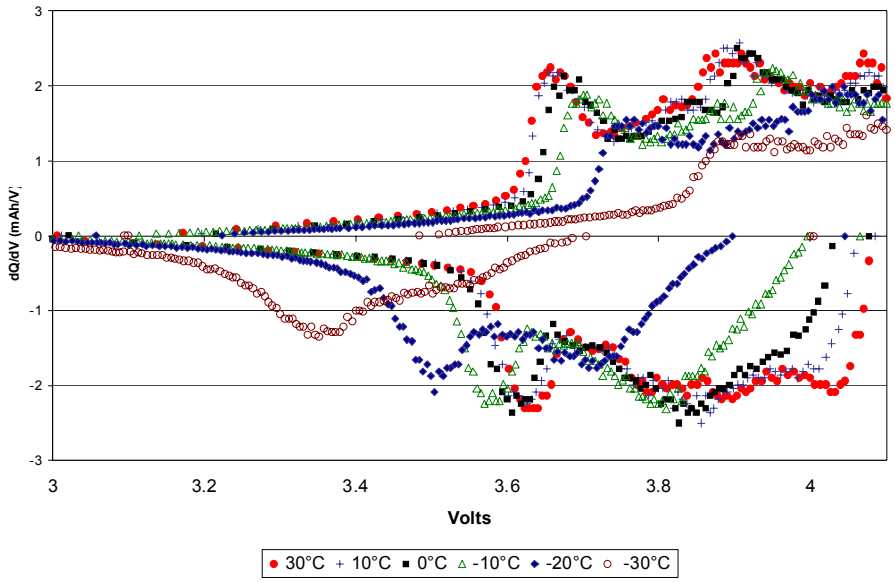

Figure III-16. Differential Capacity vs Temperature at C/10 Rate (gen 2 BC).

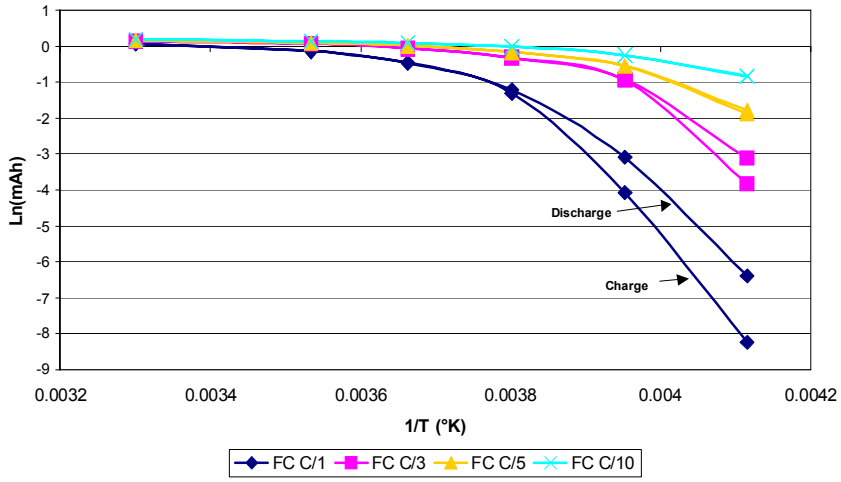

Figure III-17. Combined Charge/Discharge Polarization curves (gen 2 BCs, Formation Group C).

III.C.3 Low Temperature Electrolyte Modeling

The role of lithium ion desolvation in low-T battery performance was investigated utilizing key cell measurements and AEM tools (e.g., Li-STEP parameter). EIS measurements were obtained to gain insights on the role of the SEI in low-temperature performance loss in Li-ion cells, and trends seen in Nyquist semi-circle regions (interfacial impedance) support and confirm the AEM interpretation of the role of lithium desolvation in interfacial phenomena. This is seen by comparing Figure III-18 and Figure III-19. Figure III-18 shows Arrhenius plots of the EIS-derived Nyquist semicircle widths at various temperatures for the gen 2 electrolyte, and Figure III-19 shows Arrhenius plots of the isolated lithium desolvation component of the Li-STEP parameter for the same electrolyte. In Figure III-18, there is little difference in slopes between cells having high and low power fade, and

for cells at 60 and 100% SOC. This result supports the general notion that lithium desolvation is a ubiquitous barrier in Li-ion cells that requires approximately the same activation energy (E_a) regardless of the cell age or SOC, given a stable electrolyte chemistry. Regarding Figure III-19, Li-STEP activation energies account for about 40-50% of the net E_a observed from the EIS semi-circle analysis, suggesting that the activation energy tied to lithium transport through the SEI is markedly influenced by the lithium desolvation process.

- The AEM was used to provide data packages of predicted electrolyte properties (gen 2 and gen 3-type electrolytes) to ANL for use in the cell modeling work, see Section III.C.4.
- The AEM has been expanded to accommodate additional low-temperature electrolyte additives, based on discussions with Dr. Smart of JPL and others. These additives include the solvents ethyl propionate (EP), methyl butyrate (MB), n-propyl acetate (nPA), and 1,3-dioxolane (DIOX). The salt LiTFSI was also added to the AEM library.
- Large-Scale Simulations (LSS) for multi-solvent electrolytes were performed for EC-PC-DMC-$LiPF_6$, EC-γBL-EP-$LiPF_6$, EC-γBL-DMC-EP-$LiPF_6$, PC-γBL-DMC-DIOX-$LiPF_6$, EC-γBL-EA-LiBOB, and others. LSS are used to optimize the solvent proportions according to a chosen criterion (e.g., conductivity, diffusivity, or other parameter) over salt concentration and temperature. The optimized electrolyte formulations are good candidates for studies covering low temperature performance and cycling stability. Optimization of the system EC-γBL-EP-$LiPF_6$ is shown in Figure III-20 for two temperatures of interest.

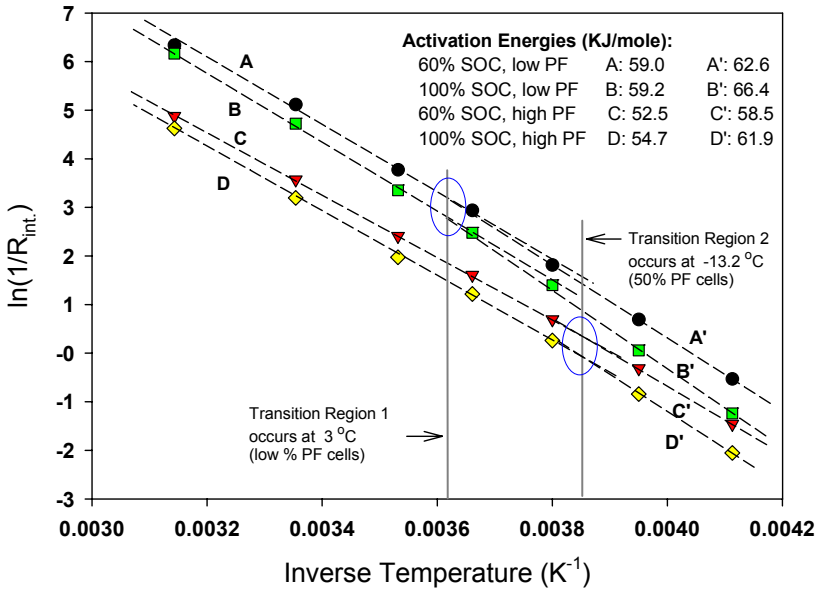

Figure III-18. Activation energy determination

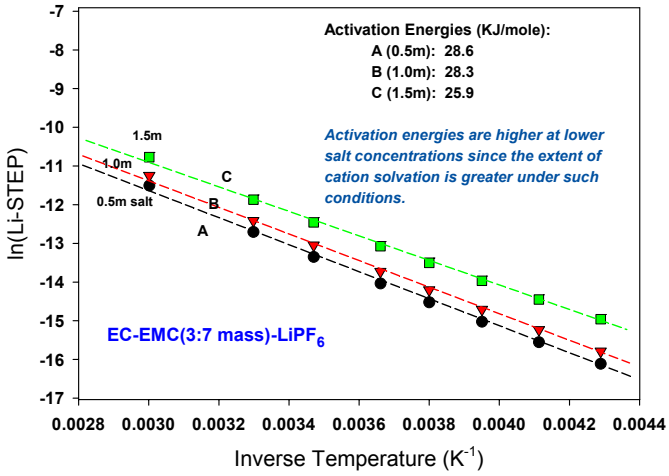

Figure III-19. Activation energies of the desolvation contribution to the LiSTEP parameter

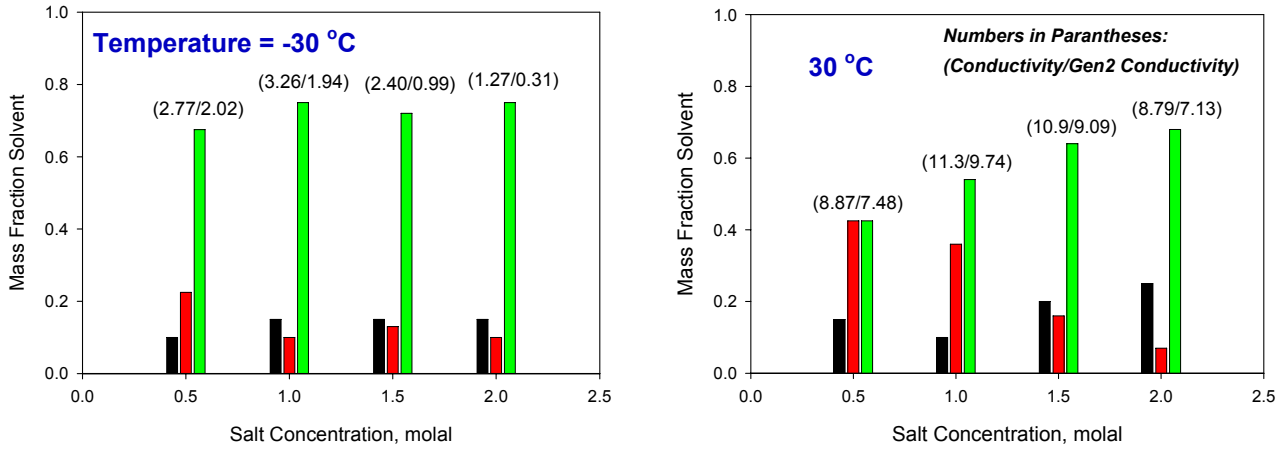

Figure III-20. Optimization results for EC-γBL-EP-$LiPF_6$

III.C.4 Low Temperature Cell Performance Modeling

The electrochemical cell modeling effort was expanded this year to examine the low temperature performance of Li-ion cells and determine the factors that contribute to the poor low-T performance of Li-ion cells. To accomplish this, the electrochemical model described in section III.B.4 was extended to low temperatures. Because of the significant data base, the initial efforts have focused on the gen 2 positive electrode. While not conclusive, the observed increase in impedance with a wide variety of electrode active materials suggests that the nature of the active material is not critical. Even with limiting initial work to the gen 2 positive electrode, determining the temperature dependence of all the model parameters was a rather daunting task. Fortunately, this effort has received support from K. Gering at INL who calculated the electrolyte parameters (see section III.C.3) and from A. Jansen at ANL who conducted experimental studies on the low-T electrochemical performance of gen 2 micro-reference electrode cells (see section III.C.2).

Dr. Gering, using the AEM, has supplied an extensive set of thermodynamic and transport parameters for the gen 2 electrolyte as a function of temperature and salt concentration. The parameters were fitted to analytical functions of salt concentration and temperature in order to utilize them in the electrochemical model. The AEM predictions agreed relatively well with room temperature experimental data taken at ANL and Illinois Institute of Technology (IIT). The greatest variations tended to occur at either very low or very high salt concentrations where only limited experimental data was obtained. Experimental studies of the salt diffusion coefficient as a function of temperature, conducted this year at ANL, also suggest that the predictions are within the error of the measurements.

The low-temperature AC impedance studies on gen 2 micro-reference electrode cells (see Figure III-21) were critical in the determination of the other parameters in the model. The increase in the high frequency intercept at low temperatures was important for more accurately establishing the separator tortuosity. This new higher tortuosity value was used to better define the electrolyte salt diffusional limitations and ultimately eliminated the need for assuming multiple oxide active material particle fractions. Besides the electrolyte parameters, most of the remaining parameters with significant temperature dependence were linked to SEI phenomena. The apparent changes with temperature of the interfacial impedance established the importance of the individual parameters and greatly simplified parameter determination. As an example, the data above 0°C was used to establish the diffusional parameters in the SEI. The exchange current density for the electrochemical reaction was then determined from the data below 0°C. It should also be noted that a much higher electrochemically active area for the oxide had to be used to match the long time-constant associated with the interfacial impedance below 0°C and to maintain a reasonable value for the double-layer capacitance. The electrochemical model simulation of the positive electrode for various temperatures with the new parameter set is given in Figure III-21.

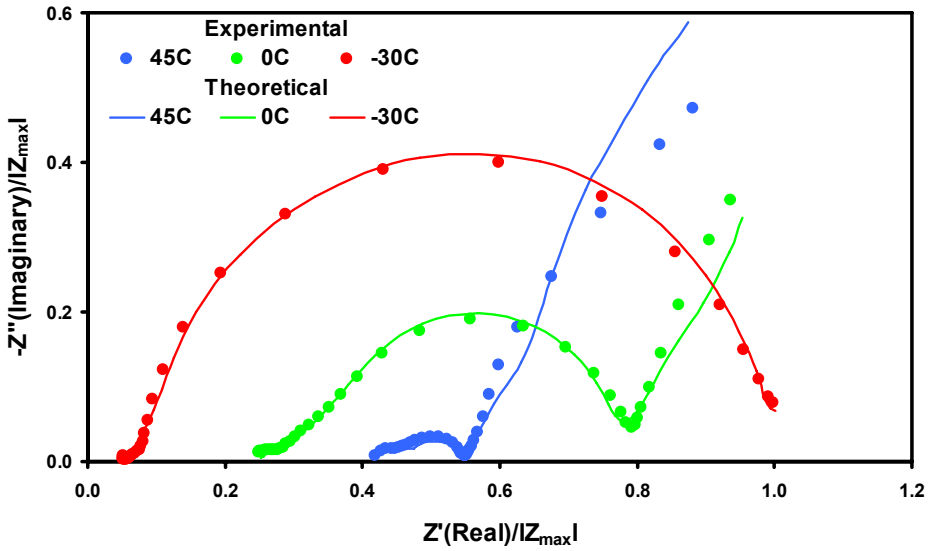

Figure III-21. Simulation of the experimental gen 2 positive electrode AC impedance at the indicated temperatures

As described above, creating a temperature dependent parameter set for the positive electrode required modification of all the SEI adjustable parameters. The new information gained from the low-temperature studies has had a particularly strong impact on the parameter set causing a review of the earlier conclusions concerning the aging of gen 2 positive electrodes (see Appendix H of the diagnostic report on gen 2 Li-ion cells[13]). The overall result of this reevaluation indicates that the general conclusions are still valid. However, the low-temperature studies have influenced a few specific observations concerning the degradation of interfacial properties. They have definitively established that order-of-magnitude parameter changes are possible with only subtle interfacial modifications. They have also confirmed that several phenomena combine to generate the total interfacial impedance at room temperature. Finally, the potential impact of a decrease in the lithium diffusion coefficient through the film on the oxide appears to be more significant than originally assumed.

The electrochemical model of the gen 2 positive electrode with the temperature dependent parameter set was used to examine the increase in impedance at low temperatures. The studies resulted in several important observations. First, bulk transport effects in the electrolyte and oxide active material are only a small part of the overall electrode impedance at low temperatures. Further, the oxide active material/electrolyte interfacial phenomena in the SEI limit the low-temperature performance. More specifically, diffusion of lithium ions through the interface accounts for a significant portion of this impedance and below 0°C electrochemical kinetics also has a major impact and is responsible for the change in slope in an Arrhenius plot of the electrode HPPC impedance. Finally the observed importance of interfacial phenomena, particularly kinetics, is consistent with Dr. Gering's theories on the impact of solvation.

[13] "Diagnostic Examination of Generation 2 Li-ion Cells and Assessment of Performance Degradation Mechanisms," D. Abraham editor, **ANL-05/21**

III.D Understand and Enhance Abuse Tolerance

Objectives

- Understand the role of each cell component in the abuse characteristics of high-power Li-Ion cells.
- Identify and develop more stable cell components that enhance the inherent abuse tolerance of Li-Ion cells.
- Validate inherent abuse tolerance enhancements at the cell level & quantify them.

Approach

- Establish role of each cell component on the thermal characteristics of the gen 2 cell chemistry.
- Using this information, identify alternative cell components and additives that possess the potential to enhance thermal abuse tolerance and evaluate their impact (mainly via DSC).
- Fabricate 110 mAh sealed prismatic cells and 18650 cells with the most promising cell components and additives to validate and quantify respective enhancements.
- Establish overcharge characteristics of gen 2 cells.
- Identify methods to enhance overcharge tolerance and evaluate in 18650 cells.

Accomplishments/Findings

- Developed mechanistic understanding of anode and cathode reactions that contribute and lead to thermal runaway.
- Identified more stable cathode materials and electrolyte additives that enhance inherent abuse tolerance in 18650 cells. Demonstrated that $Li_xNi_{1/3}Co_{1/3}Mn_{1/3}O_2$ cathode shows improved overcharge tolerance.
- Developed Li-ion thermal abuse model based on measured cell reactions.
- Used diagnostic analysis of abused cell materials at onset of thermal runaway to characterize electrode decomposition.
- The negative electrode showed the most change during cell heating. The SEI originally present on the graphite particles decomposed at the higher temperatures and was replaced by a surface film. Surface and near-surface regions of the graphite particles were damaged during cell heating.
- The positive electrode showed little change when the cell was heated to 150°C, except for the decomposition of organic films that were present on the electrode.
- Significant morphology changes were observed on the separator on cell heating. Polypropylene swelling and polyethylene melting at elevated temperatures contributed to shut-down of the separator pores.

Future Studies

- Component Level Studies
  - Continue evaluations of more stable cathode materials
  - Continue evaluations of electrolyte additives that form more stable SEI layers on the positive and negative electrode
  - Continue evaluations and development of electrolyte additives that enhance overcharge abuse tolerance

- Cell Level Studies
  - Determine the benefit of new additives in stable cathode cells.
  - Determine the benefit of shutdown separators on abuse tolerance.
  - Determine the effect of cell anode/cathode balance on abuse tolerance.
  - Develop database of quantitative thermal reaction parameters for cell components.
  - Develop Thermal Abuse Model to more accurately predict cell thermal response based on measured cell properties.
- Overcharge Response
  - Investigate structures of overcharged electrodes at regions of reaction and thermal runaway.
  - Determine effect of additives and alternative electrolytes on overcharge response and gas generation.
  - Measure effect of improved separators on overcharge response.
  - Investigate conductive polymers and redox shuttle additives as overcharge protection materials.

Selected Publications
Please see list at the end of this chapter.

III.D.1 Introduction

This subsection provides highlights and progress on understanding the factors that limit the inherent abuse tolerance of high-power Li-ion cell chemistries and using this knowledge to identify alternative materials and cell components that enhance their abuse tolerance. The cell chemistries used in conventional Li-ion cells are thermodynamically unstable. During the initial charge/discharge cycle, passivation films are formed on the active surfaces of the electrodes which stabilize the system. In the past, detailed studies were performed on the individual components of the gen 2 cell and the cell chemistry system was thoroughly studied in terms of its thermal and overcharge abuse characteristics. This year, studies were performed that further elucidated the reaction mechanisms at both the negative and the positive electrodes and information gained from these studies was used to identify cell materials and electrolyte additives that can help stabilize the cell chemistry and enhance its abuse tolerance. These inherent abuse tolerance enhancements were verified at the cell level using industry-coated electrodes in SNL-built 18650 cells. Also, an effort was initiated to model the abuse behavior of 18650 cells, employing different materials and cell chemistries, with the goal of predicting the behavior of full-size HEV cells.

Figure III-22 provides a schematic of how activities in this focus area relate to each other, while Table III-9 provides a summary of how the DOE laboratories contribute to this focus area.

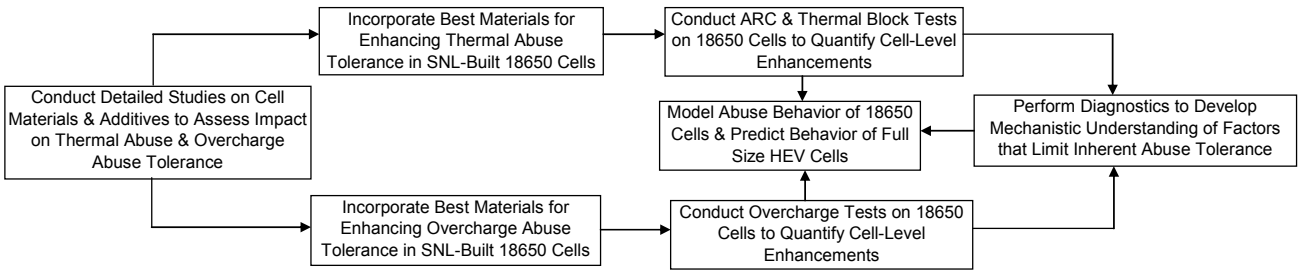

Figure III-22. Diagram of activities conducted under the "Abuse Tolerance" focus area.

Table III-9. Summary of DOE laboratory contributions to the "Abuse Tolerance" focus area.

	ANL	BNL	INL	LBNL	SNL
Secure Advanced Materials	X				
DSC and ARC on Advanced Materials	X				
ARC and Thermal Block Tests on 18650 Cells					X
Overcharge Tests with Advanced Materials	X				X
Diagnostics on Abused Cell Materials and Components	X	X		X	
Model 18650 Cell Behavior					X

III.D.2 Thermal Abuse

III.D.2.1 Thermal Abuse "Component Level Study"

This study was focused on trying to isolate the effect of the cathode and anode on the thermal behavior of the full cell. Therefore, the thermal signatures and reactivities between all components at the cathode and anode were investigated separately.

Thermal reactivity at the cathode - To clarify the impact of the cathode on the thermal behavior of the cell, ANL with SNL investigated the thermal behavior of 18650 cells having the same anode "GDR", the same electrolyte 1.2MLiPF6/EC:EMC (3:7) and different cathodes ($LiNi_{1/3}Co_{1/3}Mn_{1/3}O_2$ [NMC] and $LiNi_{0.8}Co_{0.15}Al_{0.05}O_2$ (NCA)). Figure III-23 shows the results of accelerated rate calorimetry (ARC) tests conducted on 18650 cells. The cell with NMC cathode shows much lower self heat with the onset temperature taking place at ~250°C. The NCA based cell, however, shows significantly more heat generation with the reaction taking place at 190°C. This result clearly shows that the cathode plays a significant role in the thermal behavior of the full cell.

In order to more precisely clarify the role of the cathode, the thermal and structural stability of the two cathode materials were studied after being subjected to a chemical delithiation using NO_2BF_4 oxidizer. This chemical oxidation process allows the removal of 60% of lithium which corresponds to charging these cathode materials to 4.3V.

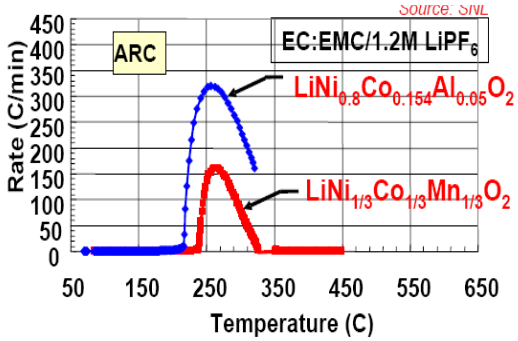

Figure III-23. ARC-test of 18650 cells having different cathode materials and similar anode and electrolyte.

Initial XRD of both $Li_{0.4}(Ni_{0.8}Co_{0.15}Al_{0.05})O_2$ and $Li_{0.4}(Ni_{1/3}Co_{1/3}Mn_{1/3})O_2$ materials shows that the layered structure remains intact and that these materials were not damaged by the oxidation process. One of the differences between $Li_{0.4}(Ni_{0.8}Co_{0.15}Al_{0.05})O_2$ and $Li_{0.4}(Ni_{1/3}Co_{1/3}Mn_{1/3})O_2$ is the degree of oxygen release during the heating process. It is speculated that the difference in the thermal behavior of these two materials is related to the amount of oxygen release from their delithiated phases. The O_2 released can oxidize the electrolyte causing a significant exothermic reaction. Figure III-24 shows the thermal gravimetric analysis (TGA) curve of $Li_{0.4}(Ni_{0.8}Co_{0.15}Al_{0.05})O_2$ and $Li_{0.4}(Ni_{1/3}Co_{1/3}Mn_{1/3})O_2$. As predicted, $Li_{0.4}(Ni_{1/3}Co_{1/3}Mn_{1/3})O_2$ material shows much less O_2 release (2wt%) than $Li_{0.4}(Ni_{0.8}Co_{0.15}Al_{0.05})O_2$ (11wt%) below 400°C . This is because of the stabilizing effect of Mn and Co in the NMC material which holds onto oxygen since these constituents do not change oxidation state during the oxidation process.

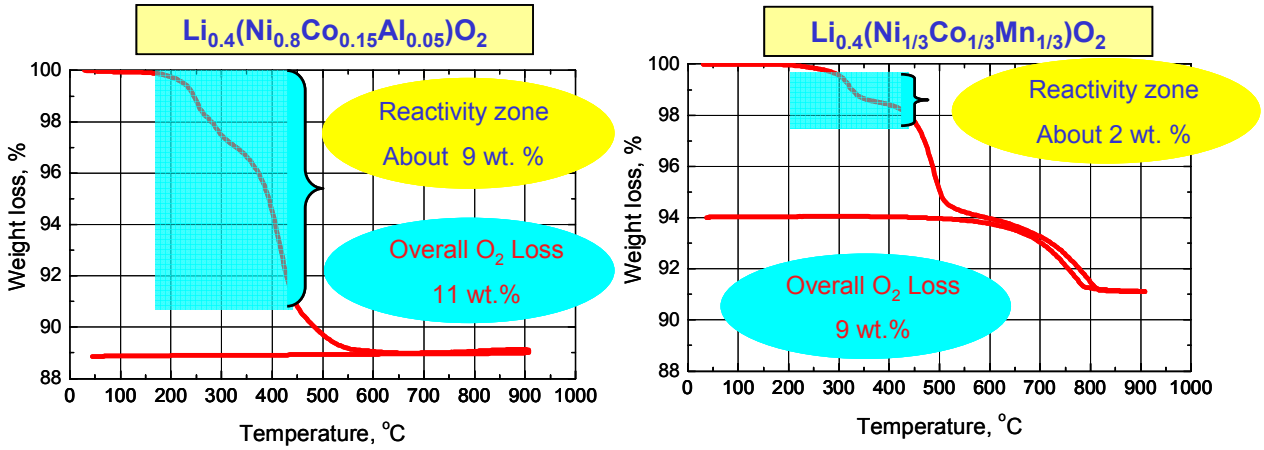

Figure III-24. Thermal gravimetric analysis (TGA), showing O_2 release from $Li_{0.4}(Ni_{0.8}Co_{0.15}Al_{0.05})O_2$ and $Li_{0.4}(Ni_{1/3}Co_{1/3}Mn_{1/3})O_2$

Figure III-25 compares the stability of $Li_{0.4}(Ni_{1/3}Co_{1/3}Mn_{1/3})O_2$ vs. $Li_{0.4}(Ni_{0.8}Co_{0.15}Al_{0.05})O_2$ during the heating process. While $Li_{0.4}(Ni_{1/3}Co_{1/3}Mn_{1/3})O_2$ material shows a quick decomposition and formation of NiO during the heating process, $Li_{0.4}(Ni_{1/3}Co_{1/3}Mn_{1/3})O_2$ shows a structural rearrangement and formation of a stable spinel phase with much less O_2 release.

Figure III-26 shows the DSC of chemically deliathed $Li_{0.4}(Ni_{0.8}Co_{0.15}Al_{0.05})O_2$ and $Li_{0.4}(Ni_{1/3}Co_{1/3}Mn_{1/3})O_2$ with and without electrolyte present. When the charged cathode alone was investigated by DSC without electrolyte, no reactivity was observed in either material. This result indicates that the thermal decomposition of these materials followed by oxygen release doesn't generate any heat by itself. However, when the electrolyte was added during the DSC study, a significant heat (ΔH =1270 J/g) was released from the reaction of $Li_{0.4}(Ni_{0.8}Co_{0.15}Al_{0.05})O_2$ with the electrolyte. However, much less heat was released from the reaction of $Li_{0.4}(Ni_{1/3}Co_{1/3}Mn_{1/3})O_2$ with the electrolyte (ΔH=670J/g) because of the smaller release of O_2. Also, one can notice that the temperature of the start of thermal signature in the DSC for $Li_{0.4}(Ni_{0.8}Co_{0.15}Al_{0.05})O_2$ was similar to that of the O_2 release from TG study (around 200°C). In the same manner, the temperature of the start of the thermal signature in TG and the temperature where O_2 is released from $Li_{0.4}(Ni_{1/3}Co_{1/3}Mn_{1/3})O_2$ is similar (around 250°C).

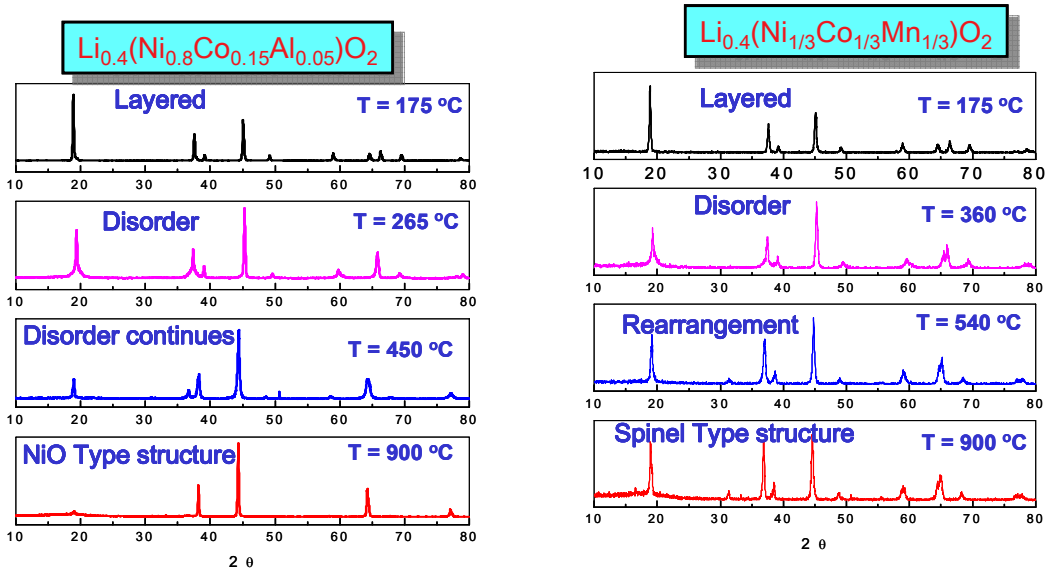

Figure III-25. XRD patterns of NCA and NMC during the heating process using TG study

Thermal reactivity at the anode - The thermal decomposition of the SEI film on the anode plays a critical role in the initiation of Li-ion thermal runaway. Therefore, an understanding of the primary and secondary SEI film formation and decomposition is important in developing new anode materials with improved safety and stability.

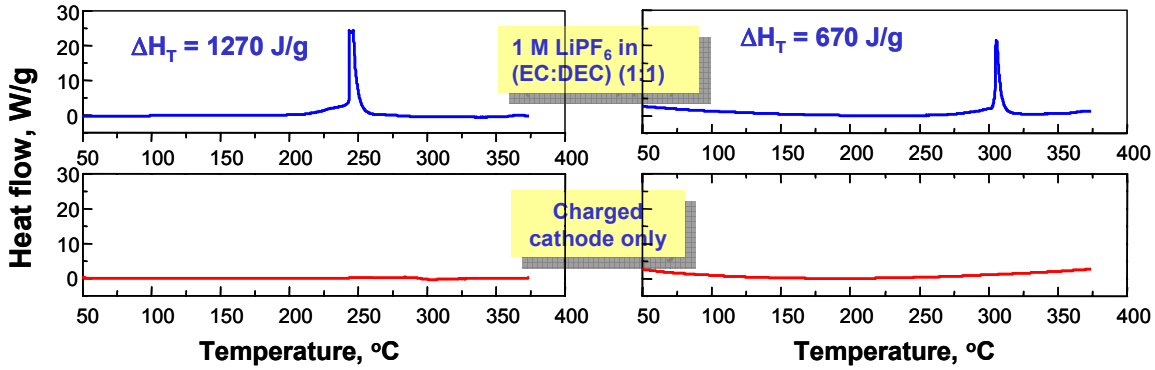

Figure III-26. DSC of $Li_{0.4}(Ni_{0.8}Co_{0.15}Al_{0.05})O_2$ and $Li_{0.4}(Ni_{1/3}Co_{1/3}Mn_{1/3})O_2$ powders in the presence and absence of the electrolyte.

Figure III-27 shows the DSC traces of Mag-10 anode intercalated with different amounts of lithium ions in the presence of electrolyte at a scan rate of 10°C/min. Only one exothermic peak (-70 J/g) at ~70°C is detected in the fully deintercalated sample (Li_0C_6). Since the electrolyte does not react until 250°C, that peak can be attributed to SEI (primary SEI) decomposition. No further reactions are detected at higher temperatures for fully deintercalated samples. However, as the degree of lithiation in the carbon increases ($Li_{0.18}C_6$, $Li_{0.37}C_6$, and $Li_{0.57}C_6$), a broad exothermic reaction peak is detected starting just after the primary SEI decomposition, and continuing to ~300°C. It has been concluded that the broad peak is due to the reaction between intercalated lithium and remaining salt and EC. This newly formed SEI film (secondary or progressive SEI film) decomposes as the temperature increases. This progressive reaction continues until the amount of lithium is reduced below the value at which the reaction can be measured.

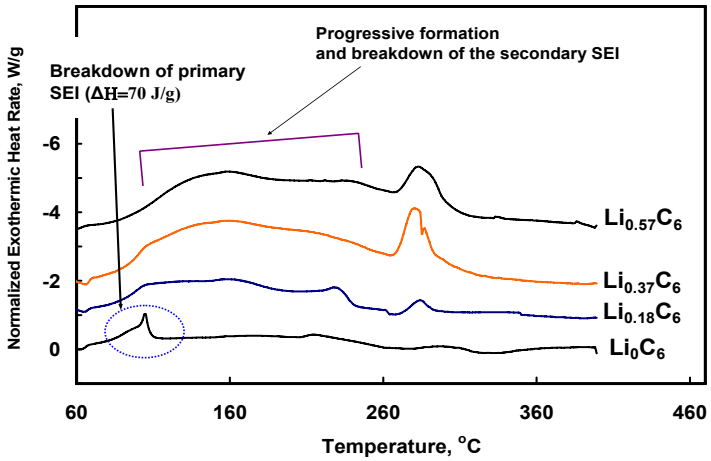

Figure III-27. DSC traces of intercalated Mag-10 anode at different of states of charge in the presence of electrolyte

The amount of heat generated as a result of the primary and secondary SEI film breakdown was calculated and normalized to the sample weight and BET area for MCMB 2528 and carbon fiber anodes. It was also observed that the morphology of the carbon anode influences the formation of primary and secondary SEI films as shown in Table III-10.

Table III-10. Thermal parameters of MCMB and Carbon Fiber anodes

	Overall Heat generation	**ΔH ; SEI** decomposition (80°C ~ 200°C) Normalized By sample	**ΔH ; SEI** decomposition (80°C ~ 200°C) Normalized By Area of sample	BET Area (m^2/g)
MCMB 2528	1552 J/g	507 J/g	429 J/m^2	1.18
Carbon Fiber	2151 J/g	1171 J/g	419 J/m^2	2.8

This program has found that certain additives in the electrolyte can modify the primary and secondary SEI film and thereby improve the thermal stability. The criteria for selection of additives are: 1) ability to form stable SEI, 2) wide potential window for electrochemical stability, and 3) acceptable solubility in alkyl carbonate organic solvents (EC, DMC, etc). Here are described the effects of vinylene carbonate (VC) and lithium bis(oxalato) borate (LiBOB) additives on the thermal stability of gen 2 and gen 3 electrodes. Figure III-28 (a) shows the DSC traces of three fully lithiated carbon fiber samples cycled with gen 2 electrolyte containing 0 wt%, 1 wt% and 2 wt% VC additives, respectively. It is clear from these figures that the onset temperature of the primary SEI decomposition increases, while the exothermic heat corresponding to the primary and secondary SEI decompositions decreases with increasing amount of VC additive. Figure III-28 also shows the accumulated heat flows during the primary SEI decomposition. These figures clearly indicate that higher VC concentrations results in improved thermal stability of the anode.

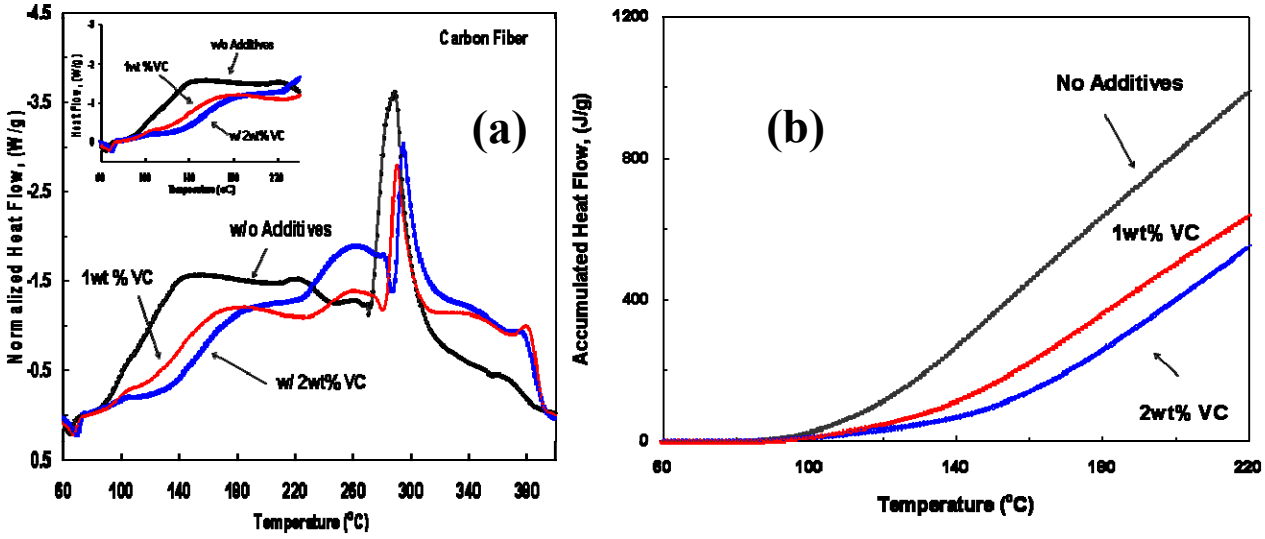

Figure III-28. (a) DSC traces of fully lithiated Carbon Fiber with different amounts of VC in the electrolyte and (b) Accumulated heat generation from DSC

The improved thermal stability of the anode in a VC containing electrolyte is likely due to two reasons. First, VC has a higher reduction potential than EC. Second, the reduction of VC forms some polymeric compounds on the anode particles surface, which are more thermally stable than compounds formed in the EC/EMC reduction.

Another additive, LiBOB, was evaluated in cells with MCMB-10 anode and gen 3 electrolyte (1.2 M $LiPF_6$ in EC+PC+DMC, 1:1:3 wt% ratio). A comparison of the LiBOB and VC additive on the thermal behavior of the gen 3 anode is shown in Figure III-29(a). It is evident from this figure that the incorporation of both LiBOB and VC additives show improved thermal stability. MCMB-10 with 1.0wt% LiBOB containing electrolyte significantly reduces the exothermic heat generation in the temperature range of 60°C to 200°C. Furthermore, the onset of SEI film breakdown is also delayed to higher temperatures. Figure III-29(b) shows the effectiveness of LiBOB in terms of reduced heat generation. However, the overall thermal behavior of the gen 3 anode depends on the type of additive incorporated in the electrolyte. For example, additive VC shows relatively lower heat generation compared to the LiBOB between 150 and 300°C. However, below 150°C, LiBOB shows reduced heat generation and also somewhat delayed exothermic reaction.

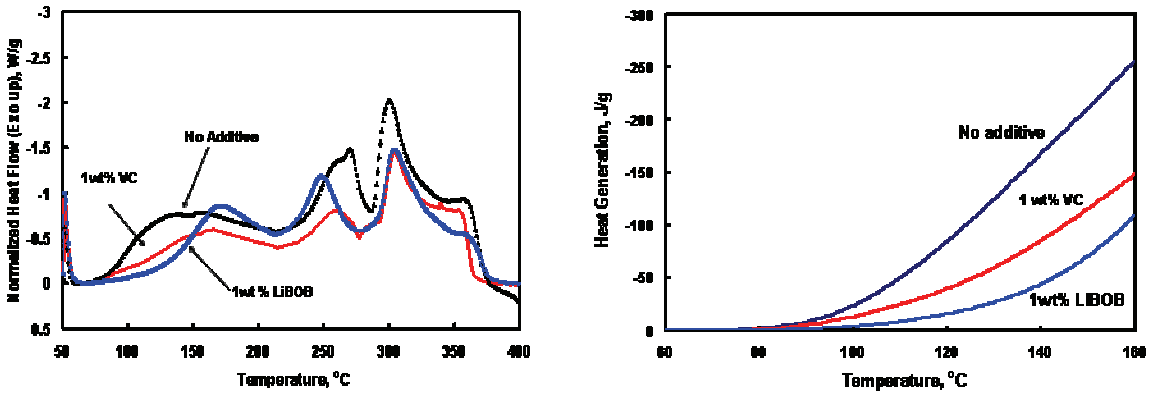

Figure III-29. A comparison of (a) DSC traces of fully lithiated MCMB-10 with different additives in Gen-3 electrolyte and (b) Accumulated heat generation

III.D.2.2 Cell-Level Studies

The thermal abuse program has concentrated on characterizing and demonstrating improved abuse tolerance in full cells based on new stable electrode materials and additives. Improved abuse tolerance in 18650 size cells (constructed at SNL) has been demonstrated using such methods as ARC and thermal ramp tests. New materials evaluated have included:

- Cathode – $LiNi_{0.8}Co_{0.15}Al_{0.05}O_2$; Anode – 6%GDR; EC:EMC/$LiPF_6$ (gen 2)
- Cathode – $LiNi_{1/3}Co_{1/3}Mn_{1/3}O_2$; Anode – 6%GDR; EC:PC:DMC
  - Salt effects: $LiPF_6$; LiBOB
  - Additives:
    - SEI enhancer – Vinyl ethylene carbonate (VEC)
    - Flame retardant – Phosphazene-based "Phoslyte B and C"
    - Perfluoro-compound SaFE-LYTE™
- Cathode – stabilized $LiMn_2O_4$ spinel; Anode – 6%GDR; EC:PC:DMC/$LiPF_6$
- Cathode – $Li_{1.1}Ni_{1/3}Co_{1/3}Mn_{1/3}O_2$; Anode – MCMB; EC:PC:DMC/$LiPF_6$

18650 cells with 900 mAh nominal capacities were built for abuse measurements. The thermal abuse response of these cells and the flammability of the vented gases were measured using a thermal

block apparatus developed at SNL that allows determination of the onset of cell heat generation and also records the flammability of the vented gases/electrolyte in the presence of an external ignition source. Cells were ramped in open air at a rate of 6˚C/min until thermal runaway.

Thermal Ramp Response/Flammability Study - The gen 2 baseline cells without additives showed self-generated heating beginning at 150°C with thermal runaway at 195°C. The vent gases ignited and burned for several seconds after runaway. The cell heating rate during the thermal ramp was calculated from the temperature difference between the cell and thermal block. The cell thermal response during forced thermal ramp was clearly divisible into three regions:

- low-rate onset region up to 140°C,
- acceleration region from 140°C -190°C
- final runaway region above 190°C.

The thermal ramp of a cell with the new $Li_{1.1}Ni_{1/3}Co_{1/3}Mn_{1/3}O_2$ cathode showed a lower self-generated heating rate at the 140°C onset temperature and the runaway temperature increased to 225°C. Cell venting was seen to be much more benign and low-rate compared to gen 2 baseline cells with no incidents of high-rate disassembly.

The thermal abuse tolerance of these cells was also improved using electrolyte additives. VEC was used to improve the protective SEI layer on the anode which delayed the onset of the anode reactions. Fire retardant additives not only reduced the flammability of the vent gases but can also help passivate the electrode surfaces. The effects of these additives (VEC/Phoslyte B, SaFE-LYTE^{TM}) are shown in Figure III-30. The thermal runaway temperature of cells with these two additives increased to 240°C and 250°C respectively. The flammability of the vapors was also reduced although the liquid electrolyte at the cell vent still burned at a low rate.

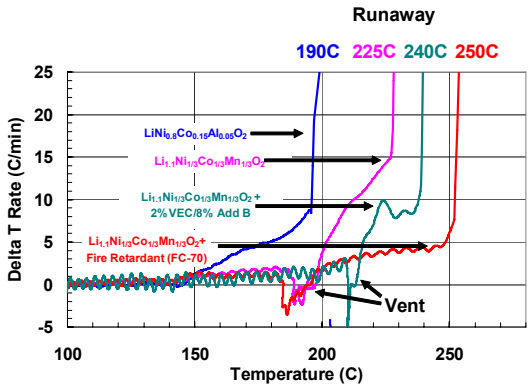

Figure III-30. Heating rates for new stable cathode materials and additives compared to gen 2 baseline 18650 cell during ramp to thermal runaway.

ARC Study - Cells with these materials were also evaluated for heat and gas generation using ARC (Figure III-31). The new $LiNi_{1/3}Co_{1/3}Mn_{1/3}O_2$ cathode material resulted in higher thermal runaway onset temperature, lower peak heating rate and reduced enthalpy of reaction. The $LiMn_2O_4$ spinel showed even more reduction in reactivity.

$LiPF_6$ salt has been known to react, producing PF_5, which can in turn result in degradation reactions including solvent decomposition. LiBOB salt does not produce this reaction product and thus was tested in cells with the Ni-based chemistry. It was found that LiBOB resulted in a 20°C-40°C lower thermal runaway onset temperature without a significant decrease in heat output and thus is not a suitable salt replacement for these types of cathodes.

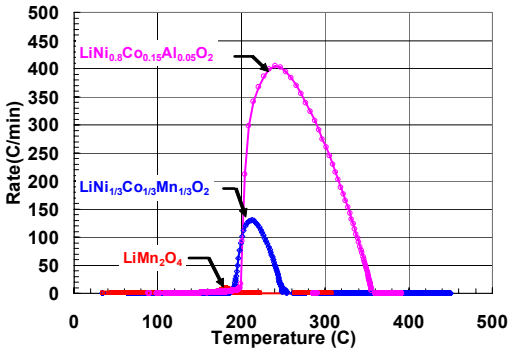

Figure III-31. ARC heating rates for different cathode materials compared to gen 2 baseline cell.

The relative contribution of the anode and cathode electrodes to thermal runaway was determined by disassembling a charged 18650 cell and re-sealing the individual electrodes/electrolyte in 18650 cans. ARC runs clearly showed the high-rate thermal runaway was dominated by the cathode. Figure III-32 shows that the heating rate profiles for a full cell and the cathode only cell were almost identical.

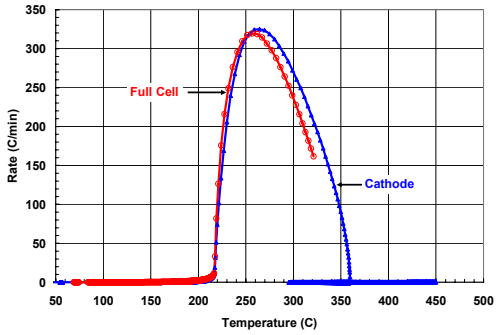

Figure III-32. ARC profiles of full 18650 cell and cell with only cathode/electrolyte.

The high-rate cathode reaction is believed to come from decomposition of the cathode with oxygen as a product which oxidizes the electrolyte at a high rate. TGA measurements of cathode materials have shown that the mass loss is a function of the degree of lithiation and is given by:

$$Li_y MO_2 \rightarrow (1+y)\, Li_{\frac{y}{1+y}}\, M_{\frac{1}{1+y}}\, O + \frac{1-y}{2} O_2$$

Solvent combustion from this cathode reaction gives 1.44 kJ/g in agreement with DSC measurements which have given 1.35-1.46 kJ/g.

Thermal Abuse Modeling - A thermal abuse model has been developed in collaboration with Battery Design Co. (Dr. Robert Spotnitz) as part of the Battery Design Studio® software. This model is based on detailed cell construction parameters and material properties to simulate the cell thermal response to ARC, DSC and thermal ramp. Experimental cell properties can be entered into the model or the program can determine these values as best fits to the reaction model chosen. Arrhenius-based thermal reaction terms are used with generalized reaction order expressions to model anode, cathode and electrolyte decomposition reactions. An example of a generalized cathode rate expression is (α is degree of conversion):

$$R = k \exp\left[\frac{-E_a}{RT}\right] \alpha_{pos}^{m} \left(1-\alpha_{pos}\right)^{n} \left[-\ln\left(1-\alpha_{pos}\right)\right]^{p} c_{solvent}^{r}$$

This model has simulated the measured DSC, thermal ramp and ARC runs using a consistent set of material reaction parameters. Initial attempts at fitting the cathode reaction clearly showed that a two-step reaction was involved: an initial Arrhenius-type surface reaction followed by the cathode decomposition/solvent combustion reaction. The sensitivity of this model to reaction parameters is shown in Figure III-33 for a DSC simulation and comparison to experimental data. The model can be used to determine these reaction parameters within a narrow range and then these values can be used to predict other cell thermal behavior. The simulation results for an ARC run are shown in Figure III-34 where a decomposition/combustion reaction for the cathode has been used. The model will be very useful for predicting larger cell performance using these values.

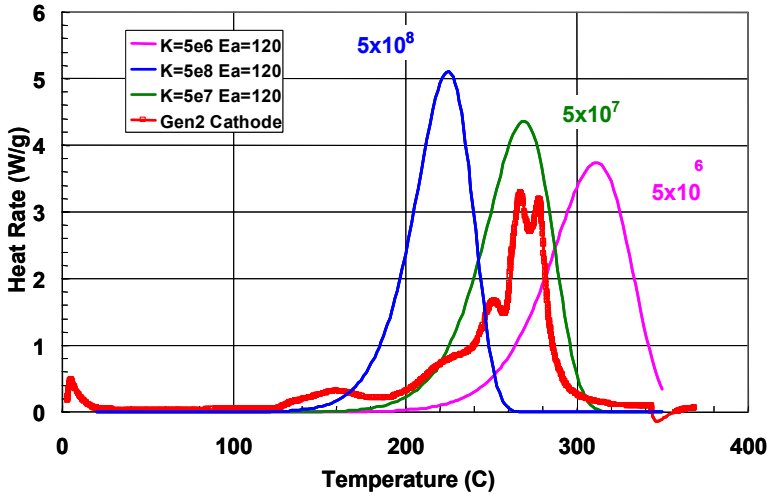

Figure III-33. Model simulation results compared with DSC data for cathode material.

SNL collaborated with ANL and LBNL in identifying surface decomposition products of thermally abused cells. Cells were quenched from an ARC run to the onset temperature of thermal runaway (150°C). The electrodes were removed for surface diagnostic analysis which revealed that the anodes had a thick coating of reaction products while the cathode had undergone little reaction.

III.D.3 Overcharge Abuse

The goal of this work is to determine the effects of electrochemical overcharge and thermal decomposition leading to cell thermal runaway. Overcharge studies have been performed using a custom apparatus designed to allow quantitative measurements of the heat generation of cells during overcharge and simultaneous real-time gas monitoring. ATD has previously demonstrated that high-rate overcharge can lead to thermal runaway. It has also been shown that, for extended overcharges at low rates, thermal runaway does not automatically occur for cells based on gen 2 materials as long as the cell temperature remains below the separator melt temperature of 135ºC.

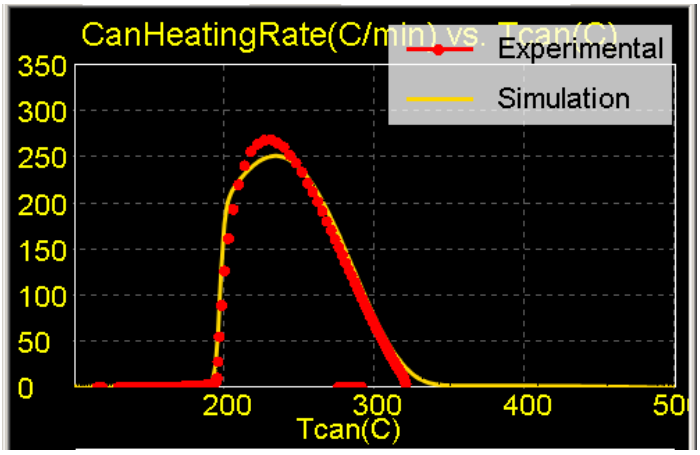

Figure III-34. Model simulation results of ARC cathode reaction in 18650 cell compared with measured ARC data of enclosed cathode/ electrolyte.

Overcharge of gen 2 cells with different anode carbons (flaky Mag10, spherical 6%GDR) were measured and compared. Figure III-35 shows that the voltage profile and heat outputs were nearly identical during overcharge. This shows that the overcharge thermal response is primarily a function of the cathode in these cathode limited cells.

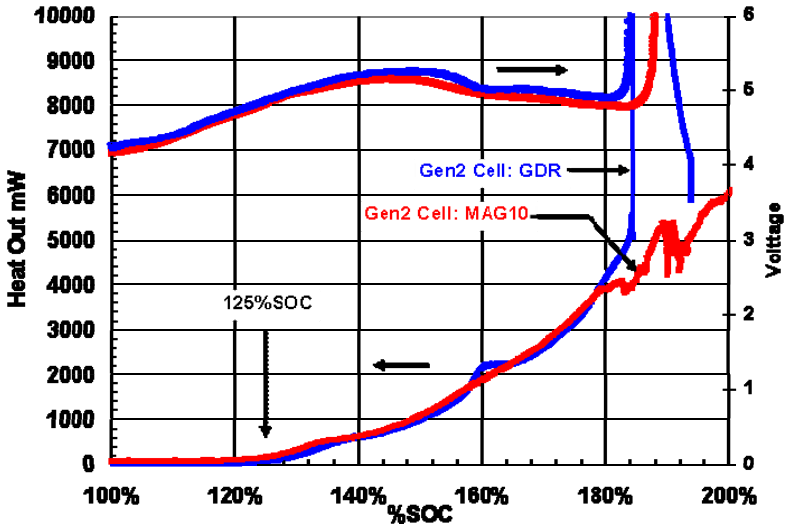

Figure III-35. Cell voltage and heat output for gen 2 cells with different anode carbons

Gen 2 cells show earlier onset of heat generation compared to $LiCoO_2$ cells, Figure III-36. The Li_xCoO_2 cells have a greater Li content at full charge (x=0.5) compared to gen 2 cathodes (x=0.38) and can be overcharged to greater extent before complete delithiation. However, both cathodes showed increased heat output at x=0.2.

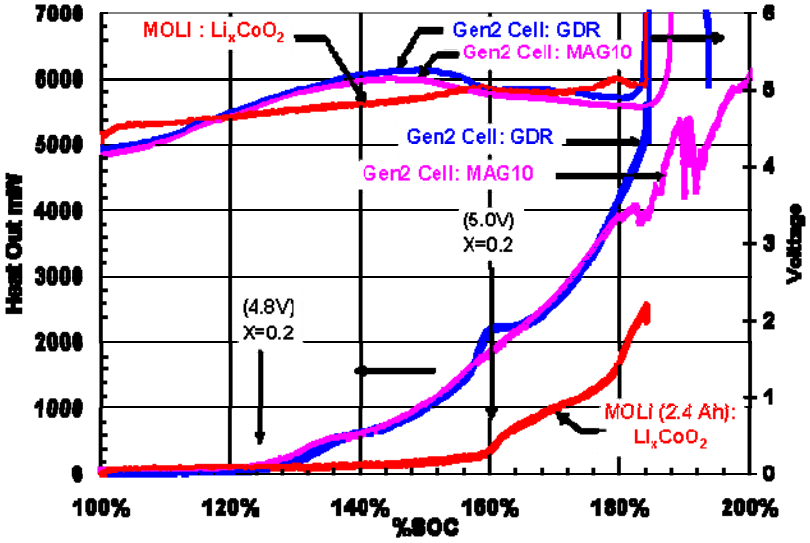

Figure III-36. Comparison of overcharge response of gen 2 cells with a $LiCoO_2$ cell

The program has begun characterization of cells with the new $LiNi_{1/3}Co_{1/3}Mn_{1/3}O_2$ cathodes. These cells have shown improved overcharge abuse tolerance. Gen 2 cells show increased heat generation at 125% SOC while the new cathode material does not show increased heat output until above 150% SOC. Figure III-37 shows a comparison of cells with this cathode, gen 2 baseline cathode and a $LiCoO_2$ material.

These new cathode cells went into thermal runaway during 1 C-rate overcharge. Runaway was immediately preceded by a sharp increase in voltage across the cell which resulted from separator shutdown. The cell skin temperature was measured as 120°C which corresponded to an internal temperature of 130°C, the temperature of polyethylene separator melt.

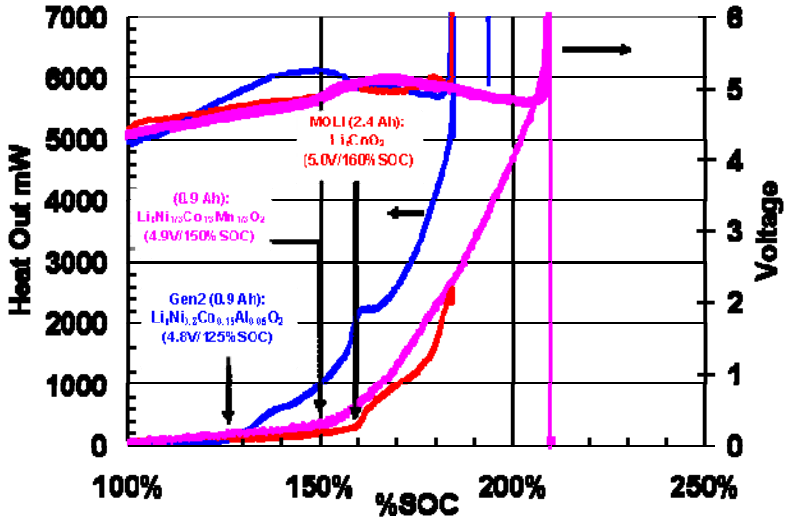

Figure III-37. Overcharge cell voltages and heat outputs for different cathode compositions

Gas evolution was monitored in real time using mass spectrometry (MS) and FTIR. Immediately preceding and during thermal runaway a large increase in hydrogen was monitored (Figure III-38) along with other gases including CO, CO_2, methane, oxygen and solvent vapors. In flowing nitrogen, no combustion of the gases was observed due to insufficient oxygen generation by the cell. This same overcharge performed in air resulted in a violent combustion of these vent gases.

Thermal runaway in overcharged cells has been closely associated with separator shutdown and the cell potential which can be high when cells are connected in series. High voltage separator breakdown was measured using an apparatus that allowed monitoring of current at increasing temperatures and applied potentials. Separator breakdown did not occur immediately after shutdown at 130°C (2 hrs) nor above the upper cell integrity limit of 160°C (7 min). Figure III-39 shows the breakdown profile immediately above the shutdown temperature. Thermal runaway at temperatures that result in separator shutdown does not result from physical breakdown of separator and shorting of the cell.

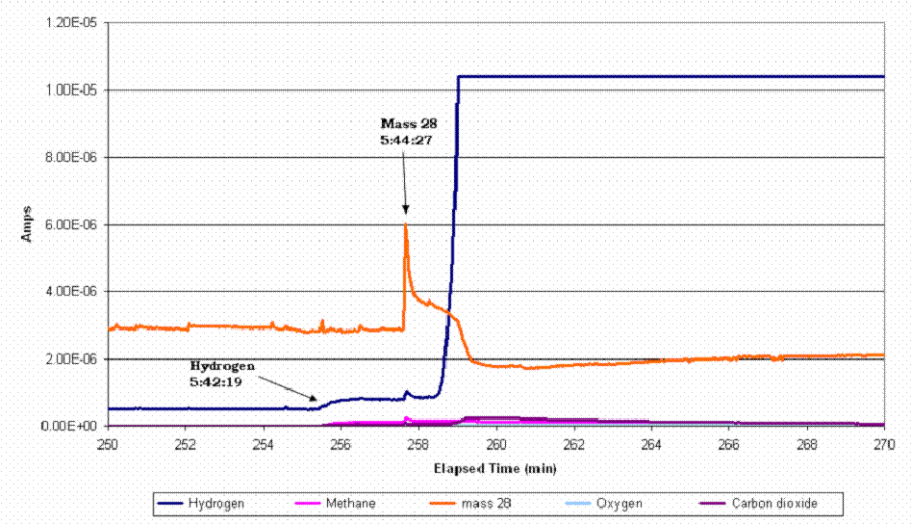

Figure III-38. Gas generation preceding and during overcharge thermal runaway

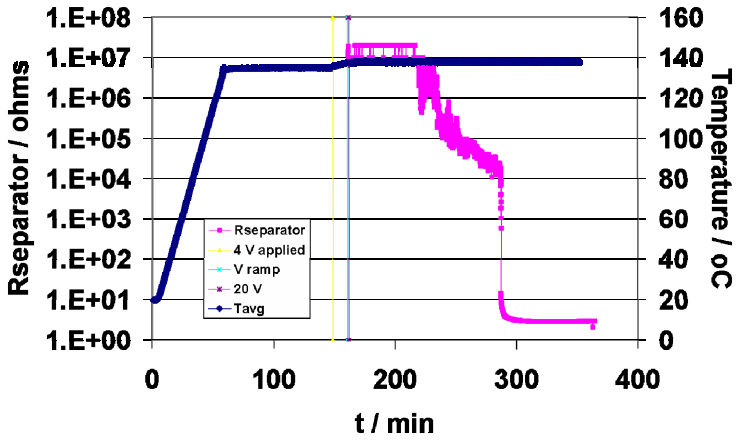

Figure III-39. High-voltage breakdown of separator above shutdown temperature

III.D.4 Diagnostic Examination

III.D.4.1 In-situ X-ray studies

Using time resolved XRD, the thermal decomposition of gen 2 cathode materials, in comparison with $Li_{1-x}Ni_{1/2}Mn_{1/2}O_2$ and $Li_{1-x}Ni_{1/3}Co_{1/3}Mn_{1/3}O_2$ cathodes at different charged states, were studied during heating from 25 ºC to 450 ºC with and without the presence of electrolyte. Comparing the XRD spectra plotted in Figure III-40, it can be seen that the decomposition temperature is about 245ºC for the $Li_{0.33}Co_{1/3}Ni_{1/3}Mn_{1/3}O_2$ at 100% SOC. This temperature is about 200°C for the gen 2 ($Li_{0.33}Ni_{0.8}Co_{0.15}Al_{0.05}O_2$) cathode at the same SOC. These results provide clear correlation between the thermal stability and the structural changes of the cathode materials when heated to high temperatures.

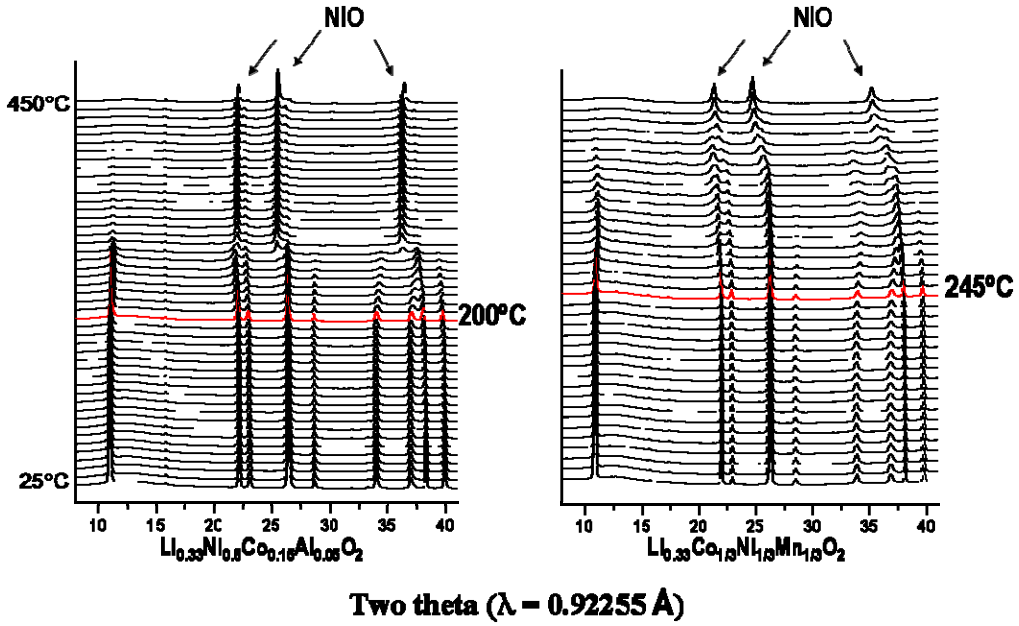

Figure III-40. Time resolved XRD spectra for gen 2 and the 1/3 cathodes heated from 25°C to 450°C with electrolyte.

As shown previously, the presence of electrolyte can significantly accelerate the thermal decomposition of the cathode material. Thus, it is important to determine if a surface coating can improve thermal stability by isolating the cathode material from electrolyte. Figure III-41 shows the time resolved XRD spectra of MgO coated $LiNi_{1-x}Co_xO_2$ cathode during heating compared with uncoated material under the same conditions. The thermal decomposition of the coated cathode starts at significantly higher temperatures. In addition, the decomposition process in the coated cathode was much slower than the uncoated one. At 450°C, in the uncoated cathode, the decomposition products of NiO and metallic Ni were clearly observed, while these compounds were not observed in the coated cathode. These data demonstrate that thermal stability can be significantly improved by surface coating the cathode materials or by modifying the electrolytes.

Soft (200 eV to 1000 eV) XAS at the O K-edge and the metal $L_{\alpha,\beta}$-edges, in both the fluorescence yield (FY) and the partial electron yield (PEY) mode, has been used to probe the electronic structure of gen 2 and $Li_{1-x}Co_{1/3}Ni_{1/3}Mn_{1/3}O_2$ materials at various charged and over-charged states. By using the surface sensitive PEY detection mode together with the bulk probing FY detection mode simultaneously, the differences between the electronic structures at the surface and in the bulk were studied. The oxygen K-edge XAS of gen 2 cathode at various charged and over-charged states are plotted in Figure III-42. In the uncharged state Ni^{3+} is observed in the FY data; there is no signature of Ni^{2+} bonded oxygen. On overcharge to 5.2V, the Ni^{3+} converts to the unstable Ni^{4+}, which has a higher propensity for oxygen loss. In the PEY mode a clear peak representing Ni^{2+} bonded oxygen ions is observed for the uncharged sample. On overcharge to 5.2V, the peak representing the Ni^{2+} bonded oxygen showed higher intensity than the lower charged states, even higher than the initial intensity for the uncharged state. This increase in Ni^{2+} results from the loss of surface oxygen from the gen 2 oxide, thus indicating the severe instability of the overcharged oxide.

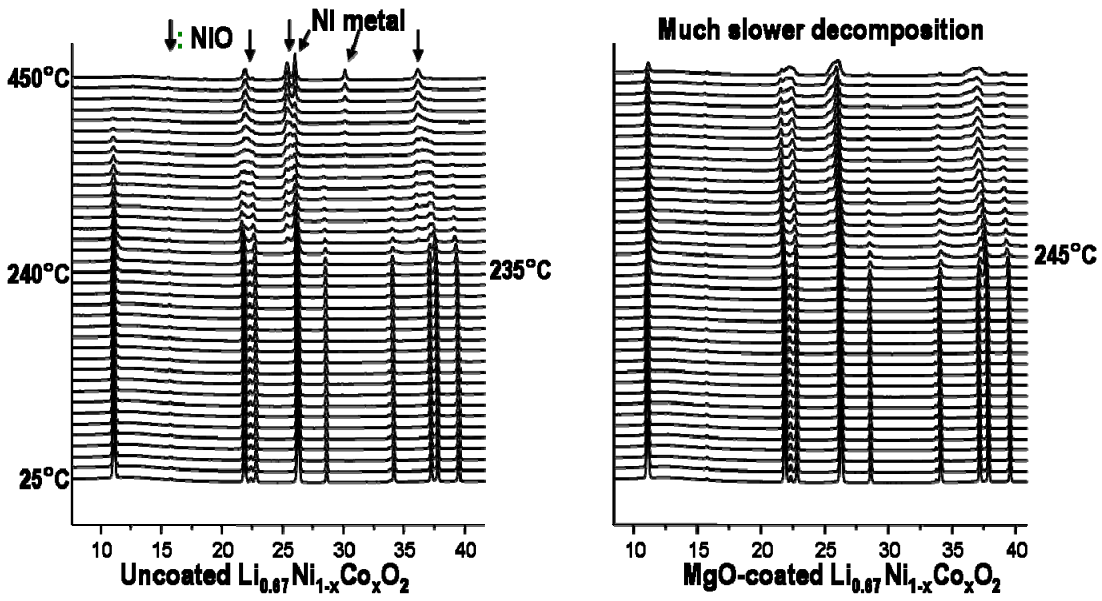

Figure III-41. Time resolved XRD spectra for uncoated $Li_{0.67}Ni_{1-x}Co_xO_2$, and MgO coated

III.D.4.2 Ex-situ examination of components from thermally abused 18650 cells

In an effort to decipher the sequence of events leading to thermal runaway, components from 18650-cells that were heated to 150° and 160°C were examined. The cells were heated in an ARC, then air-quenched to room-temperature to preserve thermal history. The quenched cell was transferred to an Argon glove box for disassembly. Electrode and separator samples from the still-charged cell were removed, sealed in hermetic containers and transferred for diagnostic study.

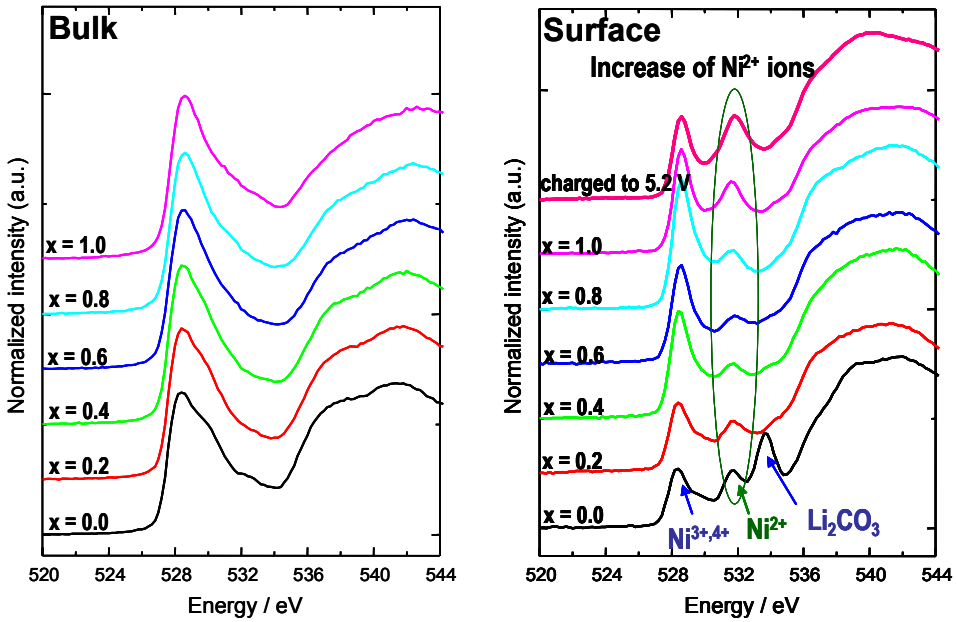

Figure III-42. Oxygen K-edge XAS spectra gen 2 cathode at various charged and over-charged states

A representative SEM image from the 150°C cell negative electrode sample is shown in Figure III-43. It is apparent that the graphite surfaces are covered by a thick layer of products that results either from electrolyte decomposition and/or from reaction of Li with the electrolyte. The PVdF binder that holds graphite particles together showed a distinctly different morphology after heating: the binder probably melted on heating and then solidified when the cell was quenched to room temperature. XRD patterns from the abused cell samples were very similar to that of the Mag-10 graphite: there was no indication of amorphization within the graphite bulk. In addition, peaks that arise from LiC_x compounds formed during graphite-lithiation were not observed. The absence of LiC_x peaks suggests that the Li diffused out and reacted with the electrolyte at the graphite surface during cell heating, as previously speculated.

Evidence for the presence of new compounds on the negative electrode sample surfaces was obtained by Raman spectroscopy and X-ray photoelectron spectroscopy (XPS). In the Raman data the graphite D and G bands were completely obscured by signals from a thick and uniform surface film. The data were consistent with the presence of organophosphates in the surface film: peaks corresponding to Li_2CO_3 were not observed. Evidence for LiF, Li_2O, Li_xPF_y, and Li-bearing alkyl fluorophosphates compounds was observed in the XPS data. In addition to surface film compounds, the Raman data also indicated that the surface and near-surface regions of the graphite particles were damaged during cell heating. This local graphite degradation/exfoliation probably results from the violent deintercalation of lithium ions from the graphite at elevated temperatures.

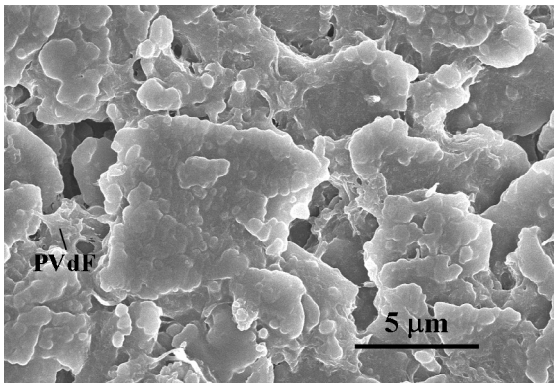

Figure III-43. SEM image of negative electrode sample from cell that was heated to 150°C

For the positive electrode, XRD data from the 150°C cell sample showed peaks that were typical of delithiated $LiNi_{0.8}Co_{0.15}Al_{0.05}O_2$; there was no evidence for oxygen loss from the sample. Similar conclusions were derived from a Raman data of the sample. However, XRD and EDS data showed evidence for a small amount of oxygen loss in the 160°C cell sample. In addition, enhanced primary particle separation observed in SEM images suggested pressure buildup within the electrode. Examination of the Al current collector showed no indication of enhanced pit formation that could have resulted from the higher test temperature. Raman study of the positive electrode showed no spectral signature of any surface film species. However, the XPS data showed the presence of inorganic compounds on the electrode surface, such as LiF, Li_xPF_y and $Li_xPO_yF_z$.

III.E Cell-Level Cost Reduction

Objectives

- Identify and secure advanced low-cost cell materials from international material suppliers and evaluate samples for high-power HEV applications.
- Develop lower-cost high-power cell chemistries — using the most promising materials — and conduct preliminary performance, life, and safety evaluations to establish their viability.
- Explore novel approaches for reducing the cost of cell packaging.

Approach

- Refine rapid screening test protocols to assess the suitability of novel materials. Employ protocols to evaluate material capabilities, provide feedback to the material suppliers.
- Produce cells from the most promising low-cost materials and conduct preliminary evaluations on their performance, life, and safety characteristics, using sealed prismatic cells.
- Thoroughly examine aged/tested cells for adhesion, wetting, and gassing problems.
- Develop a new flexible pouch design that limits permeation of electrolyte and moisture.
- Develop a new class of organoclay nanocomposite materials that improve the sealant layer barrier properties and the adhesion of the sealant layer to the aluminum foil layer.

Accomplishments/Findings

- Established and maintained contacts with material suppliers in Japan, Korea, and Europe.
- Obtained samples of advanced natural and synthetic graphite materials, advanced layered and 3D spinel cathode materials, electrolyte salts, separators, and binder materials for evaluation.
- Conducted screening tests on advanced materials and provided feedback to suppliers.
- Determined that cost savings associated with flexible packaging does not appear to offset the increased risk of reducing the cell life.

Future Studies

- Solicit samples of separator materials from industrial firms that are developing low-cost separators under the FreedomCAR and Fuel Partnership.
- Continue conducting screening tests of new materials and providing feedback to the suppliers.
- Evaluate Mn spinel/Li titanate cells for application in high power HEV batteries.
- Evaluate Li iron phosphate as a low cost, abuse tolerant cathode material.

III.E.1 Introduction

This subsection provides highlights and progress on cell-level cost reductions. Since the beginning of this program, researchers have been searching for lower cost cell materials and components that possess enhanced stability. These cell materials include: electrode active materials, conductive additives for the positive electrode, electrode binders, electrolyte salts, electrolyte solvents, and electrolyte additives. Where it makes sense to do so, a limited amount of internal R&D is performed to develop more stable materials (primarily in terms of electrolyte components and positive electrode materials). Also, the program has been studying the use of flexible cell packaging as a means of reducing the cost of cell containment. In this connection, some internal R&D has been conducted on

the development of suitable new organoclay nanocomposite technology that offered promise for significantly enhancing the oxygen, moisture, and electrolyte vapor barrier properties of conventional polymer films used for flexible packaging. All of these activities were continued during the last year.

Figure III-44 provides a schematic of how activities in this focus area relate to each other, while Table III-11 provides a summary of how the DOE laboratories contribute to this focus area.

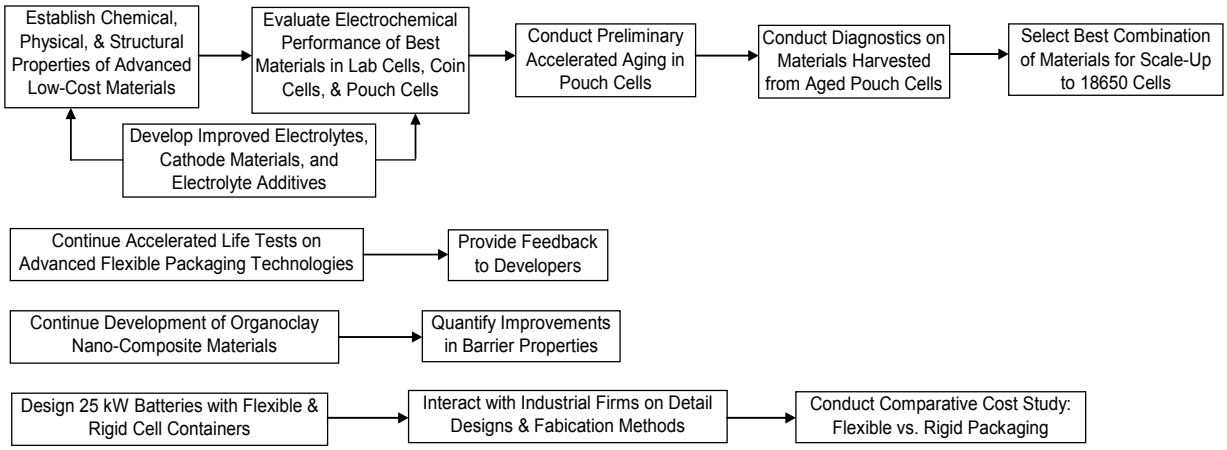

Figure III-44. Diagram of related activities conducted under the "Cost Reduction" focus area.

Table III-11. Summary of how the DOE laboratories contribute to the "Cost Reduction" focus area.

	ANL	BNL	INL	LBNL	SNL
Secure and Evaluate Advanced Materials	X				
Develop Electrode and Electrolyte Materials	X		X		
Preliminary Accelerated Aging Studies	X				
Cell Component Diagnostics	X	X		X	
Accelerated Aging of Flexible Pouch Technologies	X				
Develop Optimal Organoclay Technology	X				
Produce and Evaluate Organoclay Films	X				
Assess Cost Relative to Rigid Packaging	X				

III.E.2 Material Screening and Development

In this section is reported the performance of three promising systems for HEV applications based on spinel manganese oxide, $Li_{1+x}Ni_{1/3}Co_{1/3}Mn_{1/3}O_2$ and carbon coated olivine (C-$LiFePO_4$).

1. The lithium manganese oxide spinel cathode material - Lithium manganese oxide spinels are very attractive cathode materials for high power applications; they have excellent rate capability, and could offer lower cost, and better safety characteristics than the nickel system. However, it is known that graphite/$Li_{1-x}Mn_2O_4$ cells suffer significant capacity fade and impedance rise at and above 55°C. This capacity fade is generally attributed to Mn dissolution from the spinel cathode induced by HF in the electrolyte. Once the Mn^{2+} ions are dissolved in the electrolyte, they migrate to the carbon

anode and reduce to active metallic manganese at the surface of the carbon. The manganese metal appears to play a catalytic role in poisoning the carbon SEI layer leading to high interfacial impedance. Therefore, one promising way to address the instability of the $LiMn_2O_4$/graphite system is to replace the $LiPF_6$ that generates strong acids such as HF during the hydrolysis process. This program has been investigating two salts (LiBoB and perfluoroborane cluster salts ($Li_2B_{12}F_xH_{12-x}$)), that offer the possibility of increasing the calendar life of the spinel at high temperature.

In the present work, manganese dissolution was significantly reduced and the cycling performance of the spinel system was improved through the use of LiBoB. Also, the rise of impedance with aging at high temperature was reduced. However, after extensive cycling of the spinel/graphite cell with LiBoB at 55°C, significant swelling of the pouch cell took place which led, in some case, to cell venting. The analysis of the gas using GC-MS showed a significant amount of CO_2, perhaps due to the oxidation of the oxalate site of the LiBoB salt from the oxygen released by the delithiated cathode. As a result of this, electrolytes based on LiBoB as a main salt in the electrolyte may not be suitable for Li-ion batteries. However, since LiBoB generates a stable passivation film, it could be still used as an additive in $LiPF_6$ based electrolytes.

The ATD program, in close collaboration with Air Products, has also been investigating a new class of salts based on weakly coordinating perfluoroborane cluster salts, e.g. lithium fluorododecaborates ($Li_2B_{12}F_xH_{12-x}$). An initial investigation of spinel $LiMn_2O_4$/graphite using 0.4M $Li_2B_{12}F_xH_{12-x}$ /EC:EMC shows that the cell exhibits excellent cycle life up to 100 cycles at 55°C (see Figure III-45) with no capacity fade. As a reference, the cell based on the same system using $LiPF_6$ based electrolyte shows significant capacity loss at 55°C.

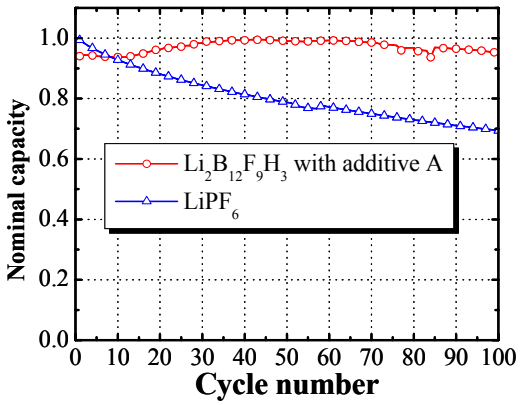

Figure III-45. Comparison of cycle life of $LiPF_6$ and $Li_2B_{12}F_9H_3$ based electrolytes in a graphite/MN spinel cell.

In addition to their function as lithium electrolytes, these salts are able to function as tunable redox shuttles. The electrolyte's unique oxidation chemistry provides inherent protection against overcharge, an important safety issue for lithium batteries. This overcharge protection is shown as a reversible redox peak with a tunable oxidation onset potential around 4.5 V vs. Li/Li^+ (Figure III-46). The redox potential is tunable by controlling the degree of fluorination in the fluoro-dodecaborate anion, i.e. lower fluorination provides a lower overcharge voltage.

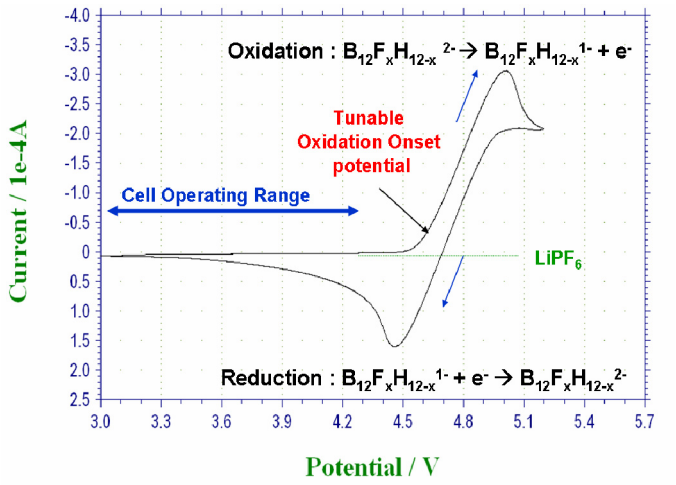

Figure III-46. Cyclic voltammetry of $Li_2B_{12}F_xH_{12-x}$ in 3:7 EC:DEC (Pt working) showing the overcharge redox shuttle in comparison to $LiPF_6$

The 1C overcharge cycling behavior for a GDR negative and gen 2 positive electrode with the partially fluorinated $Li_2B_{12}F_9H_3$ and $LiPF_6$ in 3:7 EC:DEC is shown in Figure III-47. The cell exhibits stable voltage plateaus at ~4.5 V for almost 100 hours under overcharge with negligible capacity fade. Extended overcharge protection at 1C to 2C-rates has been observed, and significantly higher rates appear obtainable over shorter periods of time. The electrolyte also provides overcharge protection for other cathodes including spinel and olivine based materials.

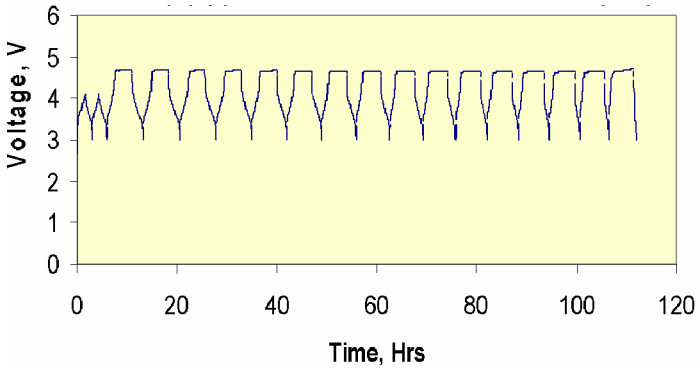

Figure III-47. Overcharge cycling behavior for a GDR anode and gen 2 positive electrode with the partially fluorinated $Li_2B_{12}F_9H_3$

2. $Li_{1+x}Ni_{1/3}Co_{1/3}Mn_{1/3}O_2$ cathode material - The layered $Li(Ni_{1/3}Co_{1/3}Mn_{1/3})O_2$ system is more stable than the gen 2 system recently investigated. The increased stability of this cathode derives from the stabilizing role of Mn and Co and the presence of a small amount of active tetravalent nickel in the material when charged. Figure III-48a shows the ASI vs. %SOC of 18650 cells based on graphite/ $Li(Ni_{1/3}Co_{1/3}Mn_{1/3})O_2$ with $LiPF_6$:EC:DEC +2%VEC electrolyte. The cell impedance when aged at 55°C and potentiostated at 60% SOC shows no sign of increase after being aged for

over 350 days. However, the initial impedance is still high because of the VEC additive. AC impedance with 0.5, 1, 1.5 and 2%VEC shows the interfacial impedance of the cell increases significantly with VEC concentration. However, the capacity of the cell with 2% VEC after 400 days was very stable, exhibiting less than 12% fade (Figure III-48b).

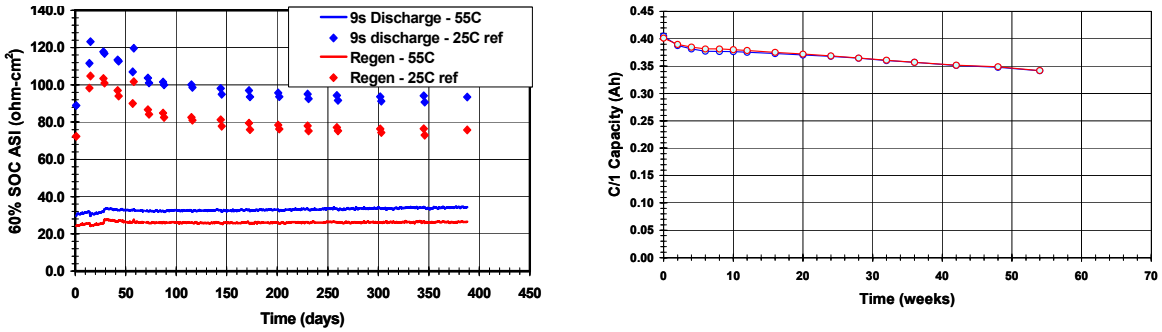

Figure III-48. a) ASI of 1/3 material, b) capacity fade with time

3. $LiFePO_4$ cathode material - Olivine $LiFePO_4$ was also investigated at ANL as a potential cathode for HEV batteries. This material has outstanding safety but its power performance is poor because of its insulating characteristics. To improve the rate capability, the material was carbon coated (2wt%) at the particle level by cracking propylene gas on olivine powder at 700°C using a rotary furnace or a fluidized bed. Figure III-49a shows the ASI of $LiFePO_4$ /graphite and C-$LiFePO_4$/graphite cells as a function of SOC. The $LiFePO_4$ electrode made with15% of super-P (SP) carbon black additive shows the highest ASI values. For the cells made of the $LiFePO_4$ coated with 2% carbon film using the ANL process, the ASI was considerably lower. This result shows that coating olivine particles with a few monolayers of carbon improved the electronic conductivity of the particles, which leads to improved performance.

Furthermore, using a gas phase process for coating the carbon could result in some carbon present in the pores of the olivine particles, creating a conductive network. Preliminary HPPC tests show that the cell almost met the power requirement for some HEVs. However, when cycled at 37°C and 55°C, the cell showed a significant capacity fade while no sign of capacity decrease was observed up to 100 cycles at room temperature (Figure III-49b). Further study using reference electrodes has shown a significant increase in the interfacial resistance at the carbon anode. Also, a stability test of the olivine powder in the electrolyte reveals some Fe dissolution (500 ppm) when the olivine powder was aged in the electrolyte at 55°C for a few weeks. Based on the above result and on EDS data that shows Fe metal presence at the carbon surface, it appears that the mechanism of capacity fade of C-$LiFePO_4$ at high temperature is similar to that of the spinel manganese oxide system.

III.E.3 Low-Cost Flexible Cell Packaging

Low Cost Packaging-Cost Analysis - A large portion of this year's packaging effort was devoted to a detailed design study to compare the manufacturing costs between flexible package (Flex) cells and rigid aluminum container (Rigid) cells at a level of 100,000 HEV batteries per year. The results of this cost study are included in a technical report which will be available in the near future. Provided here is a summary of this report.

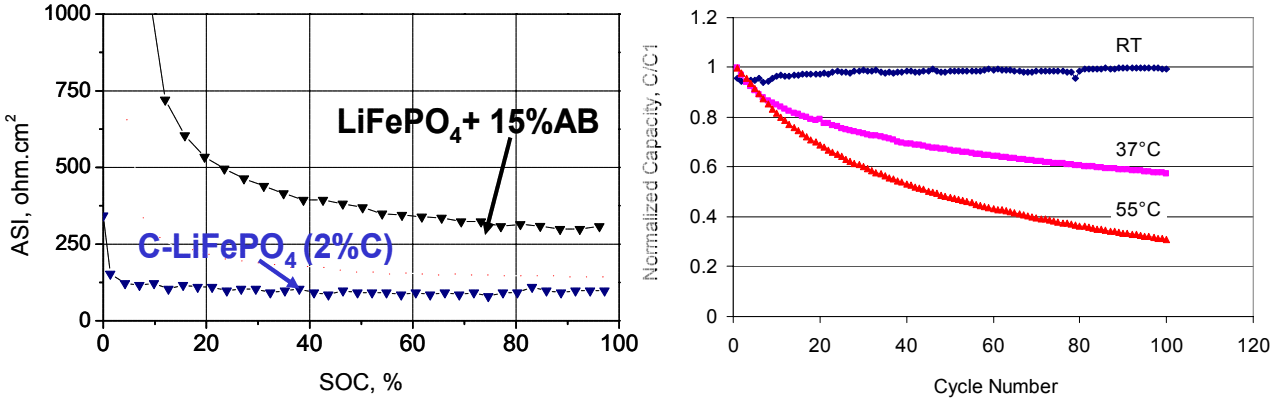

Figure III-49. a) ASI with 30 s current interrupt of $LiFePO_4$ with 15% AB and c-$LiFePo_4$ with 2% C coating. b) Cycling performance of C-$LiFePO_4$/graphite cells

Initially, the rigid cells were considered to have welded closures and to be deep-drawn containers of about the same shape as the Flex cells. As the study progressed, the method of fabricating and sealing the Rigid cells was expanded to include lower cost options including double seaming and other mechanically fastened closures with polymer sealants. Both types of batteries were designed with positive electrodes containing NMC and graphite negative electrodes. The use of different electrodes would have little effect on the costs of the cells. It was found that 20-Ah cells could be designed with excellent heat rejection capabilities for either type of cell. Many parts in the design of the Flex cells are identical or nearly identical to those of the Rigid Cell, so for these features there would be no difference in cost.

However, some of the design features of the Flex cells were different than those of the Rigid cells and would result in significant cost savings. These cost differences are summarized in Container experts assisted with this study, including a paid consultant and personnel at container manufacturing companies. Some of the companies are considering entering the business of manufacturing containers for HEV batteries. For this reason they provided valuable guidance on overall approaches to reducing the costs of the cell containers, but indicated that they were retaining the description of some specific designs and procedures for future possible work with battery manufacturers. A conclusion from discussions with the container experts is that the low manufacturing rates required for the containers for HEV batteries favors procedures requiring little experimentation and low tooling costs. These conditions favor flexible packaging, heat sealing, shallow stamping, double seaming and ultrasonic welding. It works against deep drawing and untested procedures for welding and joining.

Table III-12. Areas where Flex cells appear to have a cost advantage over Rigid cells are: 1) container fabrication and sealing, 2) terminal fabrication and sealing, and 3) intercell connections. The costs of providing cooling channels adjacent to the cells and for module and battery hardware appear to favor rigid cells slightly. Overall, Flex cell batteries appear to have an advantage of about $1.20-$3.70 per cell for a 25-kW battery of 20 cells or about $24 to $74 per battery. Of course, this analysis assumes that both cell designs will have equal reliability, safety, and life over the course of 15 years.

Container experts assisted with this study, including a paid consultant and personnel at container manufacturing companies. Some of the companies are considering entering the business of manufacturing containers for HEV batteries. For this reason they provided valuable guidance on overall approaches to reducing the costs of the cell containers, but indicated that they were retaining the description of some specific designs and procedures for future possible work with battery manufacturers. A conclusion from discussions with the container experts is that the low manufacturing rates required for the containers for HEV batteries favors procedures requiring little experimentation and low tooling costs. These conditions favor flexible packaging, heat sealing, shallow stamping, double seaming and ultrasonic welding. It works against deep drawing and untested procedures for welding and joining.

Table III-12. Cost Estimates in Comparing Flexible Package Cells and Rigid Cells

	Cost, $/cell		
	Rigid	**Flex**	**Difference[a]**
Fabrication of cell windings	b	b	$0.00
Attachment of electrodes to terminals	c	c	0.00
Container fabrication and sealing	$1.00-3.00	$0.60	0.40-2.40
Terminal fabrication and sealing	1.50-2.00	0.40	1.10-1.60
Provision for cooling channels	0.20	0.50	(0.30)
Pressure relief and pressure switch	d	d	0.00
Intercell connections	0.50	0.20	0.30
Module and battery hardware	e	e + 0.30	(0.30)
Total cost advantage for Flex cells			1.20-3.70

a: Cost for Rigid Cells minus that for Flex Cells.
b: Cost of materials and fabrication for Rigid windings.
c: Cost of attaching Rigid Cell electrodes to terminals.
d: Cost of providing pressure relief and a pressure switch for Rigid Cell.
e: Cost of module and battery hardware for Rigid Cells.

Through the guidance of these experts, it was determined that a new type of container could be manufactured that would have the best features of performance and low-cost of both the Rigid and Flex containers (Figure III-50). For instance, the aluminum layer in a tri-layer sheet can be sufficiently thick to form a rigid container that can be fabricated in two halves, much like a Flex container, and mechanically joined at the edges for strength. In addition to the mechanical joint, this container can be sealed at the edges, much like a Flex container, by means of an inner polymer liner that can be heat sealed or ultrasonically welded. The terminals can be flat strips of metal sealed into the top of the container as part of the edge sealing of the container as for the Flex cell. Ridges can be stamped into one side of the container to provide cooling channels and the exterior layer of the container stock can be coated with a thin, electrically insulating, polymer layer. This type of container should have excellent sealing and durability and be less expensive than either the Flex or the Rigid containers, which the study initially considered.

Low Cost Packaging-Organoclay - Developmental work to incorporate organoclays into polyolefin was continued in FY05, but at a reduced funding level. The key goal in making organoclay nanocomposites is to adjust the thermodynamics of the final composite such that the organoclay fully disperses, or exfoliates, in the polymer matrix. Simple shearing, which is done in most

applications where clay is added as a simple mineral filler, will not create a homogenous distribution. Complete exfoliation is not a trivial matter – the polymers of greatest interest are hydrophobic in nature, while the clay is hydrophilic. In addition, the polymer has amorphous and crystalline regions throughout its matrix, and the clay platelet is two-dimensional in its properties, *i.e.*, surface sites and edge sites. The main task in this effort has been to tailor novel surfactants that will unify these different activity zones.

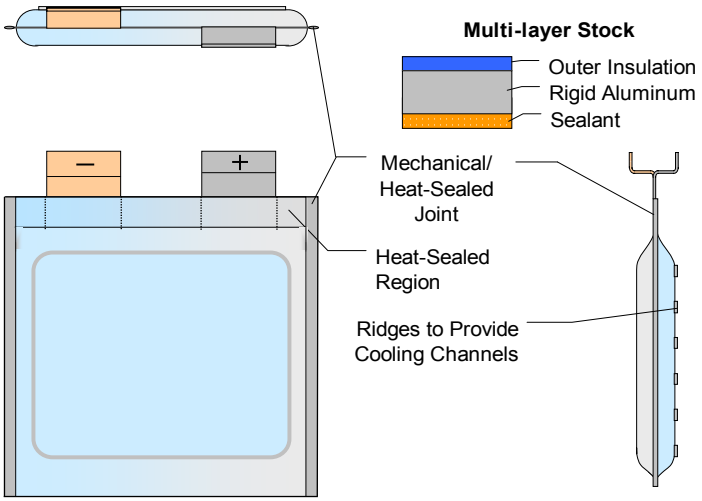

Figure III-50. Cell with rigid container and heat-sealed terminals combines the best features of rigid and flexible packaging.

Earlier work resulted in surfactants that adequately treated the edge and surface sites of the clay particle. Recently, clay surfactants were developed that blend well with the amorphous region of polyethylene. These amorphous surfactants are of high-molecular weight and are transparent, colorless, and remain as a highly viscous liquid at room temperature. Another class of surfactants were developed that blend well with the crystalline region of polyethylene. These crystalline surfactants are also of high molecular weight and have melting points close to that of polyethylene, which results in ideal mixing.

Using these new surfactants, a 70% reduction in water vapor transmission rate (WVTR) through high density polyethylene was observed with the addition of only 0.3 wt% clay. Similar results were obtained for low density polyethylene. Such impressive improvements in WVTR have not been obtained by others. These nanocomposites also displayed a significant increase in break-through time, which suggests that the increased barrier property is due to a reduction in diffusivity (increased tortuosity) and to interactions with the clay surface (solubility). The gas barrier properties of the nanocomposite were also tested and found to improve by approximately 30% for nitrogen, argon, and oxygen – and even more for carbon dioxide and hydrogen.

While these results show that organoclay nanocomposites can improve the barrier properties of common polymers, they do not improve the barrier properties by an order of magnitude. Equal levels of barrier improvement could be obtained by switching to polymers that are modified by their

molecular weight, crystallization, monomer units (copolymers, grafts, etc.), or by switching to a different family of polymers, such as polypropylene and its acid-modified derivatives.

Publication List for 2004~2005

Publication in Journals

1. **Advanced cathode materials for high-power applications.** Amine, K.; Liu, J.; Belharouak, I.; Kang, S.-H.; Bloom, I.; Vissers, D.; Henriksen, G. ; Journal of Power Sources (2005), 146(1-2), 111-115.

2. **Alternating Current Impedance Electrochemical Modeling of Li-ion Positive Electrodes**, D. Dees, et. al., *J. Electrochem. Soc.* **152** (7), A1409 (2005)

3. **Aluminum-doped lithium nickel cobalt oxide electrodes for high-power Li-ion batteries.** Chen, C. H.; Liu, J.; Stoll, M. E.; Henriksen, G.; Vissers, D. R.; Amine, K.. Journal of Power Sources (2004), 128(2), 278-285.

4. **An Overview of DOE's Advanced Technology Development Program.** G. Henriksen, D. Dees, T. Duong, and D. Howell, in Proceedings of the IEEE 62nd Semiannual Vehicular Technology Conference, Dallas, TX, September 25-28, 2005.

5. **Effect of fluorine on the electrochemical properties of layered Li(Ni0.5Mn0.5)O2 cathode materials.** Kang, S.-H.; Belharouak, I.; Sun, Y.-K.; Amine, K.; . Journal of Power Sources (2005), 146(1-2), 650-653.

6. **Effects of additives on thermal stability of Li ion cells.** Doughty, Daniel H.; Roth, E. Peter; Crafts, Chris C.; Nagasubramanian, G.; Henriksen, Gary; Amine, Khalil.; Journal of Power Sources (2005), 146(1-2) 116-120.

7. **Evaluation of macromonomer-based gel polymer electrolyte for high-power applications.** Oh, Bookeun; Amine, Khalil. Electrochemical Technology Program, CMT Division, Argonne National Laboratory, Argonne, IL, USA. Solid State Ionics (2004), 175(1-4), 785-788.

8. **High-temperature storage and cycling of C-LiFePO4/graphite Li-ion cells.** Amine, K.; Liu, J.; Belharouak, I., Electrochemistry Communications (2005), 7(7), 669-673. .

9. **Improved lithium manganese oxide spinel/graphite Li-ion cells for high-power applications.** Amine, K.; Liu, J.; Kang, S.; Belharouak, I.; Hyung, Y.; Vissers, D.; Henriksen, G. ; Journal of Power Sources (2004), 129(1), 14-19.

10. **Investigations of the Exothermic Reactions of Natural Graphite Anode for Li-ion Batteries during Thermal Runaway.** Yang, Hui; Bang, Hyunjoo; Amine, Khalil; Prakash, Jai.; Journal of the Electrochemical Society (2005), 152(1), A73-A79.

11. **Layered Li(Li0.2Ni0.15+0.5zCo0.10Mn0.55-0.5z)O2- zFz cathode materials for Li-ion secondary batteries.** Kang, S.-H.; Amine, K. ; Journal of Power Sources (2005), 146(1-2), 654-657.

12. **LiBOB-Based Electrolytes for Li-ion Batteries for Transportation Applications.** Jow, T. R.; Xu, K.; Ding, M. S.; Zhang, S. S.; Allen, J. L.; Amine, K; Journal of the Electrochemical Society (2004), 151(10), A1702-A1706.

13. **Preparation of rechargeable lithium batteries with poly(methyl methacrylate) based gel polymer electrolyte by in situ -ray irradiation-induced polymerization.** Zhou, Y. F.; Xie, S.; Ge, X. W.; Chen, C. H.; Amine, K; Journal of Applied Electrochemistry (2004), 34(11), 1119-1125.

14. **Reduction Mechanisms of Ethylene, Propylene, and Vinylethylene Carbonates.** Vollmer, James M.; Curtiss, Larry A.; Vissers, Donald R.; Amine, Khalil.; Journal of the Electrochemical Society (2004), 151(1), A178-A183.

15. **Suppressing the impedance rise of LiNi0.8Co0.2O2/graphite cells by Al, Ti and Mg doping.** Chen, Chun-hua; Xie, Song; Liu, Jun; Amine, K ; Guocheng Gongcheng Xuebao (2004), 4(1), 59-63.

16. **Synthesis and Characterization of Li[(Ni0.8Co0.1Mn0.1)0.8(Ni0.5Mn0.5)0.2]O2 with the Microscale Core-Shell Structure as the Positive Electrode Material for Lithium Batteries.** Sun, Yang-Kook; Myung, Seung-Taek; Kim, Myung-Hoon; Prakash, Jai; Amine, Khalil.; Journal of the American Chemical Society (2005), 127(38), 13411-13418.

17. **Synthesis and electrochemical analysis of vapor-deposited carbon-coated LiFePO4.** Belharouak, I.; Johnson, C.; Amine, K., Electrochemistry Communications (2005), 7(10), 983-988.

18. **Synthesis and electrochemical behavior of layered Li(Ni0.5-xCo2xMn0.5-x)O2 (x = 0 and 0.025) materials prepared by solid-state reaction method.** Sun, Y.-K.; Kang, S.-H.; Amine, K; Materials Research Bulletin (2004), 39(6), 819-825.

19. **Synthesis and improved electrochemical performance of Al(OH)3-coated Li[Ni1/3Mn1/3Co1/3]O2 cathode materials at elevated temperature.** Jang, S. B.; Kang, S.-H.; Amine, K.; Bae, Y. C.; Sun, Y.-K.; Electrochimica Acta (2005), 50(20), 4168-4173.

20. **Synthesis of Nanostructured Li[Ni1/3Co1/3Mn1/3]O2 via a Modified Carbonate Process.** Park, S.-H.; Shin, H.-S.; Myung, S.-T.; Yoon, C. S.; Amine, K.; Sun, Y.-K. Chemistry of Materials (2005), 17(1), 6-8.

21. **Thermal Response and Flammability of Li-ion Cells for HEV Applications**, E. P. Roth, D.H. Doughty, SAE 2005 World Congress and Exhibition, April 11-14, 2005, Detroit, MI.

Patent and Patent Applications

22. **Battery having electrolyte including one or more additives.** Yoon, Sang Young; Nakahara, Hiroshi; Amine, Khalil. (USA). U.S. Pat. Appl. Publ. (2005), 31 pp., Cont.-in-part of U.S. Ser. No. 496,231,. CODEN: USXXCO US 2005106470 A1 20050519 Patent written in English.

23. **Method and apparatus for preparation of spherical metal carbonates and lithium metal oxides for lithium rechargeable batteries.** Kang, Sun-Ho; Amine, Khalil. (The University of Chicago, USA). U.S. Pat. Appl. Publ. (2005), 33 pp., Cont.-in-part of U.S. Ser. No. 699,484. CODEN: USXXCO US 2005058588 A1 20050317 Patent written in English.

24. **Long life lithium batteries with stabilized electrodes.** Amine, Khalil; Kim, Jaekook; Vissers, Donald R. (USA). U.S. Pat. Appl. Publ. (2005), 13 pp. CODEN: USXXCO US 2005019670 A1 20050127 Patent written in English.

25. **Cathode material for lithium ion batteries.** Belharouak, Ilias; Amine, Khalil. (USA). U.S. Pat. Appl. Publ. (2004), 20 pp. CODEN: USXXCO US 2004157126 A1 20040812 Patent written in English.

35 **Lithium based electrochemical cell systems with suppression of gas evolution.** Hyung, Yoo-Eup; Vissers, Donald R.; Amine, Khalil. (The University of Chicago, USA). U.S. Pat. Appl. Publ. (2004), 7 pp. CODEN: USXXCO US 2004151951 A1 20040805 Patent written in English.

36 **Anode material for lithium batteries.** Belharouak, Ilias; Amine, Khalil. (The University of Chicago, USA). U.S. Pat. Appl. Publ. (2004), 13 pp. CODEN: USXXCO US 2004131941 A1 20040708 Patent written in English.

37 **Layered cathode materials for lithium ion rechargeable batteries.** Kang, Sun-ho; Amine, Khalil. (The University of Chicago, USA). U.S. Pat. Appl. Publ. (2004), 24 pp. CODEN: USXXCO US 2004091779 A1 20040513 Patent written in English

38 Nickel-titanium-phosphate cathodes for lithium ion batteries. Belharouak, Ilias; Amine, Khalil. (USA). U.S. Pat. Appl. Publ. (2004), 10 pp. CODEN: USXXCO US 2004265696 A1 20041230 Patent written in English.

39 Production and use of layered Li1+xNi□ Mn□ O2-based cathode material for Li-ion rechargeable batteries. Kang, Sun-Ho; Amine, Khalil. (The University of Chicago, USA). U.S. Pat. Appl. Publ. (2004), 9 pp. CODEN: USXXCO US 2004234854 A1 20041125 Patent written in English.

Extended Abstracts

40 Layered Composite Cathode Material for High-Energy Li Batteries. Kang, S-H.; Park, S-H.; Sun, Y-K.; Amine, K.. Abstracts of Papers, 2nd International Conference on Polymer Batteries and Fuel Cells (PBFC-2), Las Vegas, NV, United States, June 12-17, 2005, Abs-11.

41 Science and Technology of Layered Composite Cathodes for Li Batteries. Johnson, C. S.; Kang, S-H.; Kim, J-S.; Li, N.; Vaughey, J. Y.; Amine, K.; Thackeray, M. M.. Abstracts of Papers, 2nd International Conference on Polymer Batteries and Fuel Cells (PBFC-2), Las Vegas, NV, United States, June 12-17, 2005, Abs-52.

42 Electrochemistry of 0.5Li2MnO3·0.5LiNi0.5Mn0.5O2 Composite Cathode Material Doped with Co and F. Kang, S-H.; Kempgens, P.; Greenbaum, S.; Kropf, A. J.; Amine, K.. Abstracts of Papers, 2nd International Conference on Polymer Batteries and Fuel Cells (PBFC-2), Las Vegas, NV, United States, June 12-17, 2005, Abs-57.

43 Siloxane-based Electrolytes for Rechargeable Lithium Ion Batteries. Wang, Q.; Amine, K.; Vissers, D. R.; Zhang, Z.; Rossi, R.; West, R.; Yoon, S-Y.; Tsukamoto, H.. Abstracts of Papers, 2nd International Conference on Polymer Batteries and Fuel Cells (PBFC-2), Las Vegas, NV, United States, June 12-17, 2005, Abs-103.

44 Miniature Size Hermetically Sealed Lithium Rechargeable Battery with Liquid Siloxane Electrolyte for Implantable Medical Applications. Yoon, S-Y.; Nakahara, H.; Tsukamoto, H.; Wang, Q.; Amine, K.; Zhang, Z.; West, R.. Abstracts of Papers, 2nd International Conference on Polymer Batteries and Fuel Cells (PBFC-2), Las Vegas, NV, United States, June 12-17, 2005, Abs-121.

45 The Effect of Additives on the Thermal Behavior of Li-ion Anodes. Bang, H. J.; Joachin, H.; Amine, K.; Prakash, J.. Abstracts of Papers, 207th ECS Meeting, Quebec City, Canada, May 15-20, 2005, Abs-153

46 The Electrochemical Behaviors of Manganese Spinel Electrodes at High Temperature. Kim, J .; Amine, K. Abstracts of Papers, 206th ECS Meeting, Honolulu, HI, United States, October 3-8, 2004, Abs-289.

47 Synthesis and Electrochemical Properties of Li[Ni1/3Co1/3Mn1/3]O2-*x*F*x* via Co-precipitation. Kim, G-H .; Myung, S-T.; Kim, M-H.; Sun, Y-K.; Amine, K.; Kang, S-H.. Abstracts of Papers, 206th ECS Meeting, Honolulu, HI, United States, October 3-8, 2004, Abs-333.

48 Investigations of the Exothermic Reactions of Natural Graphite Anode for Li-ion Batteries during Thermal Runaway. Yang, Hui; Bang, Hyunjoo; Amine, Khalil; Striebel, Kathryn; Prakash, Jai. Abstracts of Papers, 206th ECS Meeting, Honolulu, HI, United States, October 3-8, 2004, Abs-389.

49 Source of Thermal Reactivity at the Positive and Negative Electrode in Lithium Batteries. Amine, K.; Belharouak, I.; Hyung, Y.; Henriksen, G.; Abstracts of Papers, 206th ECS Meeting, Honolulu, HI, United States, October 3-8, 2004, Abs-393.

50 Layered $Li_{1+x}(Ni_{1/3}Co_{1/3}Mn_{1/3})O_2$ as Cathode for high Power and High energy Li-ion Batteries. Liu, J.; Belharouak, I.; Amine, K.; Pan, X. Q.; Sun, H. P.; Abstracts of Papers, 206th ECS Meeting, Honolulu, HI, United States, October 3-8, 2004, Abs-492.

51 **Degradation Mechanism of LiMn2O4/Graphite Li-ion Cells.** Amine, K.; Liu, J.; Kang, S. H.; Kahaian, A,; Belharouak, I. Vissers, D.; Henriksen, G., Abstracts of Papers, 206th ECS Meeting, Honolulu, HI, United States, October 3-8, 2004, Abs-493.

52 **Inorganic Olivine Phosphate as Important Cathode Materials for High Power and High Energy battery Applications**. K. Amine, I. Belharouak, and C. Johnson. Abstracts, the 5th International Symposium on Inorganic Phosphate Materials'05, 2nd IMPHOS Workshop, Kasugai, Japan, September 06-08, 2005, p. 25 (2005)

53 **New process of coating olivine $LiFePO_4$ with monolayer of carbon using a gas phase reaction;** K. Amine, I. Belharouak and C. Johnson; Abstracts, Li-ion batteries Discussion LiBD-3 2005 – Electrode materials. Arcachon, France, May 22-27, 2005, T12 p.65-66 (2005)

54 **Thermal and Structural Stability of $Li_{1+x}(Ni_{1/3}Co_{1/3}Mn_{1/3})O_2$ Advanced Cathode;** I Belharouak, W. Lu, D. R. Vissers, and K. Amine; Accepted by Abstracts, 208th Meeting of the Electrochem. Soc., Los Angeles, CA, October 16–21, 2005

55 **New Titanium Oxyphosphate Material for Lithium Batteries;** I. Belharouak, M. Balasubramanian, D. P. Abraham, and K. Amine**;** Accepted by Abstracts, 208th Meeting of the Electrochem. Soc., Los Angeles, CA, October 16–21, 2005

56 **Effect of Excess Lithium on Power and Cycleability of $Li_{1+x}(Ni_{1/3}Co_{1/3}Mn_{1/3})O_{2+y}$;** J. Liu, I. Belharouak, and K. Amine**;** Abstracts, 208th Meeting of the Electrochem. Soc., Los Angeles, CA, October 16–21, 2005

57 **In-Situ Thermal Study of $Li(Ni_{1/3}Co_{1/3}Mn_{1/3})O_2$ Using Isothermal Microcalorimetric Techniques;** W. Lu, I. Belharouak, D. R. Vissers, and K. Amine**;** Abstracts, 208th Meeting of the Electrochem. Soc., Los Angeles, CA, October 16–21, 2005

58 **Poor Cycling Performance of C-$LiFePO_4$/Graphite Li-ion Cells at High Temperature;** K. Amine, J. Liu, and I. Belharouaki**;** Abstracts, 208th Meeting of the Electrochem. Soc., Los Angeles, CA, October 16–21, 2005

59 **Li Ion Battery Abuse Tolerance Testing - An Overview** , D.H. Doughty, Advanced Automotive Battery Conference (AABC) (session organizer and 2 invited presentations), Honolulu, HI, June 2005

60 **Heat and Gas Generating Reactions of Li-ion Cell Materials Under Abuse Conditions**, E. P. Roth, D. H. Doughty, Advanced Automotive Battery Conference (AABC) (session organizer and 2 invited presentations), Honolulu, HI, June 2005

61 **Development and Characterization of Li-ion Batteries for the FreedomCAR Advanced Technology Development Program**, E. P. Roth, D. H. Doughty, IEEE Vehicle Technology Conf. 2005-Fall, Dallas, TX, Sept. 25-28, 2005

62 **Modeling of Thermal Abuse Response of 18650 Li-ion Cells**, E. Peter Roth, Daniel H. Doughty, Robert M. Spotnitz, Gowri S. Yeduvaka, 207th Meeting of the Electrochemical Society, May 15-20, 2005 Quebec City, Canada.

IV. LONG-TERM RESEARCH

The Long-Term Research Program, also called the Batteries for Advanced Transportation Technologies (BATT) program, is supported by the DOE's FreedomCAR and Vehicle Technologies program (DOE-FCVT) to research and analyze new materials for high-performance, next generation, rechargeable batteries for use in HEVs and EVs.

Background and Program Context

The development of an advanced battery for automotive applications is difficult, although companies are making progress each year. Current HEV batteries are all NiMH, but Li-ion continues to show promise due to the promise of improved performance, reduced weight and volume, and potentially lower price and longer life. Thus, there remains a need to identify and understand performance and lifetime limitations to help guide the search for new materials to enable the use of Li-based batteries. The Long-Term Research Program addresses fundamental issues of chemistries and materials associated with lithium battery candidates for vehicular applications. The program emphasizes the identification and mitigation of failure modes, coupled with materials synthesis and evaluation, advanced diagnostics, and improved electrochemical models. Battery chemistries are monitored continuously with periodic substitution of more-promising components based on advice from within this program, from outside experts, and from assessments of world-wide battery R&D.

The work is carried out by the Lawrence Berkeley National Laboratory (LBNL) and several other organizations. The program has carried out investigations into three baseline systems (Figure IV-1):

- The $LiNi_{1/3}Mn_{1/3}Co_{1/3}O_2$ (called 123 or 1/3) cathode material in a high-energy cell with a $LiPF_6$/PC-EC-DMC electrolyte and a carbon-coated graphite anode. The cathode is less expensive than the Gen 2 cathode, plus the lower-cost PC-containing electrolyte is possible due to the amorphous carbon coating on the anode that prevents anode exfoliation.

- The low cost and abuse tolerant $LiFePO_4$ system, using a PC-EC-DMC based electrolyte. The program is working to develop significantly improved materials using liquid or gel electrolytes. This is regarded as a moderate-energy, low-voltage system that is inherently stable and low cost.

- A high-rate spinel system with a liquid-electrolyte, aiding work in the applied research program to develop a low-cost high-power battery.

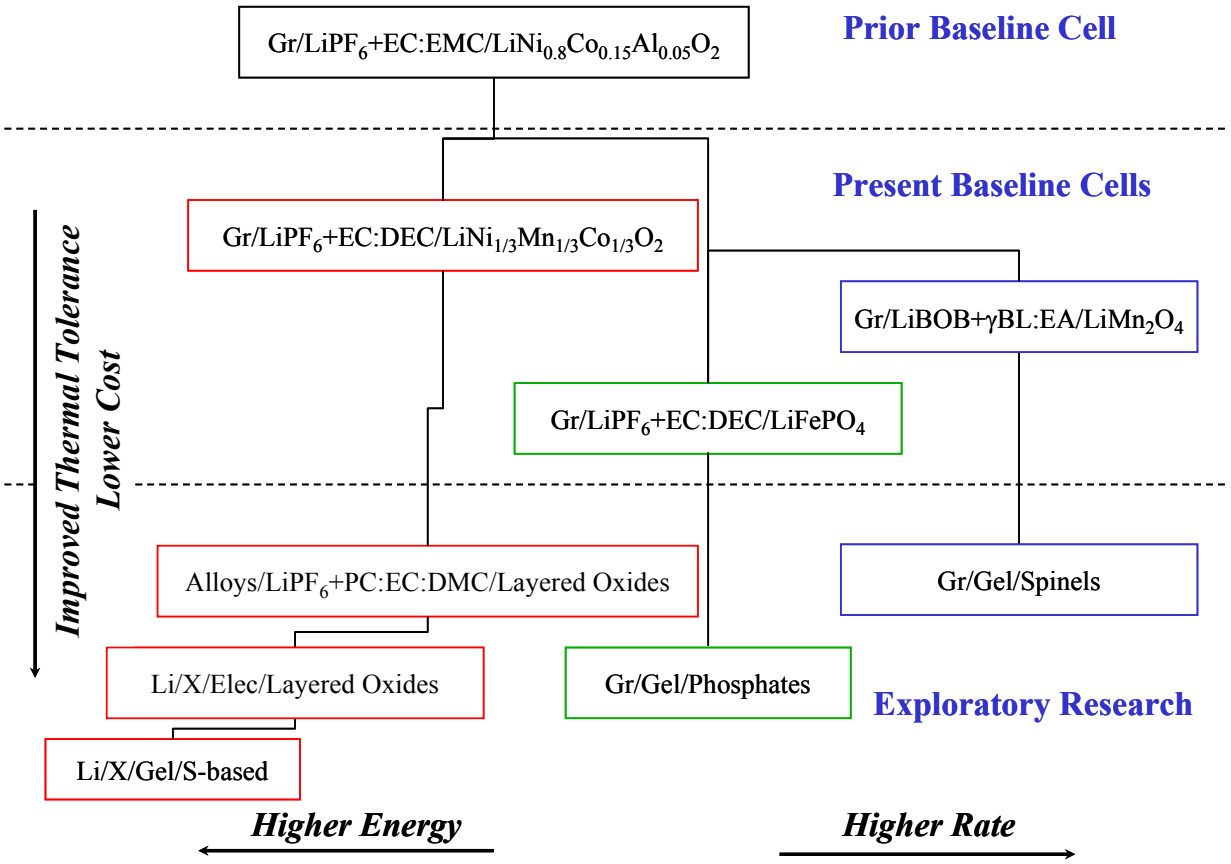

Figure IV-1. Overview of Long-Term Research Chemistries

The program, and this document, is organized into the following research areas:

IV.A New Cathode Systems, Performance and Limitations
- IV.A.1 $LiFePO_4$ Systems
- IV.A.2 Mn Spinel Systems
- IV.A.3 Nickelate Systems

IV.B New Anode Materials

IV.C Novel Electrolytes and their Characterization,

IV.D Li-Ion Modeling, Diagnostics, and Cell Analysis

These task areas provide the program with additional focus on the issues and possible solutions associated with some of the most promising chemistries in the Li-ion battery field while also permitting the researchers to collaboratively address the barriers common to all of these chemistries. Brief descriptions of each research area follow.

- The ***$LiFePO_4$ System*** task includes studies of capacity and power fade in the iron phosphate system, including the performance of iron phosphate in gel polymer electrolytes. This cathode material promises more abuse tolerant performance at a relatively low cost. Researchers investigate the impact of processing steps on performance, and perform theoretical investigations on the impact of carbon coatings on performance.

- The ***Mn Spinel Systems*** task aims to understand the failure and degradation modes in the Mn spinel system using various material doping, cell cycling, empirical and ab-initio calculations, and advanced diagnostics. Researchers are also evaluating electrode materials from multiple suppliers.

- The ***Nickelate Systems*** task aims to understand the failure and degradation modes in the 123 and other nickelate systems using cell builds, cell cycling, empirical and ab-initio calculations, and advanced diagnostics. Researchers are also developing and evaluating self-actuating overcharge protection mechanisms.

- The ***New Anode Materials*** task aims to find improved composite negative electrodes containing one (or more) metal components within a graphite matrix, for example, C/Sn and C/Sb systems.

- The ***Novel Electrolyte Materials*** task involves investigating the limitations of polymers, ionic liquids, and single-ion conducting gels in Li-polymer and Li-ion cells that offer tremendous promise for low cost and abuse tolerant batteries. Post-test analyses and spectroscopic and microscopic techniques are used to investigate morphology, structure, and compositional changes of electrode materials.

- The ***Modeling and Diagnostics*** tasks involve the use of advanced diagnostics techniques to investigate interfacial properties of high power batteries by studying the SEI formation and its change with cycling using FTIR. It also involves studying the changes in electrode structure at high temperatures using XAFS, XRD, NMR and other techniques. Several modeling approaches are used to understand cell behavior and fundamental material properties, including ab-initio calculations, macroscopic cell calculations, and molecular dynamics simulations. The latter is used to study Li transport through polymers and near model interfaces.

This chapter summarizes the research activities of this program in FY 2005. The website for the Long-Term Research Program is found at http://berc.lbl.gov/BATT/BATT.html.

IV.A New Cathode Materials

The overall objective of the following tasks is to evaluate advanced cathode materials for Li-ion batteries. Current materials suffer a number of shortcomings, including expensive raw materials (particularly with the recent increase in Co and Ni price), and relatively poor response to abuse conditions. As a result, this program is investigating three baseline chemistries, $LiFePO_4$, $LiMn_2O_4$, and $LiNi_{1/3}Mn_{1/3}Co_{1/3}O_2$, and several more exploratory systems including composite cathodes, that offer improvements over $LiCoO_2$.

There is one modeling effort that spans all three baseline chemistries. This effort is evaluating the performance of the three baseline cell chemistries; identifying the limiting mechanism in each; understanding the low temperature limitations of the baseline systems; and investigating degradation mechanisms towards development of a cycle-life model. Results from this modeling work are presented in the sections below.

IV.A.1 $LiFePO_4$ System: Performance and Limitations

Objectives

The primary objective of the iron-phosphate research is to overcome the inherently poor conductivity of this material to permit cell developers to take advantage of its relatively low cost and good abuse tolerance characteristics.

Approach

One project has explored methods for maximizing the high-power performance of $LiFePO_4$ composite cathodes. These include introducing a variety of electronically conductive additives and optimizing electrode structure using carbon rods. Another project concentrates on enhancing the capacity and rate of this material by replacing electrochemically inactive additives such as carbon and Polytetrafluoroethylene (PTFE) in conventional cathodes with active polymers. Another group is investigating the affect of carbon coatings and additives on the cathodes rate capability.

Another group is exploring low-temperature hydrothermal synthesis as a lower-manufacturing approach to this material.

In-situ, time resolved, XRD has been performed to understand the response of this cathode material to elevated temperatures in both the charged and uncharged states.

Finally, experimental and theoretical data have been used to model this material. One PI has performed ab-initio calculations to investigate the energy barriers in the material. Another has applied a full cell model and performed experiments to extract unknown parameters, and then used these optimized models to compare the baseline chemistries.

Accomplishments

New Conductive Carbons – Recent efforts included fabricating and testing $LiFePO_4$ cathodes containing new combinations of conductive carbons, in particular carbon fibers.

Cells utilizing carbon-coated $LiFePO_4$ active material in the cathode with a Li counter electrode were fabricated and tested. The cathode slurries contained a total of 3.5% by weight carbon additives to promote electronic conductivity. The three additives used were graphite (GR), carbon black (CB), and carbon fiber (CF). The vapor-grown carbon fibers, obtained from Pyrograf Products, have diameters in the range 70-200nm and lengths in the range 50-100µm. Assembled cells were tested according to BATT protocols. Shown in Figure IV-2 are results for three cells of different carbon compositions: one containing carbon fiber, one containing graphite and carbon black, and one containing a mixture of the three types of carbon.

Before discussing the results, note that each of the curves represents data from a single cell, and that the reproducibility of the results is still being established. Furthermore, as indicated on the plot, the respective cathodes differed in thickness; researchers are working toward better control of electrode thickness so different cells can be directly compared. Control during the casting process is made especially difficult with fibers present in the cathode slurry.

As depicted in Figure IV-2, the discharge capacity at low discharge rates for a standard cathode (graphite + carbon black) was about 82% of theoretical, while that for the carbon-fiber-only cathode was approximately 70%. The best performance, 87% of theoretical capacity, was obtained for the mixture of carbon particles and fibers. At high discharge rates, cathodes containing carbon fiber performed better than the standard cathode, despite greater thicknesses that adversely affect performance.

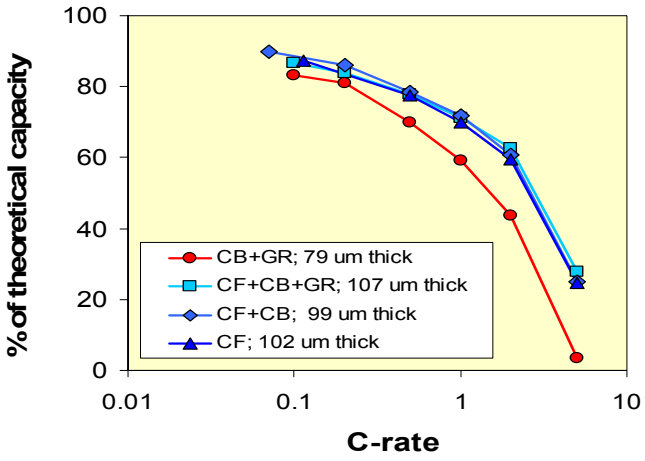

Figure IV-2. Capacity vs. discharge rate for cells with varying conductive-carbon compositions and thicknesses.

New Conductive and Electroactive Polymers – The goal of this work is to replace non-electrochemically active conductive additives with conductive polymers which are active, to achieve better access of electrolyte to oxide; and increase capacity, see Figure IV-3. Recently, researchers succeeded in chemically attaching ferrocene groups to every other pyrrole of a polypyrrole (PPy) backbone. Figure IV-4a compares its discharge/charge curves *vs.* Li with that of PPy without a redox-couple attachment. A plateau near 3.5 V is clearly associated with the ferrocene redox couple, but the capacity remains too small. Therefore, they extended the concept to physically attach

$LiFePO_4$ to PPy. Figure IV-4b compares discharge/charge curves of a $LiFePO_4$/PPy composite *vs.* Li^+/Li^0 containing no carbon black or PTFE with those of the conventional $LiFePO_4$/C/PTFE in a weight ratio 75:20:5. At C/5, the capacity increased from 105mAh/g for the conventional composite to 132mAh/g for the composite with PPy.

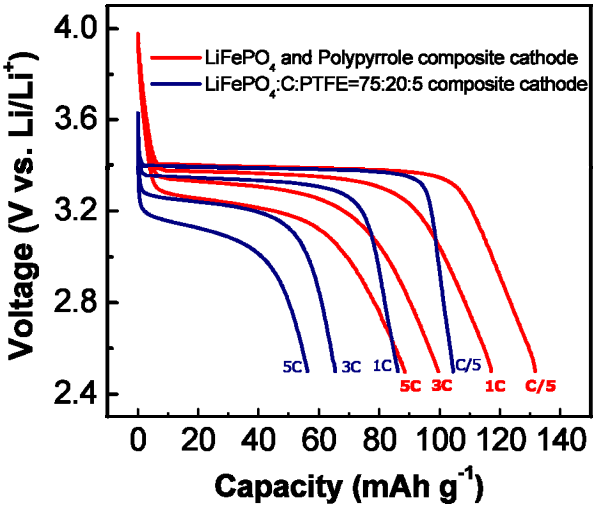

Figure IV-3. Rate capability of iron phosphate with and without conductive polymer

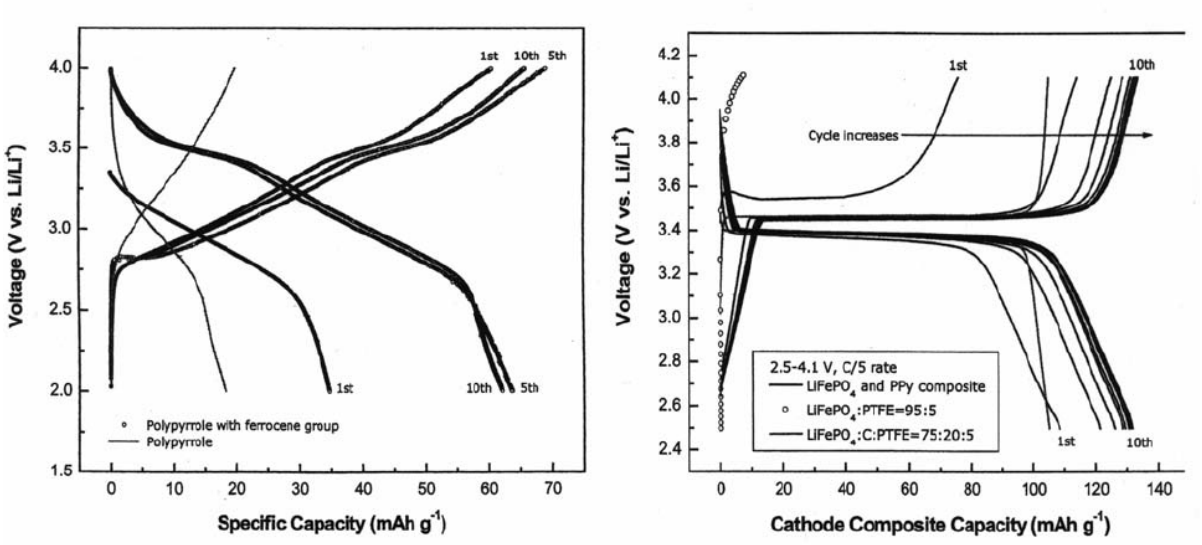

Figure IV-4. a) PPy with ferrocene group, b) cathode composite capacities

Conductivity Improvements – The rate capability of the best-performing $LiFePO_4$ in this program is substantially improved when carbon-coated current collectors are used, Figure IV-5. Mathematical modeling (see below) indicates that this material nearly matches the performance at high rates of $LiFePO_4$ samples from Phostech, but is worse at low rates. This is most likely attributable to a wide particle size distribution. Future work will be devoted towards decreasing this and should result in further improvement. Several samples processed with ferrocenecarboxylic acid and pyromellitic acid are currently under test.

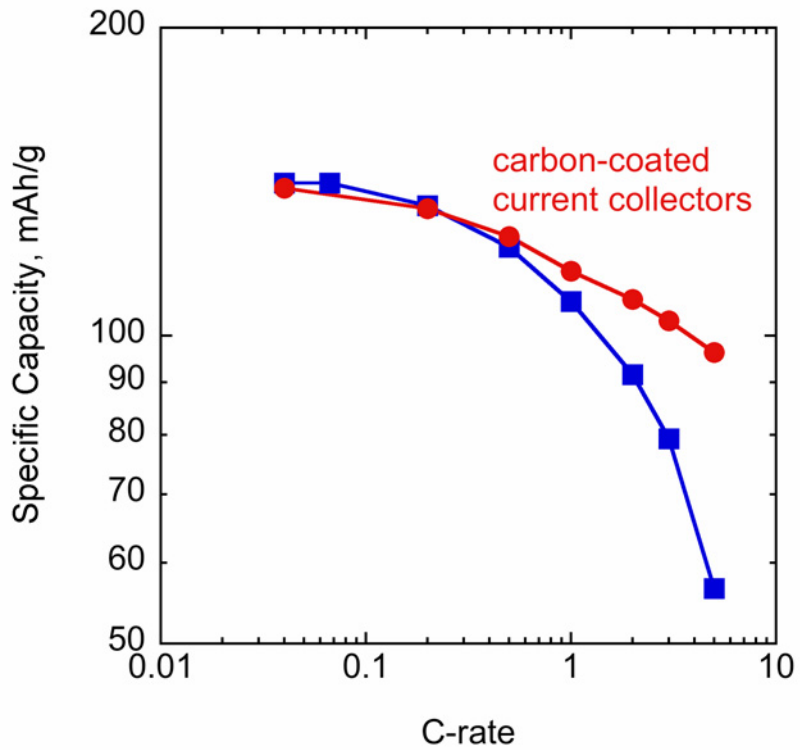

Figure IV-5. Rate data for Li/$LiFePO_4$ cells containing materials prepared with 6% PA and 1% ferrocene promoters (carbon content 1.45 wt%).

$LiFePO_4$ samples calcined with 6 or 8 wt% pyromellitic acid (PA) and 1% ferrocene were electrochemically characterized. (These materials contain 1.45 and 1.64% residual carbon respectively). Figure IV-6 shows a comparison of rate data for cells containing $LiFePO_4$ prepared with and without PA and iron nitrate or ferrocene promoters.

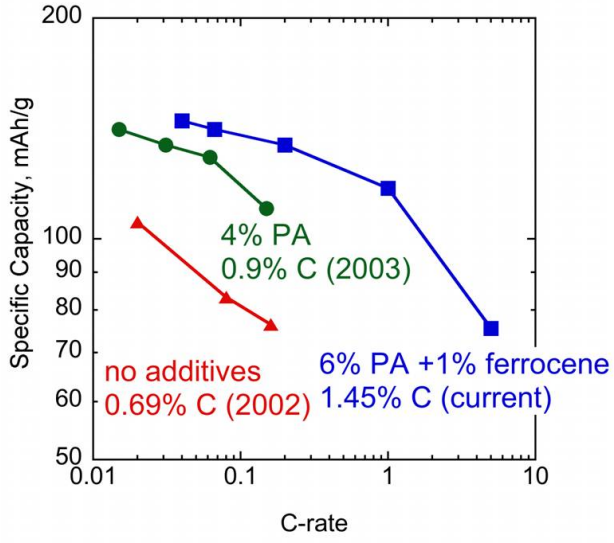

Figure IV-6. Improvements in electrode performance

The addition of ferrocene during synthesis results in better performance for the 6% PA series, but not the 8% series. The *in situ* carbon structure studied by Raman microprobe spectroscopy by Kostecki et al, indicates lowered sp^3 carbon content and D/G (disordered to graphene carbon) ratios, resulting in higher electronic conductivity for the better performing material. This team plans to characterize cells built with carbon-coated current collectors to determine how much the resistance at the current collector/cathode interface affects rate capability.

Hydrothermal Synthesis – Other researches are exploring low-temperature hydrothermal synthesis as a low-cost route to this material. They have synthesized the material from 120–200°C and achieved the same lattice parameters as the high-temperature material and with minimal iron on the Li site.

If the iron to phosphate ratio can be increased beyond that in $LiFePO_4$, then it may be possible to increase the cathode capacity beyond 170mAh/g. The all ferric $Fe_{1.36}PO_4(OH)$ compound has been synthesized, in which one third of the available iron sites are vacant (the all ferrous compound $Fe_2PO_4(OH)$ has all the iron sites occupied). The cycling behavior of this compound is shown in Figure IV-7(a), where the capacity obtained at 21°C is 170mAh/g, approaching the theoretical value of 192mAh/g. The protons in this compound can be partially exchanged for lithium ions. This ion-exchanged material shows improved capacity retention on cycling, as shown in Figure IV-7(b). The fully discharged compound has ~2 Li/PO_4 group. Note that the complete reduction of all the ferric to ferrous would result in a capacity of 192mAh/g.

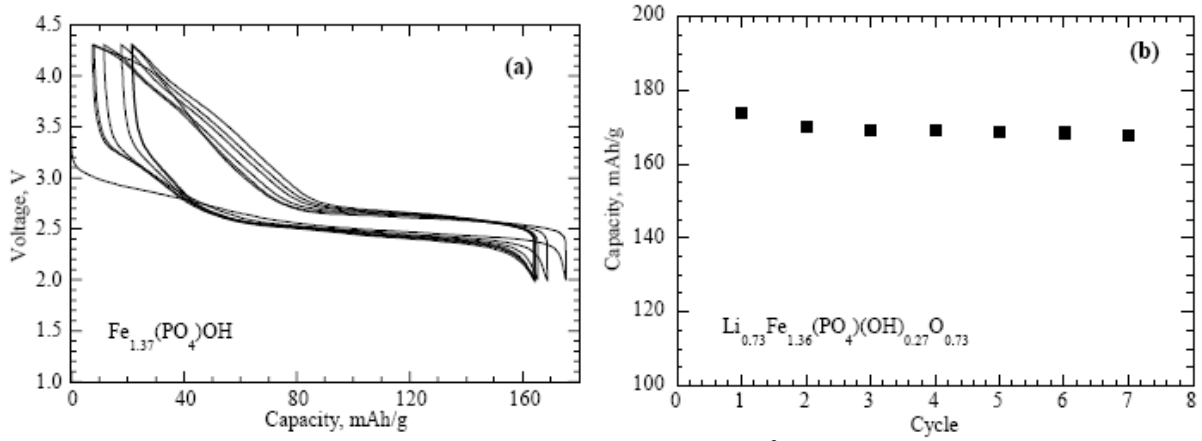

Figure IV-7. (a) Cycling of Li^+ in $Fe_{1.37}(PO_4)OH$, at 0.5 mA/cm^2 (15 mA/g) and (b) the capacity on cycling of $Li_{0.73}Fe_{1.36}(PO_3)(OH)_{0.27}O_{0.73}$ at 0.2 mA/cm^2 (15 mA/g).

In situ XRD Diagnostics – The diagnostics group has used *in situ* time-resolved XRD to monitor temperature-induced structural changes in carbon-coated $LiFePO_4$ provided by Hydro-Québec. Studies were carried out on charged electrodes in the absence and presence of electrolyte. The electrolyte accelerates thermal decomposition of the charged cathode material. The presence of the electrolyte changes the paths of the structural changes and lowers the temperatures for onset of the reactions. As the extent of Li-ion deintercalation increases, the thermal decomposition takes place at lower temperatures.

Time-resolved XRD patterns for $Li_{0.5}FePO_4$ in the absence and presence of electrolyte and heated from 25 to 600°C are shown in Figure IV-8(a) and (b). The structure of the charged $Li_{1-x}FePO_4$ with electrolyte shows dramatic changes with increasing temperature compared to that without electrolyte. In the absence of electrolyte, no structural decomposition is seen until ~515ºC. In the presence of electrolyte, decomposition reactions begin ~390ºC. A temperature-driven solid solution of Li_xFePO_4 was observed below decomposition temperatures of the charged $Li_{1-x}FePO_4$ cathode with or without electrolyte. The formation of the temperature-driven solid solution of Li_xFePO_4 is much clearer in the cathode with electrolyte.

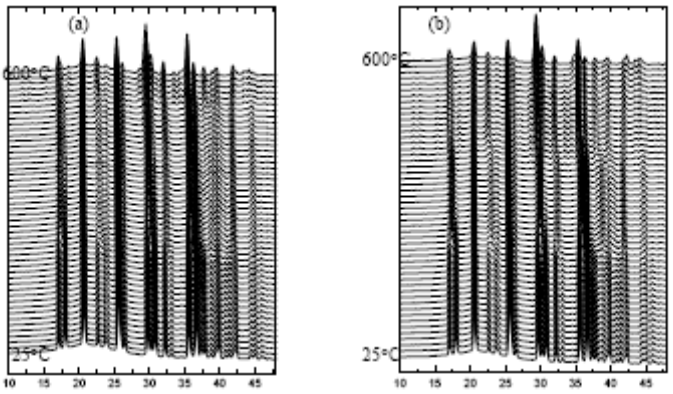

Figure IV-8. Time-resolved XRD patterns for $Li_{0.5}FePO_4$ in the absence (a) and presence (b) of electrolyte, when heated from 25 to 600°C.

P K-edge XAS experiments in the FY mode were performed for $Li_{1-x}FePO_4$ electrodes at different x values. Upon Li deintercalation, pre-edge peaks start to appear in the lower energy region of the main edge. The gradual increase of pre-peak intensities with the Li-ion deintercalation shows that these pre-edge peaks originate from the hybridization of P 3p states with the Fe 3d states. It is interesting that such hybridization occurs in spite of the presence of oxygen atoms that separate phosphorus from iron.

These techniques have also been used to investigate thermally induced structural changes. As an example, this group has shown that $FePO_4$ is more thermally stable than the NiMn material.

Theoretical Investigations – Theoretical efforts to predict electronic and ionic conductivity in electrode materials (and hence rate capability) are coming to fruition. Figure IV-9 shows the calculated activation barrier for a free polaron in $LiFePO_4$. While this barrier is reasonably low, there is a significant association energy, on the order of 130 meV, between the hole carrier in $LiFePO_4$ and the Li vacancy that creates it. The binding energy and polaron migration barrier lead to an activation barrier >400 meV, which is in reasonable agreement with what has been measured experimentally by several groups. This group is currently extending the modeling effort to other materials and is constructing a more general predictive capability of ionic and electronic transport in electrode materials. In addition they have started to test a methodology for predicting the oxygen release of electrodes at high states of charge in order to address abuse behavior of these materials.

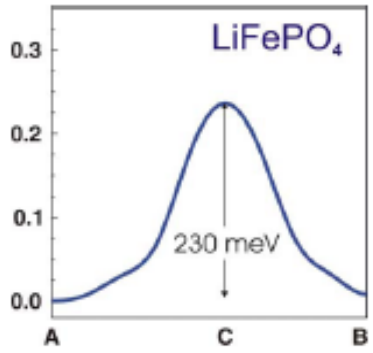

Figure IV-9. Energy path for a polaron transition between two equivalent Fe sites in $LiFePO_4$ The barrier is ~230 meV, but is increased when the Li vacancy is near the Fe^{3+} hole.

Full Cell Modeling – The main focus of this project was to model the three BATT baseline chemistries and to compare them to each other and to the DOE goals. This task is now complete and is summarized in Figure IV-10 and in *JECS*, **151,** A1517 (2004). The graph shows the simulations for the baselines ($LiFePO_4$, $LiNi_{1/3}Co_{1/3}Mn_{1/3}O_2$ and $LiMn_2O_4$) *vs.* a natural graphite anode with 10% excess anode capacity and for the $LiNi_{1/3}Co_{1/3}Mn_{1/3}O_2$ cathode charged to 4.3 V with a Li metal anode with two times excess anode capacity. The electrolyte in all cases is 1M $LiPF_6$ in 1:1 EC:DEC. The Li-metal simulations were performed on a cell that has the same liquid electrolyte, but with the Li covered with a single-ion conducting glass described in Patent application No. US 2004/0191617 A1 by the Polyplus Battery Company. The resistance of the glass layer (taken from this patent) is included in the model. The lines were generated by optimizing the thickness and porosity of the electrodes for a wide range of discharge-times (corresponding to the sloped lines). Therefore, the design of the cell for a 3 h application is significantly different from that for a 2 min application. The graph shows the advantage of using the Mn spinel for HEV applications and also allows one to quantify the improvements needed in the other two cathodes for them to be competitive with the spinel. It is clear that the layered material may prove to be an ideal HEV material, if the other attributes that make a good battery (cost, life, and abuse tolerance) are acceptable.

However, it is also clear that all graphite-based systems have little hope of achieving the EV needs. Li-metal based systems offer hope in this regard, assuming that the metal can be protected from side reactions and from the formation of dendrites.

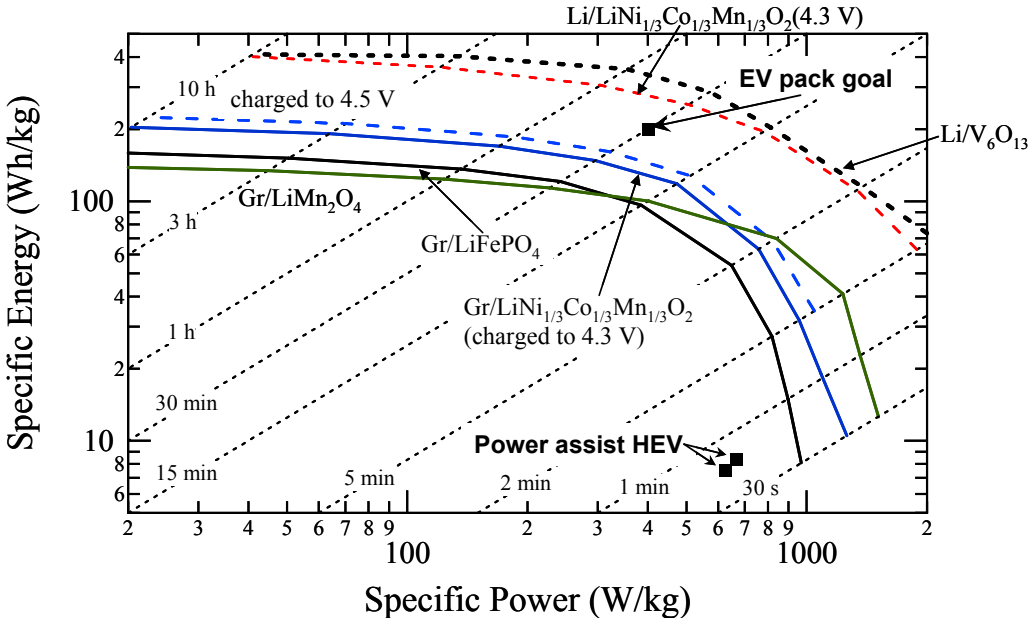

Figure IV-10. Ragone Plot comparing BATT baseline chemistries

This group also investigated in more detail the performance of $LiFePO_4$, particularly the difference between its charge and discharge capabilities. They have found, Figure IV-11, that the diffusion coefficient in $FePO_4$ is ~6 times larger than that in $LiFePO_4$.

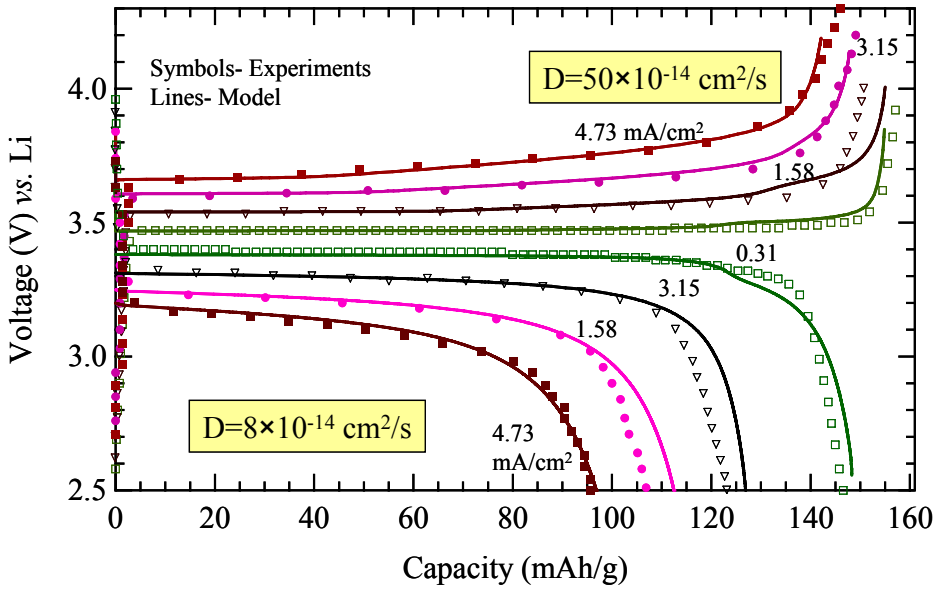

Figure IV-11. Charge and discharge capacity of iron phosphate.

Future Plans

Cathode and Cell Optimization – Produce a new generation of $LiFePO_4$ cathode material at Phostech and other labs, some specific tasks include:

- Determine the behavior of the olivine phase formed hydrothermally at 200°C,
- Further tune the morphology and composition to optimize the performance,
- Narrow the particle size distribution and make particles smaller,
- Further characterize materials to understand role of carbon,
- Dope the olivine phase on the iron site, and
- Measure Li diffusion in the olivine phase.

Conductive Carbon – Researchers are evaluating the feasibility of using the Hall effect to directly determine the cation transference number in battery electrolytes. While a precedent does exist for the measurement of the Hall Effect in liquid electrolytes[14], earlier researchers have argued that experimental results indicate anisotropic transport properties in the presence of a strong magnetic field; and hypothesized that the mobilities of the ions differ between electric-field and Lorentz driving forces. Thus, this group is constructing a Hall effect apparatus in order to test this hypothesis and assess the viability of the technique.

Additional work in the conductive carbon area will include

- Sending optimized fibrous cathode samples to other groups for analysis,
- Determining the effect of fiber-additive compositions on cycle life and failure mechanisms, and
- Investigating possible improvements through novel structured current collectors.

Full Cell Modeling: Simulations to date are based on optimizing the performance for a fixed time-of discharge from 0% to 100% DOD. However, HEV designs use pulses and a more limited cycling range. In order to simulate this behavior the existing model will be used to follow the HEV protocol. This will be used as a basis to understand the impact of changing the voltage cut-offs, differences in the rate capability between charge and discharge, effects of thickness and porosity of electrodes, and the impact of the SOC range of cycling. Some specific enhancements to the modeling will include:

- Determining if the history-dependent behavior has any impact,
- Determining what limits the cycling stability of $LiFePO_4$,
- Incorporating life-limiting mechanisms, and
- Understanding the impact of pulse current and particle size.

Finally, one group plans to perform first principle's based simulations of $LiFePO_4$ to more fully understand its inherent rate capability.

[14] P. Gérard et al., *J. Electrochem. Soc.* **137**, 3873 (1990)

IV.A.2 Spinel Systems: Performance and Limitations

Objectives

Mn is inexpensive, environmentally benign, and has inherently high rate capability. However, it suffers large capacity loss at high temperatures. Thus, the objective of this task is to develop low-cost spinel manganese oxide compositions that can offer excellent capacity retention, high rate, low irreversible capacity loss, and good storage characteristics at elevated temperatures, all consistent with the goals of the FreedomCAR program.

Approach

One approach is to develop a firm scientific understanding of the factors that control/influence the electrochemical performance of the spinel cathodes and utilize this knowledge to design and develop high performance compositions. In this regard, a variety of single and multiple cationic substitutions as well as an optimization of the microstructure and morphology are being pursued.

Researchers are also attempting to exploit high potential $LiMn_2O_4$ spinel materials (4.0-5.0 V *vs.* Li) for high-power batteries. In conjunction with the anode project described in section IV.B, they are exploring the electrochemical properties and the abuse tolerance of high-potential layered and spinel cathodes against graphite and low-potential metal oxide anodes.

Another approach is to search for, characterize, and develop low-cost, high-voltage, high-capacity layered lithium-manganese oxide 'composite' $xLi_2M'O_3 \bullet (1-x)LiMO_2$ structures with particular emphasis on electrodes in which M′ = Mn and M = Mn, Ni, Co that operate between 3.0 and 4.8 V *vs.* Li^0. These materials are showing excellent promise to replace $LiCoO_2$ as the cathode of choice for Li-ion batteries; they also hold promise for high-power applications.

Finally, in-situ XRD has been used to investigate the impact of electrolyte additives on the high temperature stability of the spinel cathode.

Accomplishments

Doped Spinels - In continuation of the investigation into cationic substitutions for Mn in the 4V spinel oxide cathodes, the storage performances of $LiMn_{1.85}Al_{0.075}Li_{0.075}O_4$ and $LiMn_{1.85}Ni_{0.04}Al_{0.035}Li_{0.075}O_4$ have been evaluated and compared against the previous best compositions such as $LiMn_{1.85}Li_{0.075}Ni_{0.075}O_4$.

The triply substituted $LiMn_{1.85}Ni_{0.04}Al_{0.035}Li_{0.075}O_4$ composition shows slightly better storage characteristics and elevated temperature cyclability than the doubly substituted $LiMn_{1.85}Li_{0.075}Ni_{0.075}O_4$ and $LiMn_{1.85}Al_{0.075}Li_{0.075}O_4$ compositions. Although the doubly and triply substituted compositions show superior cyclability, rate capability, and storage characteristics with low ICL compared to the unsubstituted $LiMn_2O_4$ cathode, they generally exhibit lower capacities. To increase the capacity while preserving the other improved parameters, small amounts of fluorine have been substituted for oxygen in the anionic lattice along with cationic substitutions to obtain compositions such as $LiMn_{1.9}Ni_{0.1}O_{4-z}F_z$, $LiMn_{1.9}Ni_{0.05}Li_{0.05}O_{4-z}F_z$, and $LiMn_{1.85}Ni_{0.075}Li_{0.075}O_{4-z}F_z$. with $0 \leq z \leq 0.2$.

The fluorine substituted oxyfluoride spinel compositions synthesized by conventional solid-state methods exhibit 5-10mAh/g higher capacities than the corresponding oxide counterparts due to a lowering of the manganese valence. Also, the fluorine substitution leads to a further improvement in cyclability both at room temperature and at 60°C while maintaining similar rate capabilities, Figure IV-12. For example, $LiMn_{1.85}Ni_{0.075}$ $Li_{0.075}O_{3.8}F_{0.2}$ exhibits an excellent capacity retention with 1% fade in 50 cycles compared to 2% fade for $LiMn_{1.85}Ni_{0.075}$ $Li_{0.075}O_4$.

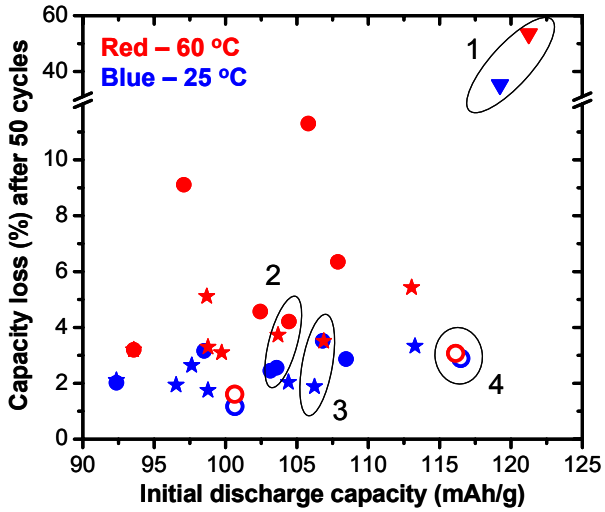

Figure IV-12. Performance of substituted spinels, where
●: $LiMn_{2-x-y}L_xxM_yO_4$ (doubly substituted oxides), ★: $LiMn_{2-x-y-z}Li_xM_yM'_zO4$ (triply substituted oxides), ○: $LiMn_{2-x-y}Li_zM_yO_{3.8}F_{0.2}$ (doubly substituted oxyfluorides) (M, M' = Ni, Al, and Cu)
1 - $LiMn_2O_4$, 2 - $LiMn_{1.88}Li_{0.06}Ni_{0.06}O_4$, 3 - $LiMn_{1.88}Li_{0.06}Ni_{0.03}Al_{0.03}O_4$, 4 - $LiMn_{1.9}Li_{0.05}Ni0_{0.8}F_{0.2}$

The influence of manganese dissolution has been investigated by soaking spinel oxide powders in 1M $LiPF_6$ in EC/DEC electrolyte at 55°C for 7 days. The fluorine-substituted compositions exhibit lower manganese dissolution (1.5–2.0%) than the corresponding oxide compositions (2.5–3.0%), possibly due to stronger metal-fluorine bonds, Figure IV-13.

Additionally, $LiMn_2O_4$ and $LiMn_{1.88}Ni_{0.06}Li_{0.06}O_4$ cathodes have been compared at various stages of cycling by Raman spectroscopy in collaboration with the University of Puerto Rico at San Juan. While the $LiMn_2O_4$ cathode contains ~35% of the second cubic phase ($F43m$) in the fully discharged state after 5 cycles, the cation-substituted $LiMn_{1.88}Ni_{0.06}Li_{0.06}O_4$ cathode predominantly retains the original Fd3m cubic phase with <20% of the second cubic phase in the fully discharged state after 50 cycles, attesting to its better cyclability.

Finally, the lattice parameter differences among the three cubic phases have been examined during the charge-discharge process with three additional compositions: $LiMn_{1.42}Ni_{0.42}Fe_{0.16}O_4$, $LiMn_{1.5}Ni_{0.42}Mg_{0.08}O_4$, and $LiMn_{1.58}Ni_{0.42}O_4$. The data obtained with these compositions support the previous conclusion that a decrease in lattice parameter difference corresponds to an increase in capacity retention. Also, the rate capabilities of the 5V spinel compositions are found to increase as the lattice parameter differences among the three cubic phases decrease. Thus the 4V and 5V spinel oxides share a common dependence of the cyclability and rate capability on the lattice parameter differences among the two or three cubic phases formed.

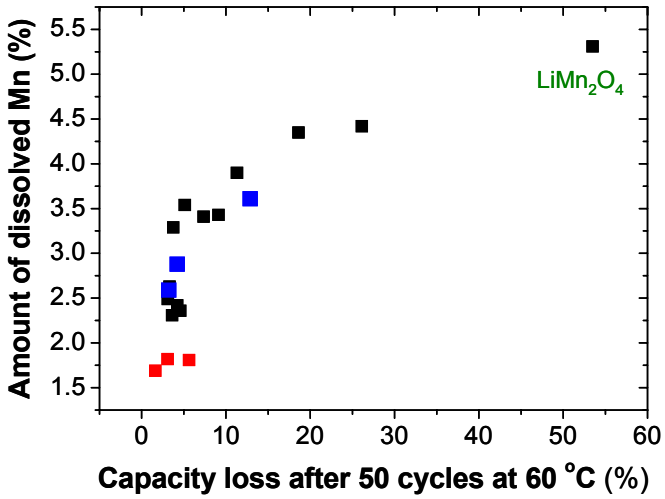

Figure IV-13. Capacity loss vs. Mn dissolution at 60°C, where

	Spinel composition
■	$LiMn_{1.9}Ni_{0.1}O_4$
■	$LiMn_{1.9}Li_{0.05}Ni_{0.05}O_4$
■	$LiMn_{1.85}Li_{0.075}Ni_{0.075}O_4$
■	$LiMn_{1.9}Ni_{0.1}O_{3.8}F_{0.2}$
■	$LiMn_{1.9}Li_{0.05}Ni_{0.05}O_{3.8}F_{0.2}$
■	$LiMn_{1.85}Li_{0.075}Ni_{0.075}O_{3.8}F_{0.2}$

In conclusion, fluorine substitution reduces Mn dissolution and leads to improved capacity retention. Samples with small lattice parameter differences exhibit better capacity retention and the percentage capacity fade decreases with decreasing lattice parameter difference between the cubic phases

Layered and Spinel Composite Cathodes – Manganese oxides exist in many structural forms, e.g.,

- α-MnO_2 (hollandite, 2x2 tunnels)
- β-MnO_2 (rutile, 1x1 tunnels)
- λ-MnO_2 (spinel, 3-d intersecting 1x1 tunnels)
- r-MnO_2 (ramsdellite, 2x1 tunnels)

Intergrown MnO_2 'composite' structures are also well known, and include γ-MnO_2 which has domains of β-MnO2 and r-MnO_2 in which r-MnO_2 is electrochemically active with respect to Li and β-MnO_2 is an electrochemically inactive, stabilizing component. γ-MnO_2 is used for primary alkaline and lithium cells.

Similarly, Li_2MnO_3 is electrochemically inactive with respect to lithium insertion/extraction, whereas $LiMO_2$ is active, Figure IV-14. The approach in this work entails embedding an inactive Li_2MnO_3 component within a layered $LiMO_2$ structure to stabilize the electrode and to reduce the oxygen activity at the surface of charged (delithiated) electrode particles.

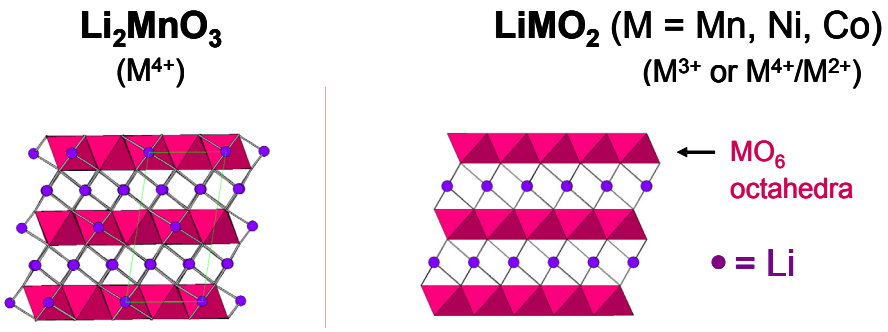

Figure IV-14. Composite $xLi_2MnO_3 \bullet (1-x)LiMO_2$ electrodes

The strategy of designing high-capacity (>200mAh/g) composite electrodes with two layered components (denoted $xLi_2MnO_3 \bullet (1-x)LiMO_2$) is being extended to composite structures with layered and spinel components, (denoted $xLi_2MnO_3 \bullet (1-x)\ LiMn_2O_4$). The goal is to design a bi-functional electrode with a high manganese content in which the layered component ensures a high capacity while the spinel component ensures high rate. The structural compatibility that exists between the (001) close-packed planes of layered Li_2MnO_3 with the (111) planes of spinel LiM_2O_4 compounds should, in principle, make the structural integration of the two components possible. For the initial investigations, the lithium-manganese-oxide system $xLi_2MnO_3 \bullet (1-x)\ Li_{(1+y)}Mn_{(2-y)}O_4$ was selected. Layered-spinel composite electrodes were synthesized by reacting the required amounts of Li and Mn salts at various temperatures.

The XRD patterns of $0.7Li_2MnO_3 \bullet 0.3Li_4Mn_5O_{12}$ products synthesized between 400 and 750°C have been obtained. Although the layered and spinel components have remarkably similar X-ray patterns, the layered component can be distinguished from the spinel component by unique peaks, which are more readily observable in the product synthesized at 750°C. Heating the product from 400 to 750°C releases oxygen, which drives the composition of the spinel component from $Li_4Mn_5O_{12}$ toward $LiMn_2O_4$ (as monitored by an increase of the lattice parameter) and, at the same time, increases the concentration of the Li_2MnO_3 component to maintain the required Li:Mn ratio in the structure.

The initial charge and discharge profiles of a $Li/0.7Li_2MnO_3 \bullet 0.3Li_4Mn_5O_{12}$ cell are shown in Figure IV-15. The capacity delivered between 3 and 4.3 V during the initial charge to 5.0 V corresponds to the oxidation of a small amount of Mn^{3+} in the parent electrode. Thereafter, two voltage plateaus distinguish the removal of Li_2O from the layered and spinel components. The first plateau between 4.5 and 4.7 V is attributed predominantly to the extraction of Li_2O from the Li_2MnO_3 component because this potential is consistent with removal of Li_2O from the Li_2MnO_3 component; the process at higher potential (4.7-5.0 V) is consistent with reports from Manthiram's group of Li extraction from $Li_4Mn_5O_{12}$ at ~5 V. The discharge profile is consistent with a composite electrode having both spinel and layered-type structural features. Preliminary data indicate that high rechargeable capacities (>200 mAh/g) are achievable from these composite structures.

Further examination of the reactivity of these materials at high potential (~4.6 V) has revealed a large first cycle irreversibility loss (>25%). Subsequent investigations showed that acid-leaching can be effective in reducing and even eliminating this first cycle ICL, while preserving a high

discharge capacity. XRD patterns of (a) the as-prepared electrode, (b) a 6-h acid-leached sample, and (c) sample (b) after a heat-treatment step were obtained. Evidence of a layered $HCrO_2$-type phase, similar to that formed by acid-leaching Li_2MnO_3[15], provided supportive evidence for the two-component character of the electrode and for a localized acid-leaching process whereby Li_2O is removed preferentially from Li_2MnO_3 domains of the $0.5Li_2MnO_3 \bullet 0.5Li[Ni_{0.375}Co_{0.25}Mn_{0.375}]O_2$ structure. On heat treatment, this metastable $HCrO_2$-type phase was observed to transform into the configuration of the parent composite structure.

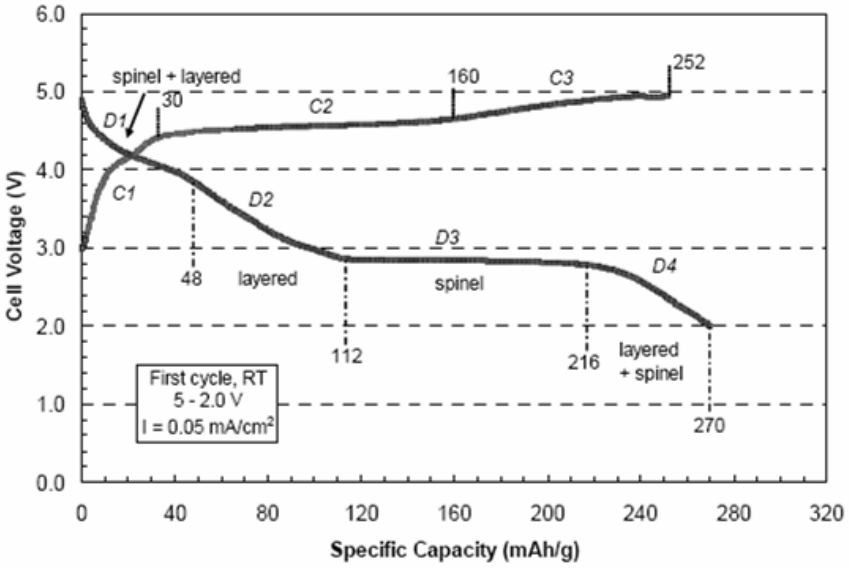

Figure IV-15. Initial charge/discharge profiles of a $Li/0.7Li_2MnO_3 \bullet 0.3Li_4Mn_5O_{12}$ cell

Mn Dissolution Studies – Several groups have reported that Mn dissolution at elevated temperature leads to capacity fade of Mn spinel/graphite cells. To investigate this, samples of spinel manganese oxides were stored in a 1M $LiPF_6$ 1:2 EC/DMC solution at 55ºC for several weeks, and test strips were used to determine if metal dissolution was occurring as a function of time. Li cells containing these materials were cycled at the same temperature, Figure IV-16. Results indicate that spinel and O3 layered materials underwent the most Mn dissolution. $LiNi_{0.5}Mn_{0.5}O_2$ and $LiNi_{1/3}Co_{1/3}Mn_{1/3}O_2$ cycle well at elevated temperature, while O2 and O2/O3 layered manganese oxides show rapid fading. Surprisingly, the O3 compound shows higher capacity at elevated temperatures than at room temperature, but fading still occurs.

In situ XRD Diagnostics - *In situ* XRD work on spinel $LiMn_2O_4$ electrode during cycling at elevated temperatures has been completed. The comparison between the spectra collected from samples cycled in a conventional $LiPF_6$/EC-DMC electrolyte and a more stable $LiPF_6$/EC-DMC electrolyte using 0.1 M tris(pentafluorophenyl) borane (TPFPB) as an additive demonstrated that decomposition of the electrolytes is an important factor in capacity fading of the spinel cathodes. This decomposition causes the deposition of contaminants at the surface of electrodes, blocks Li-ion paths, and results in deactivation of cathode materials. The spectra collected from the sample which

[15] Y. Paik, C. P. Grey, C. S. Johnson, J.-S. Kim, and M. M. Thackeray, *Chem. Mat.*, **14**, 5109-5115 (2002).

underwent washing with TPFPB after multiple cycling at elevated temperature showed that the not-reactive parts of the electrode regained reactivity after washing. Since TPFPB has the ability to dissolve LiF salt into organic solvents, it is reasonable to believe that the major contaminant is LiF.

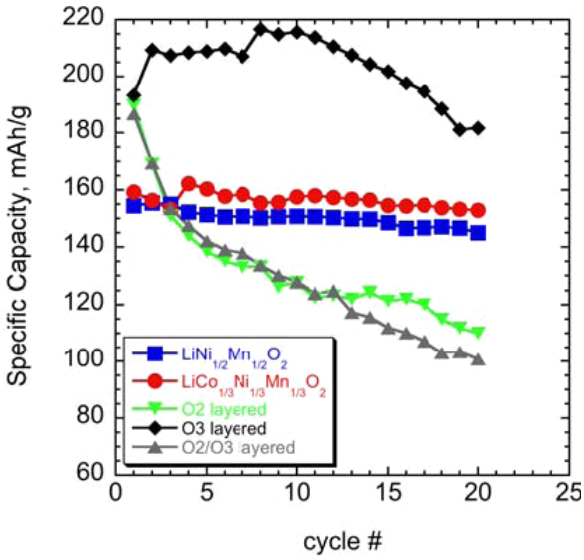

Figure IV-16. Capacity at 55ºC as a function of cycle number for $LiNi_{0.5}Mn_{0.5}O_2$, $LiNi_{1/3}Co_{1/3}Mn_{1/3}O_2$ and layered manganese oxides.

Future Plans

One result of this year's work has been that fluorine substitution is an effective way to overcome the problems of Mn dissolution and capacity fade in spinel cathodes. Thus, one focus of work in 2006 will be on optimization of oxyfluoride spinels.

Another group will continue work to optimize 'layered-layered' and 'layered-spinel' composite electrodes, specifically through:

- Analyzing rate capability, low-temperature performance and Li-ion configuration with graphite and intermetallic anodes for the most promising configurations,
- Eliminating first-cycle ICL of composite electrodes and improving impedance of acid-treated electrodes, and
- Determining the structure-property relationships of electrodes using diagnostic methods.

Some specific tasks will include varying composition to optimize capacity (200-250 mAh/g), power, and cycling stability.

IV.A.3 Nickelate Systems: Performance and Limitations

Objectives

The primary objective of this work is to evaluate alternative Ni-based cathode materials for high power Li-ion batteries. A second objective is to determine the effect of structure on cathode stability, and specifically to explore rate limitations and their relation to structure.

Approach

One approach uses solid-state NMR to characterize local structure and diffraction/TEM for long-range structure, as a function of sample preparation method, state of charge, and number of charge cycles. This is coupled with first principles calculations (density functional theory) to identify redox-active metals, determine the relative stability of different structures, and the effect of structure on cell voltages; and to identify promising cathode materials.

In-situ XRD has been used to characterize the response of layered nickelates to elevated temperatures, and to compare them to cathodes studied earlier.

Finally, groups in this task area synthesize cathode materials by various means. Physical and electrochemical properties (*e.g.,* structure, surface characteristics) are measured in conjunction with members of the diagnostic tasks. Emphasis is placed on low-cost, structurally stable materials that promise very high rate capability.

Accomplishments

Experimental/Theoretical Investigation into Layered Materials – One of the purposes of the continued investigations into the NiMn layered materials is to use $Li(Ni_{1/2}Mn_{1/2})O_2$ as a vehicle to more broadly understand structure property relations in multi-transition metal electrodes. Some of the major findings of this work are that:

- There is always 7-9% Li/Ni exchange,
- The Li in the transition metal (TM) layer octahedron shares face with tetrahedral site, thus Li removal from TM makes tetrahedral sites available for Li diffusion, and
- Li in the transition metal layer is electrochemically active, Figure IV-17.

Combined modeling and experimental work on the $Li[Li_{(1-2x)/3}Ni_xMn_{2/3-x/3}]O_2$ systems has continued, with particular focus on the structure and rate capability of the $Li(Ni_{1/2}Mn_{1/2})O_2$ material as a potential Co-free replacement for the 1/3 system. First principles modeling had suggested a structure for this material,[16] which has been confirmed with TEM on well-annealed samples. Neutron-diffraction studies suggest that the samples quenched from high temperature are more disordered, but that some long-range ordering still persists.[17] While the relation between transition metal ordering and performance is not yet clear, results indicate that the structure of this material changes significantly upon cycling and that these changes may affect the rate performance. A structural model for the changes in this material upon cycling is being developed by combining NMR, XRD, TEM and first principles modeling.

---

[16] A. Van der Ven, G. Ceder, *Electrochemistry Communications* **6**, (2004) 1045-1050.

[17] J. Bréger, N. Dupré, P.J. Chupas, P.L. Lee, Th. Proffen, J.B. Parise, C.P. Grey, *J. Am. Chem. Soc.*, in press (2005).

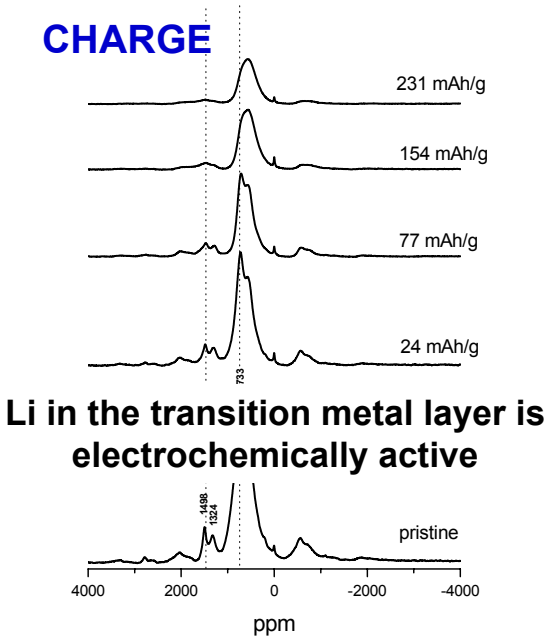

Figure IV-17. Electrochemically active Li in TM layer

Following cycling of the 1/3 material between 2.5V and 4.6 V, the local structure (as probed by Li NMR) changes slowly. The concentration of Li in the transition metal layers drops gradually, so that by 20 cycles no Li in the TM layers remains. The long-range structure (via XRD) changes more rapidly and by 2-3 cycles, evidence for longer-range ordering in the TM layers has disappeared. Similar results are seen for $Li(Ni_{1/2}Mn_{1/2})O_2$ and $Li(Ni_{1/3}Mn_{5/9}Li_{1/9})O_2$; however, it is easier to follow the disappearance of long-range order in the 1/3 material. In contrast, when the material is charged to 5.3V, essentially all of the Li is removed from the material – both from the Li layers and from the transition metal layers. XRD and neutron studies are in progress to follow the changes in Ni/Mn structure during these processes.

Analysis of the XRD patterns of the series $Li[Li_{(1-2x)/3}Ni_xMn_{2/3-x/3}]O_2$ has been completed. These patterns show additional peaks which are ascribed to Li_2MnO_3 (i.e., $Li[Li_{1/3}Mn_{2/3}]O_2$)- like ordering in the transition metal (Ni, Mn and Li) layers. This ordering is rarely perfect, and stacking faults of the layers are observed. These faults result in characteristic broadening and apparent changes in the intensities of the reflections caused by the Li_2MnO_3-type ordering, making a full analysis of the profiles difficult. The study of these faults has now been completed by using the DIFFaX program (Figure IV-18) to model the XRD data.

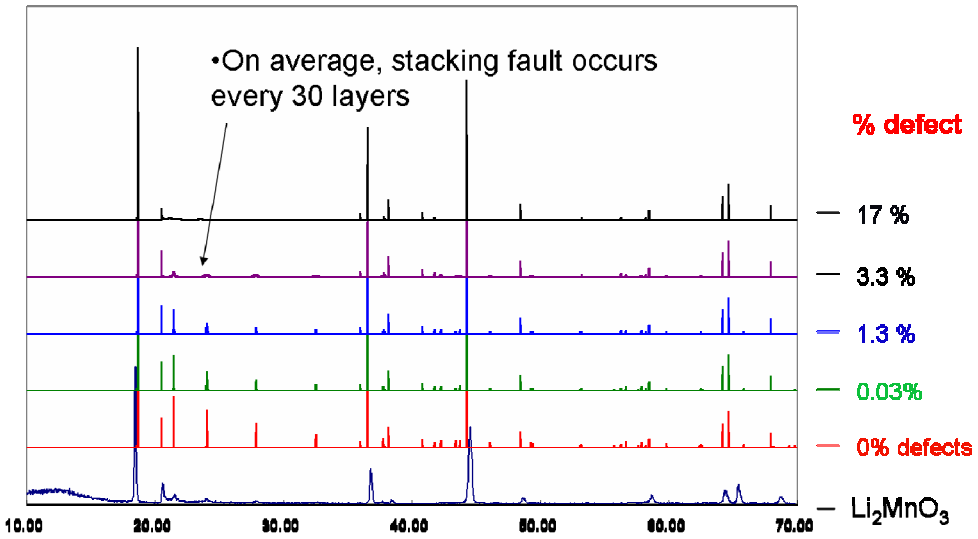

Figure IV-18. Comparison between experimental and simulated XRD patterns (calculated with DIFFaX) for Li_2MnO_3, with C2/m stacking and different percentages of stacking faults.

The results illustrate that Li_2MnO_3 samples that have been heated for 1 day contain ~10 % faults (i.e., a stacking fault on average every 10th [$Li_{1/3}Mn_{2/3}$] layer), while the number of faults drop to only 2% after heating for a month. The x = 1/2 and 1/3 materials contain similar types of stacking faults. Materials can be prepared that show much less order, by using shorter heat treatment temperatures and by quenching from high temperature. Neutron diffraction of the x = 1/2 material has been completed. The pair distribution function (PDF) analysis of the data illustrates that Ni shows a strong tendency to occupy sites near Mn in the transition metal layers. This information, coupled with the NMR data for the same sample, was used to generate a model for the local and long-range ordering in this system, Figure IV-19.

Detailed structural models from NMR, XRD, neutron diffraction, and TEM, developed as part of this work, coupled with predictions from ab-initio calculations, provide a platform with which to correlate changes in electrochemical performance with structural properties.

Some conclusions from this investigation are that:

- Disorder in Li_2MnO_3 is not caused by Li/Mn exchange but by stacking faults in the c direction,
- Li_2MnO_3-$Li(NiMn)_{0.5}O_2$ materials contain strong Li_2MnO_3 like local ordering in the a-b plane and weaker long range ordering, clearly seen by NMR, extended x-ray absorption fine structure (EXAFS), PDF and TEM,
- Stacking faults are again present which reduce superstructure peaks - in XRD,
- Ordering in low Ni materials based on Li_2MnO_3 honey comb - but with Li-Ni avoidance,
- NMR indicates Li-Ni avoidance at high Ni content and PDF calculations show Ni-Ni constraints resulting in “flower-like” arrangements,
- Li in TM layers participates in electrochemistry, and
- Short range order disappears slowly on cycling, but long range order disappears after the 1st few cycles.
- Cycling to high voltages introduces disorder on the 1st charge

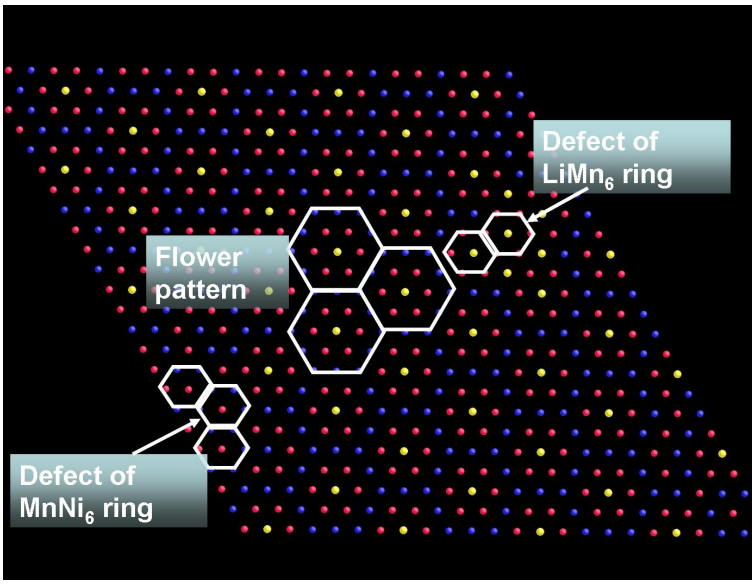

Figure IV-19. "Flower Structure" with defects.

Further Studies on $LiNi_{1-x}Mn_xO_2$. Among the oxides, the layered $LiMO_2$ structure offers good hope for high power provided complete ordering of the Li and M atoms can be achieved. Complete order requires a significant difference in the ionic radius of the Li ion and the mean ionic radius of the M atoms. A low-temperature preparation route has been used for $LiMO_2$ with M = $Ni_{1-x}Mn_x$, x < 0.5, to achieve a high degree of order of the Li atoms in alternate cation layers. Figure IV-20 compares the rate capability for x = 1/3 and 0.4 with that of $LiNi_{1/3}Co_{1/3}Mn_{1/3}O_2$. The X-ray data confirm excellent Li-ion ordering for x = 1/3, and the rate capability of the x = 1/3 sample is comparable to that of $LiNi_{1/3}Co_{1/3}Mn_{1/3}O_2$, but without Co.

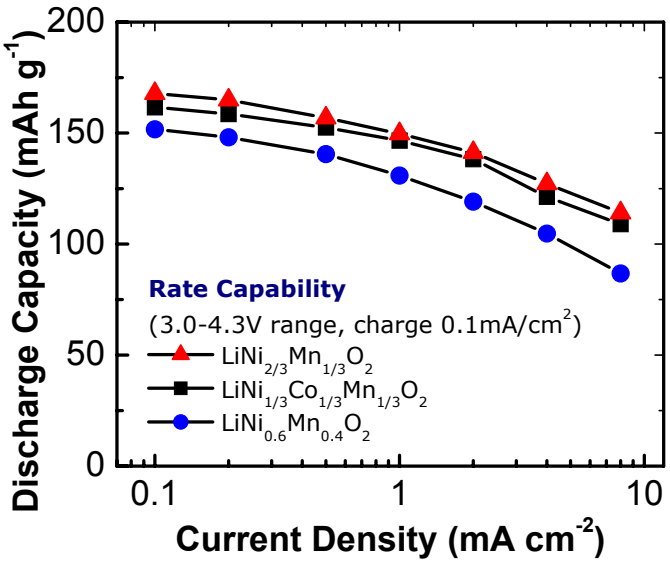

Figure IV-20. Rate capability of cathode materials

In situ XRD Diagnostics – Additional effort continued on the characterization and evaluation of the mixed metal oxides, $Li_xMn_{0.4}Ni_{0.4}Co_{0.2}O_2$. This work is a joint effort between SUNY and BNL on *in-situ* delithiation, and with the National Institute of Standards and Technology (NIST) on neutron diffraction studies of the nickel ordering. *In situ* XRD results indicate that the structural behavior of this material during charge is different than $Li_{1-x}Ni_{0.8}Co_{0.15}Al_{0.05}O_2$ cathodes. Compared with the structural changes of the $Li_{1-x}Ni_{0.8}Co_{0.15}Al_{0.05}O_2$ cathode during charge, the phase transition boundaries in $Li_{1-x}Mn_{0.4}Ni_{0.4}Co_{0.2}O_2$ cathode are smeared out. Other differences in the structural changes indicate better structural stability of the $Li_{1-x}Mn_{0.4}Ni_{0.4}Co_{0.2}O_2$ cathode.

This same compound has been cycled at a number of rates (same rate on charge and discharge). The capacity is shown as a function of rate in Figure IV-21. At low rates the capacity is about 180mAh/g. The capacity of these cells, cycled using a $LiPF_6$ salt electrolyte, decays upon cycling. Although the initial capacities were increased by using a higher charging cut-off voltage, there was only a minimal effect on the capacity after the first 20 cycles; after 50 deep cycles the capacity at a C/10 rate was 140mAh/g for cut-off voltages of 4.4, 4.6, and 4.7 volts.

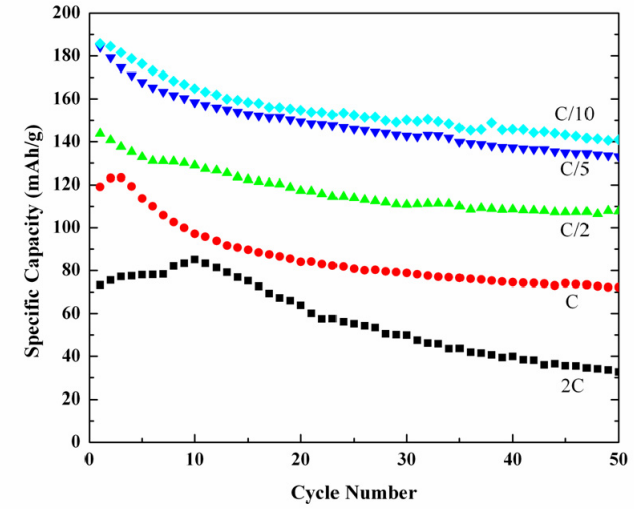

Figure IV-21. Capacity of $LiNi_{0.4}Mn_{0.4}Co_{0.2}O_2$ as a function of discharge rate.

One of the advantages of the x-ray absorption spectroscopy technique is the ability to distinguish between surface and bulk features. Figure IV-22 shows that the surface of the nickel-based cathode materials has a different electronic structure from the bulk. In addition, it as been found that the greater the nickel content in the materials, the more severe is the difference between the surface and the bulk.

Soft XAS (200 to 1000eV) at the O K-edge and the metal L-edges, in both the FY and the PEY mode, has been used to probe the electronic structure of deintercalated $Li_{1-x}Co_{1/3}Ni_{1/3}Mn_{1/3}O_2$. It is interesting to note the differences of Ni $L_{II,III}$-edge XAS spectra for $Li_{1-x}Co_{1/3}Ni_{1/3}Mn_{1/3}O_2$, at various x values, obtained by the two detection modes, PEY and FY. That obtained in the FY mode appeared in a higher energy region compared with those obtained in the PEY mode.

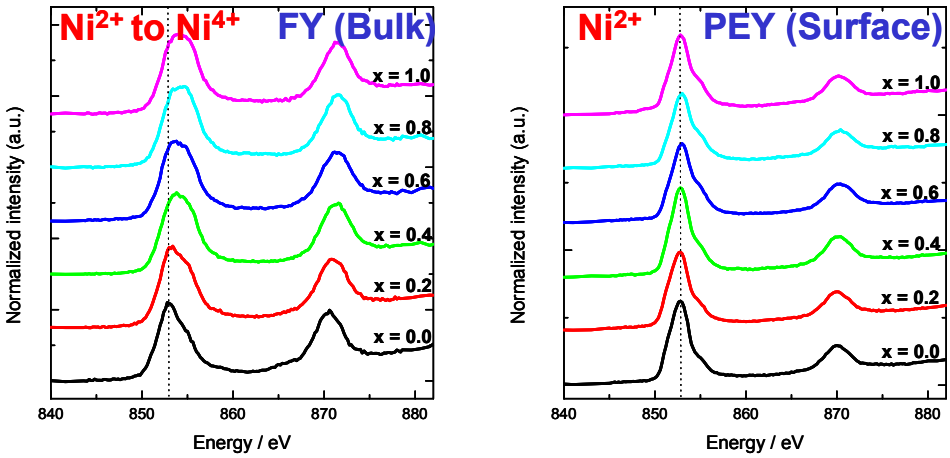

Figure IV-22. Li L-edge XAS spectra of $Li_{1-x}Ni_{0.5}Mn_{0.5}O_2$

Since the PEY and FY probe the surface and bulk respectively, it was concluded that Ni^{2+} ions at the surface are oxidized mostly to Ni^{3+} whereas Ni^{2+} ions in the bulk are oxidized further to Ni^{4+} by comparing the calculated and observed Ni L-edge XAS spectra. This difference in the electronic structure of Ni ions between the surface and the bulk is more distinguishable in the case of $Li_{1-x}Ni_{0.5}Mn_{0.5}O_2$. A previous soft XAS study on $Li_{1-x}Ni_{0.5}Mn_{0.5}O_2$ using both the FY and PEY modes showed that Ni ions on the surface remain mostly unchanged in the Ni^{2+} oxidation state during charge whereas charge compensation in the bulk is achieved mainly by the oxidation of Ni^{2+} to Ni^{4+}. The difference in electronic structures during charge between the surface and bulk is a unique feature of the Ni-based cathode materials.

Cell Modeling – This group has performed a model/experimental comparison of the 1/3 baseline chemistry involving two different cell designs and charging to two different voltages. This study established that a contact resistance was giving rise to ohmic drops. The cell development group has since fabricated an electrode on a carbon-coated current collector. These cells are currently being testing.

Future Plans – Among other tasks, researchers plan to develop rate models for multi-transition metal systems, and to apply them to the Ni-Mn-Co systems. They also plan to develop new first principles tools to perform stability predictions, and to test the capacity fade of ball milled $LiNi_{2/3}Mn_{1/3}O_2$ cathodes.

IV.B New Anode Materials

Objectives

The objectives of the tasks in this area are to replace the presently used carbon anodes with more abuse tolerant materials that, in particular, will be compatible with low-cost manganese oxide and phosphate cathodes and the associated electrolyte.

The project also addresses the need to improve irreversible capacity losses of intermetallic electrodes as well as the low-temperature operation and abuse tolerance of Li-ion cells.

Approach

One approach is to explore, synthesize, characterize and develop inexpensive materials that have a potential about 500 mV above that of pure Li (to minimize risk of Li plating) and have higher volumetric energy densities than carbon. Emphasis has been placed on simple metal alloys/composites, and on intercalating oxides. All materials have been evaluated electrochemically in a variety of cell configurations, and for thermal and kinetic stability.

Another approach has been to search for inexpensive intermetallic electrodes (primarily for EV applications) that provide a capacity of 300mAh/g and ~2000 mAh/l. This work focused on: 1) matrix reactions that, when combined with insertion reactions, may have a stronger chance of success than when topotactic reactions are used alone; 2) determining the rate capabilities of composite electrodes with Al, Si, Sn, and Sb components; 3) pre-lithiation reactions to fabricate charged electrodes for use against non-lithiated metal oxide electrodes and to overcome first-cycle ICL; and 4) low-potential metal oxide negative electrodes coupled with the high-potential layered and spinel cathodes to yield high-rate and abuse tolerant Li-ion cells.

Finally, a theoretical effort has investigated the benefits of higher potential anodes.

Accomplishments

Tin Anodes – Recently, tin foil and expanded tin grids were found to have higher capacities than graphite as a host for Li. However, the capacity rapidly decays after 10 to 15 cycles to values comparable to that of graphite. Earlier research in the BATT program showed that the intermetallic Cu_6Sn_5 showed attractive anodic behavior for several cycles. It was therefore decided to try to stabilize tin foil by binding it to a Cu-support foil through the formation of the above intermetallic, as in solder formation reactions. All the components, the Cu, the Sn and the Cu_6Sn_5 have excellent electronic conductivity and so no conductive diluent should be needed in the electrode system.

The tin-copper foil was prepared mechanically using a rolling machine to form the triple-layered structure, with a Cu-Sn alloy layer, most possibly Cu_6Sn_5, sandwiched between a tin layer and a copper layer. Electrochemical cycling at a current density of 1mA/cm^2 between voltage limits of 0 and 1.4 V is shown in Figure IV-23. The voltage plateaus are similar to those of a pure tin anode reacting with Li, as expected for the layer reacting first with the Li. However, a large capacity loss was observed after the first Li insertion, following which the capacity fell to 250mAh/g; the reason for this is not clear. Current efforts are focused on forming a sample that does not show the large capacity above 0.4 V, which suggests the presence of oxide. This oxide might be formed during the

rolling process, where the local temperature may exceed 100°C, which had to be repeated many times to reach the final thickness of ~50μm. The existence of the oxide affects both the capacity and reversibility as it may separate the tin and copper resulting in a highly resistive interface.

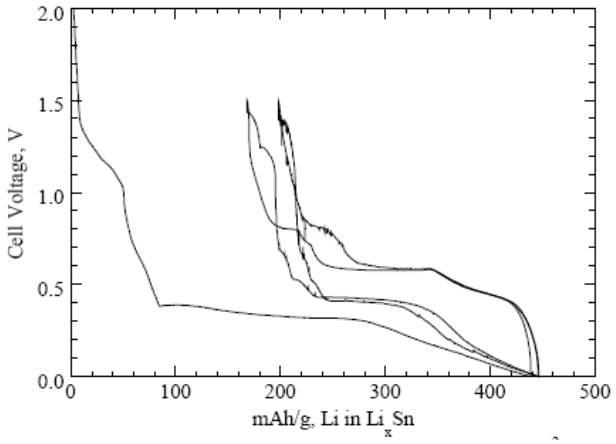

Figure IV-23. Cycling of as-prepared Cu-Sn foil at 1mA/cm^2

Recently, this group reported the electrochemistry of tin foil mounted on copper, which was inferior to tin foil itself and has thus expanded the studies of two reacting phases, the Sn-Bi system, and are exploring manganese oxides as anodes. The bismuth-tin eutectic alloy (Bi:Sn = 58:42 wt%) was mechanically rolled into a 30-40μm thick foil. Figure IV-24 shows the initial 3 sweeps at 1 mA/cm^2. The capacity reached ~550mAh/g, according to $Li_{3.5}$(Sn-Bi). After the first rather featureless Li intercalation, five plateaus are seen in the recharge and discharge processes. These five plateaus correspond to Li_1Bi, Li_3Bi, $Li_{0.4}Sn$, Li_1Sn, $Li_{2.3}Sn$ respectively, clearly showing that both tin and bismuth participate electrochemically.

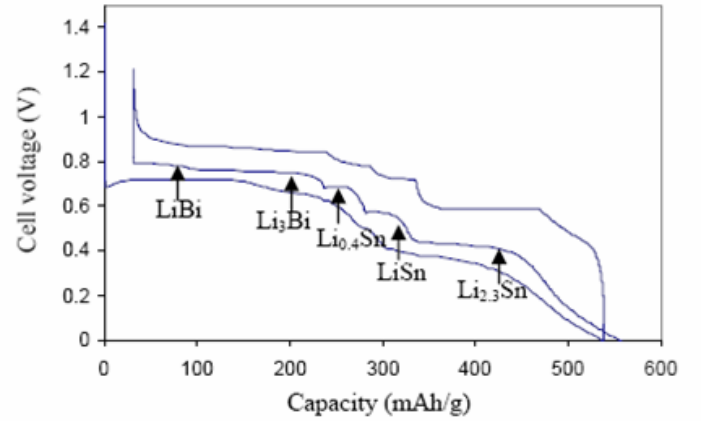

Figure IV-24. Cycling of Sn-Bi eutectic foil

Intermetallics and Li Coating – One group is investigating, in collaboration with FMC Corporation, the utility of a Li metal powder product (Lectro^{TM} Max Powder) which is stabilized by a surface coating of lithium carbonate. The coating significantly increases the air stability of the powder allowing it to be used in a lamination process. FMC, in collaboration with AEA

Technologies in the UK, has already demonstrated the effectiveness of the powder by using it to pre-lithiate graphite anodes when fabricating charged Li_xC_6/LiV_3O_8 and Li_xC_6/MnO_2 Li-ion cells. This powder is being evaluated as a prelithiation agent for non-graphitic anodes such as intermetallic Cu_6Sn_5 and the crystalline metal oxides SnO and $Li_4Ti_5O_{12}$. The purpose is: 1) to determine the extent to which the powder can reduce the first-cycle ICL at negative electrodes, and 2) to evaluate the differences between reactions of Lectro^{TM} Max Powder with insertion compounds (*e.g.*, graphite and $Li_4Ti_5O_{12}$) and with compounds that operate by displacement reactions (*e.g.*, SnO and Cu_6Sn_5). A major advantage of using Lectro^{TM} Max Powder is that the amount of Li to be added to the electrode can be accurately controlled.

Electrode laminates of SnO were pre-made; thereafter, various amounts of Lectro^{TM} Max Powder were added to the electrode surface prior to calendaring. There was little evidence that the SnO was reduced by this process or by the addition of electrolyte, as reflected by the OCV of fresh cells (2.2 V *vs.* Li). The ICL expected for the reaction: $2Li + SnO \rightarrow Li_2O + Sn$, which occurs before the formation of Li_4Sn, is 33%. This was confirmed by the initial discharge-charge reaction of Li/SnO cells. The addition of Lectro^{TM} Max Powder, for both 1.4 and 3.5 Li/SnO, increased the capacity but did not significantly reduce the ICL (Figure IV-25).

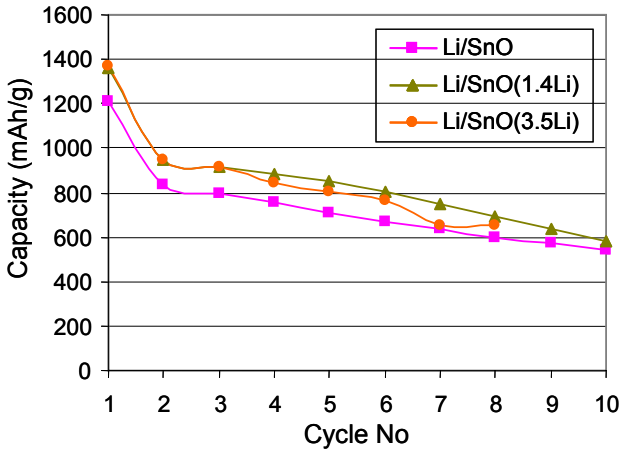

Figure IV-25. Capacity vs cycle number for Li/SnO cells

Lithium-ion cells with the configuration C(GDR)/$Li_4Ti_5O_{12}$ and Cu_6Sn_5/ $Li_4Ti_5O_{12}$, in which Lectro^{TM} Max Powder was used to prelithiate the GDR graphite and Cu_6Sn_5 electrodes, were evaluated. In both instances, good cycling stability was achieved for the initial 30 cycles, the $Li_4Ti_5O_{12}$ electrode yielding ~80% of its theoretical capacity (175mAh/g) (Figure IV-26). One conclusion from these preliminary studies is that Lectro^{TM} Max Powder is effective for prelithiating insertion electrodes such as electronically-conducting graphite that can react immediately to form Li_xC_6, whereas electrodes that operate by displacement reactions, such as SnO and Cu_6Sn_5, may not react readily with the powder, presumably as a result of insulating surface layers, reaction kinetics and activation barriers, and particle size restrictions that prevent the prelithiation reactions from proceeding to completion.

This group has also initiated studies to determine the rate capability of several intermetallic compounds. Cu_6Sn_5 and Cu_2Sb were selected for the initial investigations.

Lithium reacts with these copper-based compounds by two distinct processes:

1) Li insertion, which is accompanied by partial copper extrusion, to yield a ternary intermediate compound (Li_2CuSn and Li_6CuSb), and
2) Additional lithium insertion that leaves an active lithium Zintl phase ($Li_{3+x}Sn$ and Li_3Sb) and extruded nano-grained copper metal.

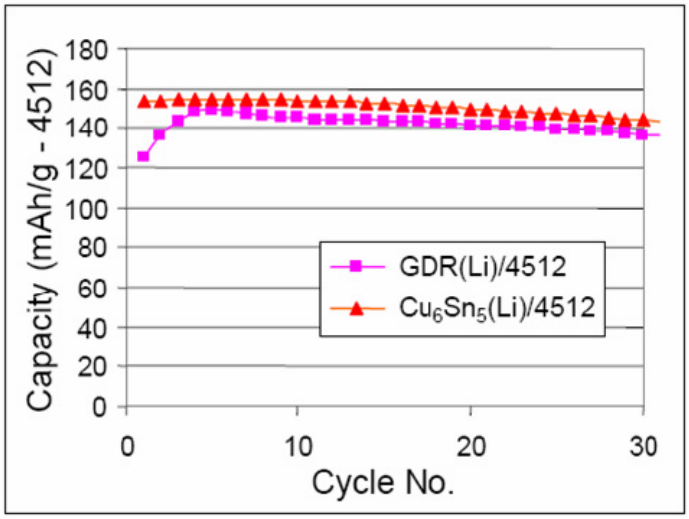

Figure IV-26. Capacity vs. Cycle No.: C/$Li_4Ti_5O_{12}$ and Cu_6Sn_5/$Li_4Ti_5O_{12}$ cells

The two processes occur at different potentials. The cycling stability and rate capability of these electrodes are dependent on the selected voltage window, the extent of metal displacement, and side reactions with the electrolyte. The effect of conductive additives, such as copper or silver, on the parent electrode matrix was also explored.

The Cu_6Sn_5 and Cu_2Sb materials were synthesized by ball-milling and sieved to 10-15μm size. Additives, such as acetylene black, copper (< 50 μm), or silver (< 50 μm) were added to the electrode at the mixing stage. Lithium half cells were constructed and tested over two different voltage windows (2.0-0 V and 1.2-0.2 V for Cu_6Sn_5; 2.0-0 V and 2.0-0.6 V for Cu_2Sb). Capacity data were collected over these potential windows using five different rates for 10 cycles. Data from the 5th cycle were typically used for the capacity vs. current rate plots in Figure IV-27; literature data for graphite electrodes (SFG10) are included for comparison.[18]

In general, Cu_6Sn_5 electrodes did not cycle well when cycled over the whole potential window (2.0-0 V), nor did they provide any rate advantage over SFG10. By contrast, Cu_6Sn_5 electrodes with an Ag additive and a smaller voltage window, showed a superior rate capability, at least between C/10- and a 1C. On the other hand, Cu_2Sb electrodes with an AB additive (10-20%) exhibited a slightly superior rate capability than SFG10 when cycled between 2.0 and 0.6 V. The best performance was obtained from a Cu_2Sb (70%), AB (20%), binder (10%) electrode, which delivered approximately

[18] B. Veeraraghavan et al, J. Electrochem. Soc., **149**, A675 (2002).

30% higher capacity than SFG10 at a 2C rate. Adding metallic copper or silver to Cu_2Sb was detrimental to electrochemical performance.

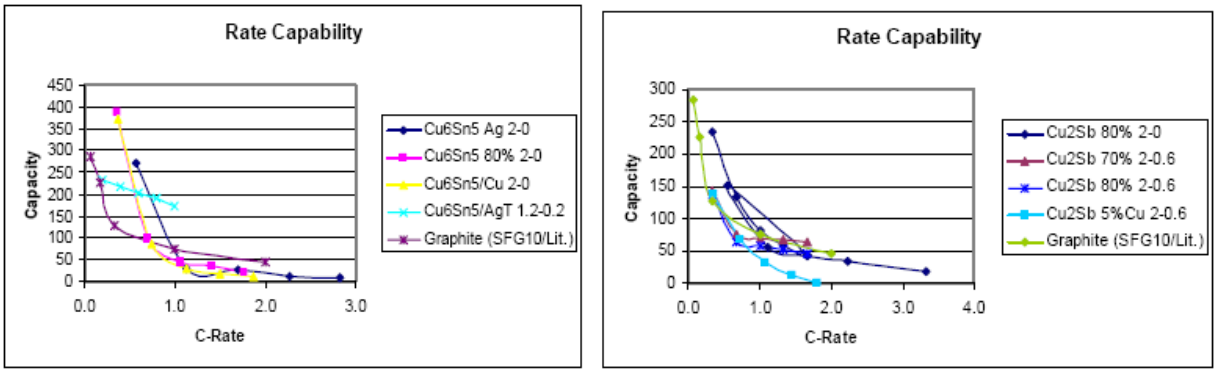

Figure IV-27. The effect of various conductive additives on the rate performance of Cu_2Sb and Cu_6Sn_5 at room temperature compared to graphite (SFG10).

Cell Modeling – Finally, the modeling team has investigated the benefits of higher potential anode materials. Side reactions (*e.g.*, SEI formation, Li deposition) can be avoided with a high-potential negative electrode. Lithium titanate was compared with graphite (*vs.* the Gen 2 cathode), as shown in Figure IV-28, with optimization carried out over positive electrode thickness and porosity.

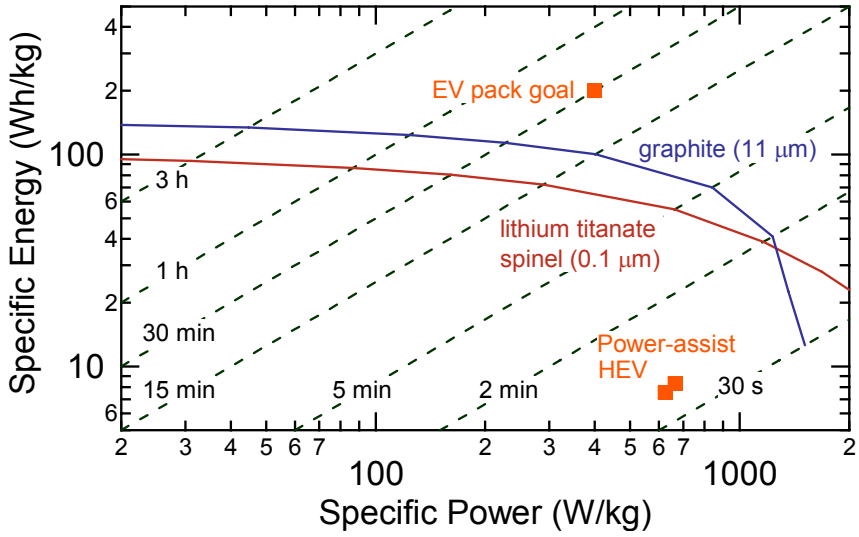

Figure IV-28. Optimized Li-titanate Spinel

Future Plans

Researchers plan to continue studies on LectroTM Max Powder to reduce the ICL of intermetallic and metal oxide (SnO) electrodes. In addition, they will determine the extent of reaction between Li powder and metal oxide and intermetallic compounds. Finally, researchers plan to evaluate 'composite' positive electrodes against the selected anodes, exploit ICL at high potentials, and continue low temperature rate studies on selected anodes

IV.C Novel Electrolytes and Their Characterization

Objectives

The objectives of this task area are to

- Determine and quantify the improvement (if any) in abuse tolerance of polymer gel electrolytes over liquid electrolytes.
- Determine the limitations on Li-ion transport in polymer gel electrolytes and develop materials capable of high-power operation at ambient temperature with lithiated carbons/Li metal alloy anodes and high-voltage cathode materials.
- Determine the feasibility of Li metal electrodes with polymer gel electrolytes and provide operating conditions that prevent dendrite growth at HEV rates.
- Synthesize new salts for which anion attachment to a suitable plasticizer, scaffold, or matrix can be accomplished; characterize battery electrolytes made from the salts.
- Gain a fundamental understanding of the transport mechanism in single ion conductor (SIC) gel electrolytes and develop new electrolytes with improved transport and mechanical properties. In addition, understand Li transport in the SEI layer.

Approach

One of the approaches used involves fabricating and testing polymer cells with an optimized gel formation which is a function of plasticizer content, and evaluation of a new polymer with an ionic liquid or liquid electrolyte as plasticizer. This effort included synthesizing and coating electrodes with low-cost materials to evaluate them in Li /polymer cells. The gel electrolyte has been compared to a liquid electrolyte at low temperatures.

Another approach is to synthesize and characterize new polymeric electrolytes, including gel and nano-structured dry polymer electrolytes. Polymers are characterized by methods such as neutron scattering, dielectric relaxation spectroscopy, rheology, and light scattering to obtain new insights into the rate-limiting transport processes. Another approach applies physical organic chemistry to electrolyte design, thereby ensuring that the sources of poor performance and failure are pinpointed and also that the problem can be corrected through materials design and synthesis.

Another team is using surface-functionalized fumed silica fillers to determine the effects of filler type and concentration on interfacial stability and cell cycling. Electrochemical characteristics are correlated with mechanical properties and materials chemistry.

Synthesis and detailed characterization of a number of SIC and ionic liquids is being performed. The structure of the SIC is varied along with the fraction of the plasticizer (EC) in gel electrolytes in order to optimize the ion transport and mechanical properties. MD simulations are being performed on transport in the electrolytes and near the SEI layer to understand structural properties and Li transport of these battery components.

Accomplishments

Evaluation of Polymer Cells – To characterize the impact of various cell parameters, effort was recently focused on the effect of a new polymer gel having low molecular weight in cells with a graphite anode and a $LiFePO_4$ cathode. The polymer is coated on a polypropylene (PP) separator

and cross-linked by two different methods: a) thermally at 60°C for 1 h, b) hybrid cross-linked by thermal and UV. In the second method, the polymer electrolyte was cross-linked first with UV, sealed in the cell, and then cross-linked thermally at 60°C for 1 hour. In both cases, the polymer electrolyte was first filled in the pores of the electrodes before UV cross-linking. Half cells of Li/EC-DMC- $LiPF_6$ gel/graphite (anode cell) and Li/EC-DMC-$LiPF_6$ gel/$LiFePO_4$ (cathode cell) that contain thermally cross linked and hybrid cross linked gels were compared with standard liquid cells.

Figure IV-29a shows the first 2 cycles at C/24 of the anode cells at 25°C. For the anode cell with gel obtained thermally, the initial (first-cycle) Coulombic efficiency is 85% and the reversible capacity is 342mAh/g. For the anode cell with hybrid cross link gel, the Coulombic efficiency is 83% with a reversible capacity of 347mAh/g. The standard anode cell shows 86% Coulombic efficiency and 337mAh/g reversible capacity respectively. For the $LiFePO_4$ half cells, a comparable result (Figure IV-29b) was obtained for a hybrid-polymer gel cell and a liquid cell, *i.e.*, 88% Coulombic efficiency for both cells and 156mAh/g and 155mAh/g for the reversible capacity respectively. These data confirm the good performance of the gel polymer obtained by the hybrid method. Figure IV-30 shows the cycling of the $LiFePO_4$ material vs. graphite at 60°C.

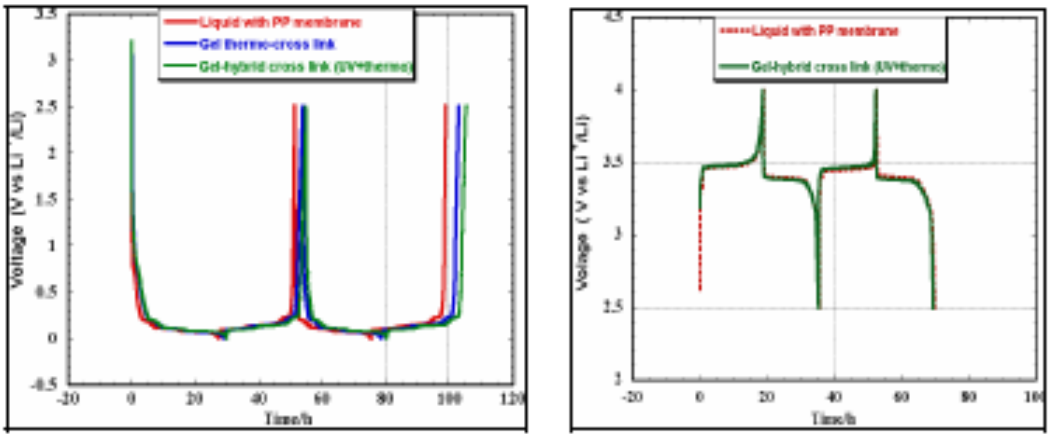

Figure IV-29a. Cycles 1 and 2 of anode half-cells with thermal gel polymer, with hybrid gel polymer, and with liquid standard in EC-DEC-$LiPF_6$. **b)** Cycles 1-2 of $LiFePO_4$ half cells with hybrid gel polymer electrolyte compared to liquid standard in EC-DEC-$LiPF_6$.

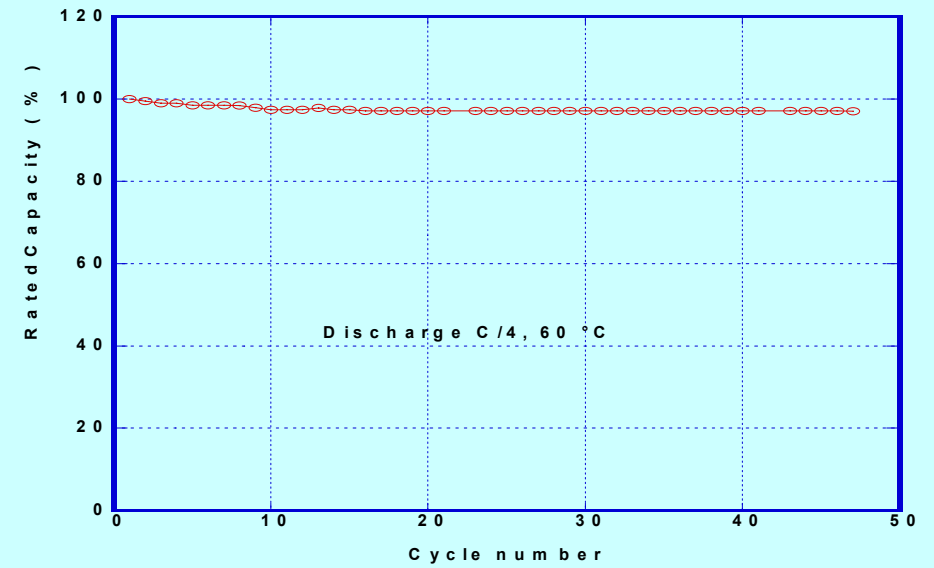

Figure IV-30 Cycling of $LiFePO_4$ at 60°C.

Nanostructured Polymer Electrolytes – One team has investigated the electrical, mechanical, and morphological characteristics of a series of a poly(styrene-block-ethylene oxide) diblock copolymer (PS-b-PEO) system, Figure IV-31. The concept of this material is to impede the growth of Li dendrites while providing tunnels for Li transport. Characterization tools include small angle X-ray scattering (SAXS), TEM, optical birefringence, and rheology. LiTFSI, was added to each sample (at an [EO]/[Li] ratio of 50) for ionic conductivity measurements. AC impedance measurements were made on these membranes to obtain the bulk ionic conductivity, Figure IV-32. The system's conductivity increases by a factor of four when the PEO volume fraction changes from 0.38 to 0.40, perhaps due to the formation of a continuous network of PEO channels. The conductivity values are approximately one quarter that of pure PEO with the same salt concentration and temperature. Below 60°C, PEO domains remain crystalline in the diblock copolymer.

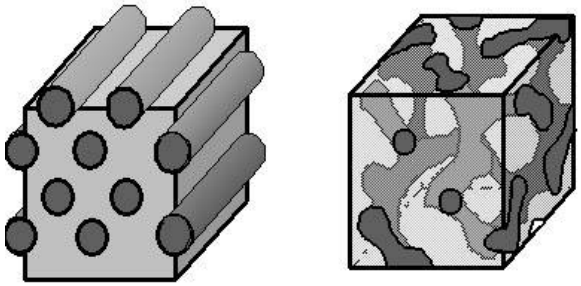

Figure IV-31. Schematic of a nanostructured polymer electrolyte

Next, the effect of salt (LiTFSI) on the crystallinity of the PEO domains was investigated. The salt acts as a plasticizer in PS-b-PEO, the crystallization of the PEO domains is suppressed at room temperature at a salt concentration corresponding to an [EO]/[Li] ratio of 15. The mechanical property of this polymer electrolyte system does not change much with temperature below the glass

temperature of polystyrene (~90°C). At 80°C, preliminary indications are that the modulus of this material exceeds the upper limit of the rheometer being used, ~10^8 Pa.

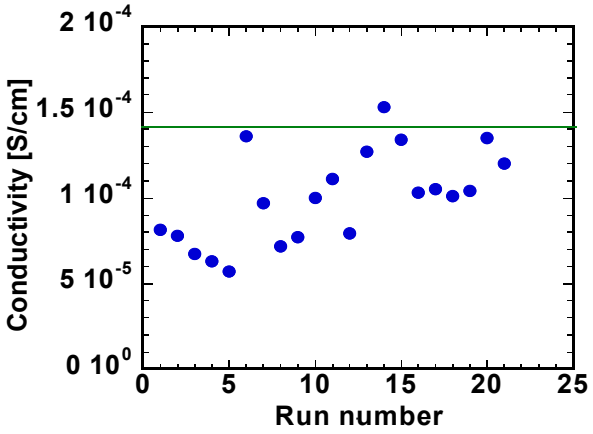

Figure IV-32. Conductivity (vs maximum) of nanocomposite polymer with [EO]/[LiTFSI]=50

A sample with volume fraction of 0.40 thus has half the ionic conductivity of pure PEO but a modulus that is at least two orders of magnitude greater than pure PEO. Tests of the stability of the Li/polymer interface of the nanostructured electrolytes are currently underway.

Abuse Tolerance of Gel Electrolytes – The purpose of this work is to understand the possible abuse tolerance advantage provided by gel polymer electrolytes. Chemical reactions of ethylene oxide based polymers and solvent components (EC, EMC) with Lewis acid salts ($LiPF_6$, $LiBF_4$, $LiAsF_6$, LiBOB) have been investigated using GC/MS, GPC and CE in addition to cell cycling with Li metal symmetrical cells. Comb-branch polymer electrolytes based on ethylene oxide units combined with Li salts were cycled with Li metal for extended periods. LiTFSI and LiBETI could be cycled indefinitely with no sign of dendrite formation, however, the Lewis acid salts behaved poorly, Figure IV-33.

Post-mortem GC analysis of the cycled cells showed little or no reaction with the well-behaved salts but many reaction products for the Lewis acid salts. Control reactions with electrolytes sealed in cells in contact with Li metal and with stainless steel electrodes showed that the products were formed with the Lewis acid salts regardless of the presence of the electrodes.

It has been observed that LiF is apparently soluble in pure EC and PC but insoluble in linear carbonates such as DMC and EMC. The reactivity of $LiPF_6$ in Li-ion electrolytes will depend on the solubility of LiF. $LiPF_6$ is completely stable in water as the LiF is soluble. In cases where the LiF precipitates, the PF_5 is sufficiently long-lived to react in another fashion such as on the EC or on PEO ether chains. More detailed studies of these reactions are underway.

Transport property measurements of LiTFSI- Poly(trimethylene oxide) (PTMO) have been carried out. The concentration cell data for the LiTFSI system show a much smaller variation in potential with concentration than with PEO. This is consistent with the lower dielectric constant of the

trimethylene oxide (TMO) system. These experiments are carried out to complete work on dry Li/polymer systems as well as provide a comparison for the gel systems that will be prepared by addition of solvent components to the cross linked polymers.

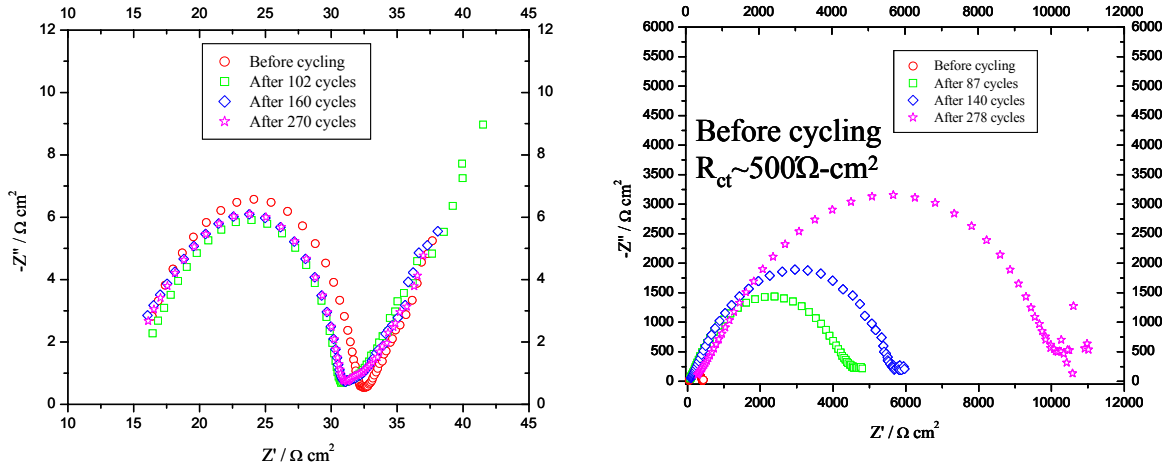

Figure IV-33. a) Li/LiTFSI /PEPE4coE2Allyl (EO/Li=20)/Li. b) Li/$LiPF_6$/PEPE4coE2Allyl (EO/Li=20)/Li impedance with cycling

Fumed Silica and other Gel Electrolytes – This work continues the exploration for suitable gel electrolytes for Li-ion batteries. This team has investigated liquid 1M LiBETI (3M)/ EC:PC:DMC:DEC (1:1:1:1) and a gel with a blend of 10 wt% fumed silica + the above liquid. Three types of fumed silica were employed and gel behavior was observed for all; that is, the elastic modulus exceeds the viscous modulus and is independent of frequency. The fumed silica has a negligible effect on conductivity. Cycling of Li(Ni)/electrolyte/Li cells shows that fumed silica improves the interfacial stability both at room and low temperature (3 ~ 5°C). The cycling efficiency is also improved.

The effect of various Li salts on the ionic transport of composite electrolytes containing single-ion conducting fumed silica[19] has been studied Figure IV-34. Four different Li salts were used, all of which improved conductivity. Although the Li transference number decreases with salt addition, it remains high relative to the electrolyte with Li salt as the sole charge carrier. Among the four salts examined, LiTFSI and LiBOB have a better ability to increase the conductivity and maintain a higher transference number than LiBETI and Li_3PO_4.

An effort has begun to investigate the effects of adding fumed oxides to BATT baseline liquid electrolytes. Two liquid electrolytes were used: 1M $LiPF_6$ + EC: DEC (1:1, vol) and 1M $LiPF_6$ + EC: EMC (1:1). Three types of fumed oxides were used: aluminum oxides (neutral and weakly acidic), silica oxides (A200 and R805), and aluminum and silica oxide mixture (COX84, 84% SiO2 + 16% Al_2O_3). Fumed aluminum oxides do not form a gel. A200, R805 and COX84 form gel electrolytes in the above two liquid electrolytes. Conductivity has been measured from -3 to 68°C. The conductivities of composite gel electrolytes are slightly lower than the counterpart liquid

[19] [Degussa R711-poly(lithium 2- acrylamido-2-methyl-1-propanesulfonate), R711-pLiAMPS, surface Li content γ = 4.2 nm^{-2}] + PEGdm (MW = 250, Li:O = 1:20)

electrolyte at all temperatures; the filler types (silica oxide and oxide mixture) and the surface groups do not have a significant effect on conductivity at the experimental conditions employed.

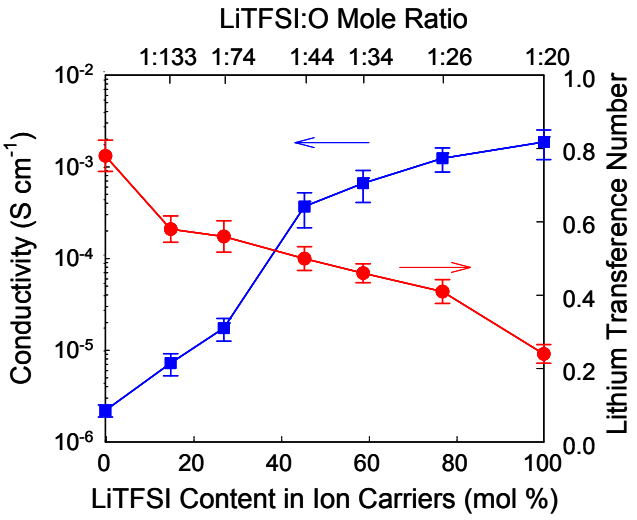

Figure IV-34. Conductivity and transference number using R711-pLiAMPS

This group has also investigated in the ability of composite electrolytes to inhibit dendrite formation, Figure IV-35. It has been found that increasing the high- to low-MW PEO mass ratio decreases dendrite formation, and that the elastic moduli for the 3:1 and 1:1 PEO600K/ Polyethylene glycol (PEG)dm250 blends show little difference.

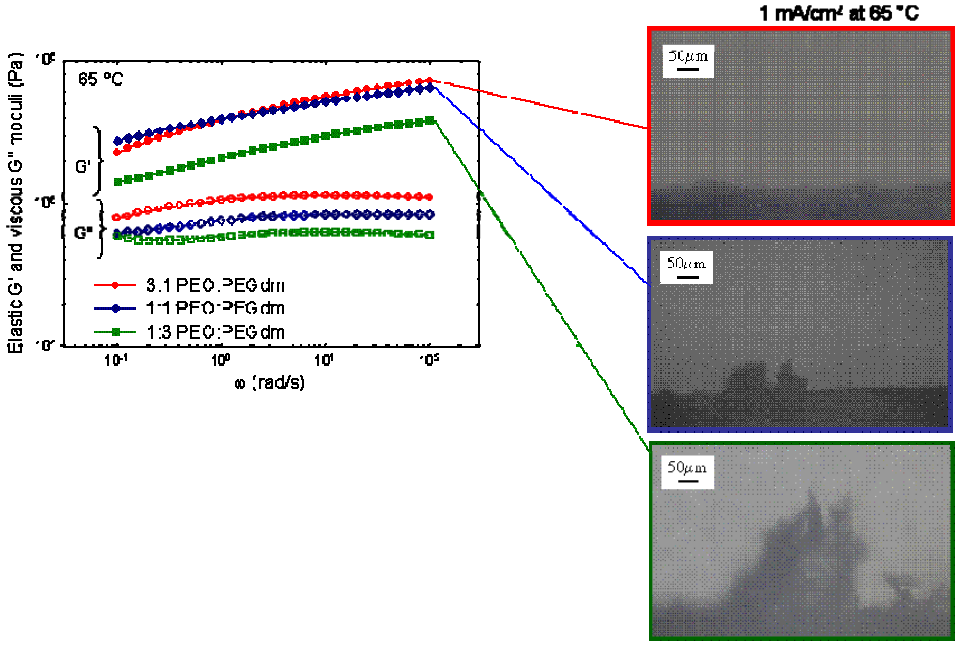

Figure IV-35. Dendrite formation in PEO:PEG blends

Single Ionic Conductors and Ionic Liquids – Progress was made in synthesizing and characterizing ionic melts which are being investigated as low cost, stable electrolytes for Li-ion and Li-metal batteries. Conductivity data were acquired for all materials, with the highest conductivities being realized for the material with X = PEG monomethyl ether of MW 550 (avg. of 11.8 EO units per chain) and salt = $SO_2N(Li)SO_2CF_3$. It is thought that this material provides the optimal combination of Li dissociation, melt viscosity, and EO:Li ratio to achieve high conductivity. Figure IV-36 shows conductivity data for two ionic melts, one with a fluorosulfonate anion and the other with a fluorosulfonimide anion linked to a PEG chain.

Work has begun to scale up the synthesis of ionic melts to produce amounts adequate for cycle testing and further reactivity testing. A special effort is required to keep the entire reaction mixture cool, since the reactions involved are highly exothermic and prior project work has showed that warm conditions can result in undesired side products.

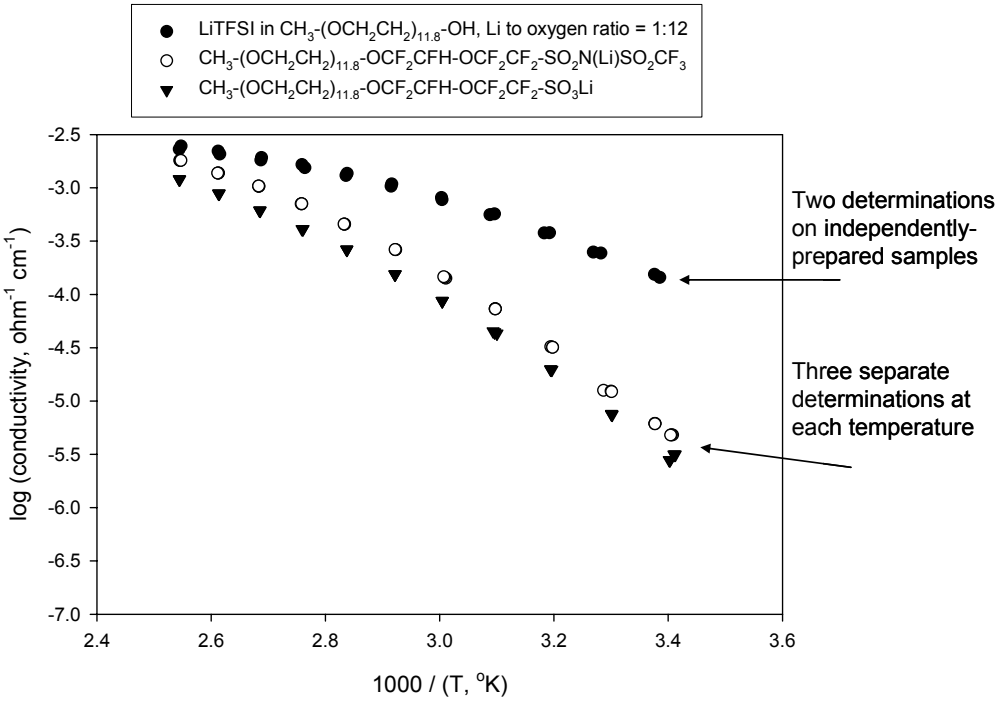

Figure IV-36. Conductivity of ionic melts.

Molecular Dynamics Simulations of Electrolyte and SEI Properties – Molecular dynamics offers one theoretical approach to understanding the fundamental limitations of various materials, and perhaps, to understand how to modify those materials on an atomic scale to improve their properties. This project is investigating the conductivity of solid and liquid electrolytes, and dynamics near the SEI layer which plays a large role in battery performance.

This work includes simulations of a number of ionic liquids with the structure LiTFSI-$(EO)_n$-LiTFSI, with n=12, 20, 40; gel and dry single-ion conductors with the (trifluoromethansulfonyl) imide anion immobilized on the comb branched polymer-host side chains with and without EC

plasticizer, and studies of the same gel electrolyte with pentaglyme. It is expected that changing the plasticizer from EC to the pentaglyme may lead to more Li complexation by the plasticizer than the polyelectrolyte host which may result in changes of the Li transport mechanism from diffusion coupled to the polymer matrix, to one involving transport by the plasticizer.

Temperature dependent conductivity was investigated for the $PEPE_{10}LiTFSI$ single ion conductor, $PEPE_5TFSI\text{-}Li + EC_6$ gel SIC, $PEPE_5TFSI\text{-}Li + EC_6$, and $LiTFSI\text{-}(EO)_n\text{-}LiTFSI$ ionic liquid and is shown in Figure IV-37. The gel SIC exhibited the smallest activation energy and the largest conductivity at low temperatures. Extrapolation to room temperature yields a value of 0.1 mS/cm for a relatively low weight fraction of plasticizer, 37 wt%. Extrapolation of the dry SIC and ionic liquid conductivity yields $\sigma(RT) \sim 0.02$ mS/cm.

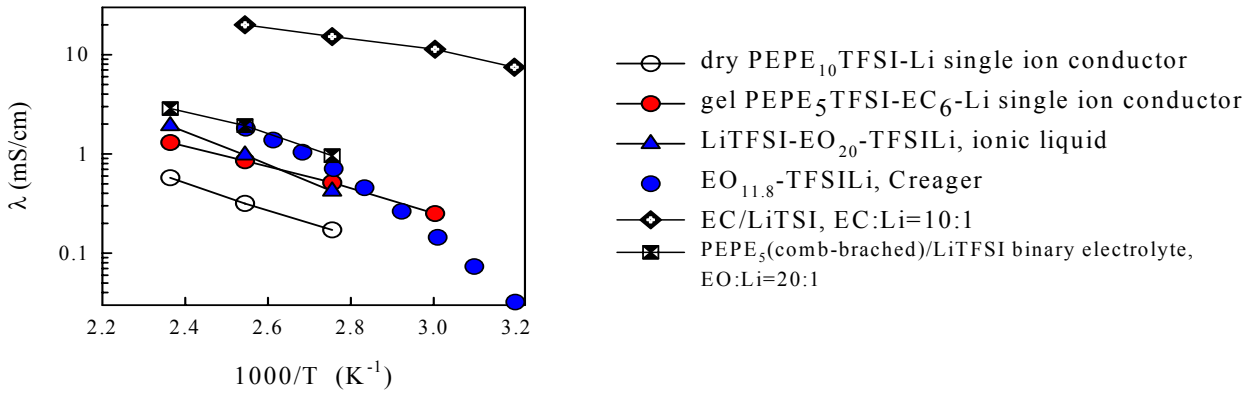

Figure IV-37. Temperature Dependence of Liquid, Plasticized and Dry Electrolytes

This group has also recently begun investigating the behavior of various salt/solvent combinations near an SEI. Li^+ transport from electrolyte to SEI layer and electrode requires overcoming additional free energy barriers associated with the presence of interface structures. The free energy for a Li to approach a neutral surface depends on the nature of the electrolyte. Specifically, Li is able to approach a neutral surface in EC/LiTFSI with no free energy penalty up to 3 Å, whereas the neutral surface from PEPE-TFSI-Li dry single ion conductor has a higher free energy barrier, Figure IV-38. Further insight into mechanism of ion transfer from electrolyte to passivation layers will be obtained from non-equilibrium simulations.

Future Plans

Evaluation of Polymer Cells – Investigate the effect of the gel electrolyte on other baselines chemistries, including $LiMn_2O_4$ and $LiNi_{1/3}Mn_{1/3}Co_{1/3}O_2$. Determine the composition of the anode (soft and hard carbons) and cathode material as a function of the content of gel electrolyte. Hydro-Québec will fabricate $LiFePO_4$ cathodes with water soluble binders (WSB) and other BATT baselines chemistries. These electrodes will be sent to LBNL for interfacial studies and Raman spectroscopy characterization. Collaborations will be established with other groups in the BATT program to select the appropriate cross link agent, amount of plasticizer and additives to obtain better electrochemical performance at low temperature. Test the stability of the Li/polymer interface in nanostructured electrolytes, commence cell testing. Evaluate the effects of cross-linking on gel formation (UV, infrared (IR) and thermal) with ionic liquid. Study the cyclability of carbon and $Li_4Ti_5O_{12}$ as reference in contact with ionic liquid and gel electrolyte

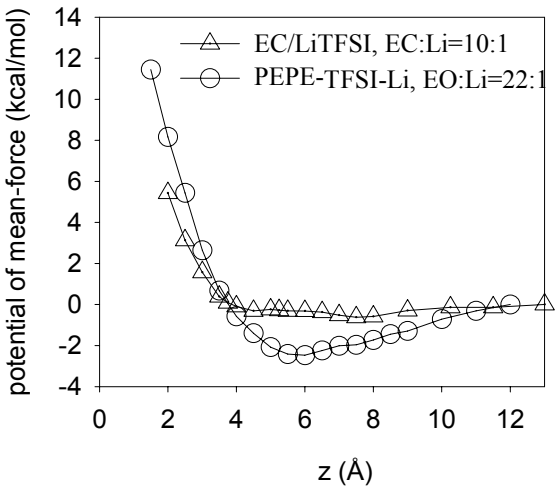

Figure IV-38. Potential of mean-force perpendicular to the neutral surface for EC/LiTFSI and $PEPE_5TFSI$-Li

Transport Property Determination – Demonstrate the ability to rapidly predict and/or measure transport properties of liquid electrolytes.

Single Ionic Conductors and Ionic Liquids – Scale-up processing of synthetic ionic liquids from grams to tens-of-grams. Perform polarization testing in Li | electrolyte | Li cells. Perform spectroscopic studies of ion-pairing and ion diffusion and compare with model results. Compare conductivity data with recent results from MD studies on similar materials to help improve understanding of the factors affecting Li transport in polyether-based ionic melts.

Molecular Dynamics – Gain further insight into mechanism of ion transfer from electrolyte to passivation layers from non-equilibrium simulations.

IV.D Li-Ion Modeling, Diagnostics, and Cell Analysis

Objectives

The primary objective of the modeling and diagnostics tasks is to establish correlations between electrode changes, interfacial phenomena, and cell degradation and failure.

The objective of the cell development task is to establish a test vehicle for the evaluation of new materials for high-power or high-energy, low-cost Li-ion cells. One project is investigating protecting cells against overcharge by means of lightweight, inexpensive protection mechanisms.

In addition, researchers are determining the influence of corrosion and passivation of Al current collectors on the capacity loss of Li-ion batteries.

Approach

The diagnostics team carries out structural characterization of active electrode components before, during, and after cycling. Specifically, *in situ* FTIR spectroscopy is used to study the interfacial chemistry in model electrode/electrolyte systems, particularly at low temperature. The spectrometer optics and spectro-electrochemical cell enable any electrode material to be studied. FTIR spectroscopy is accompanied by classical electroanalytical methods such as cyclic voltammetry and the rotating ring-disk electrode (RRDE). Additional diagnostics approaches include the use of:

- XRD, vibrational spectroscopy, and electroanalytical testing to address the primary causes of power and capacity fade by correlating them with changes in the composition and structure of active materials.
- A combination of *in situ, ex situ,* and time-resolved synchrotron techniques to characterize electrode materials. *Ex situ* soft XAS is used to distinguish between surface and bulk processes using both electron yield and fluorescence yield detectors. Time-resolved XRD techniques are also used to understand the reactions that occur in charged cathodes at elevated temperatures. Hard and soft XAS are used to study the charge-compensation mechanisms of cathode materials during cycling.
- *In-situ* and *ex-situ* Raman microscopy, scanning probe microscopy (SPM), spectroscopic ellipsometry, SEM, and high resolution transmission electron microscopy (HRTEM) are used to characterize cell components taken from baseline cells, fresh electrode materials, and thin-film or single-particle electrodes materials. Data collected includes changes in electrode surface morphology, structure, electronic conductivity, electrode surface chemistry, and SEI thickness and composition, all of which accompany cell cycle-life tests.

To improve performance, researchers are developing simulations to identify the best particle morphologies for both energy- and power-dense systems. This information is then used to develop improved anodes and cathodes by altering the content and morphologies of conductive materials. Specifically, they are developing scale-bridging models to determine the likely electrochemical performance of cathode materials, taking account of the effects of particle shape and connectivity, and determining the effect of mechanical compression, accounting for both multiple layers and cell compression.

The Al current corrosion project consists of three tasks. In Task 1, the influence of corrosion and passivation of Al current collectors on battery capacity is quantitatively evaluated. In Task 2, water concentrations ranging from 2 to 100 ppm are added to battery electrolytes with salts of $LiPF_6$ and LiBOB to investigate the influence of water contamination on the corrosion and passivation of Al current collectors. In Task 3, electrochemical tests and *in situ* Raman spectroscopy are employed to probe the mechanism of corrosion of Al current collectors.

The cell development task has focused on standardizing the cell making process and on producing repeatable cells. Novel components developed by other BATT researchers are incorporated into a standardized cell, and then tested using a standard protocol to determine cell capacity, energy, power, and lifetime characteristics. Tested cell components are then delivered to appropriate investigators involved with diagnostic projects.

Accomplishments

Interfacial Chemistry at Low Temperature – A fundamental understanding of the behavior of Li-ion cells at low temperature is critical for reducing the large impedance that arises in many such cells at low temperatures. This task involved the study of interfacial chemistry at low temperatures. The first experiments focused on interfacial phenomena observed with gen 2 anodes (MAG-10) in different electrolytes, standard gen 2 and a low-T version of gen 2 electrolyte, EC:PC:DMC (1:1:3) with 1M $LiPF_6$. Swagelok cells were used with Li counter electrodes, and *ex-situ* analysis of the graphite anodes was carried out using a combination of FTIR and XPS. Parallel experiments on Li deposition on non-carbon (Ni) electrodes were performed in the same electrolytes to establish the FTIR signatures of the SEI layer on metallic Li versus graphite.

Graphite anodes went through room temperature formation cycling at C/25 followed by HPPC testing. They were then placed in an environmental chamber, subjected to (modified) HPPC testing at –30°C, then returned to room temperature, and HPPC tested again before the electrodes were removed from the cells and examined by FTIR. In both electrolytes, the ASI increases by more than one order of magnitude at –30°C for both charge and discharge processes. The anode potential was considerably more negative during the charging pulse in the gen 2 *vs.* the EC/PC/DMC electrolyte. A typical FTIR plot is shown in Figure IV-39.

An SEI layer characteristic of metallic Li was observed after HPPC cycling at –30°C in the gen 2 electrolyte, but it was readily washed off by rinsing with DMC. The remaining SEI was identical to that formed at RT. There was clear evidence that Li was deposited on top of the graphite SEI formed at RT, a result that was probably due to a large potential drop in the electrolyte at –30°C. No spectroscopic signature of Li deposition after HPPC at –30°C in EC:PC:DMC was seen, Figure IV-40. The SEI composition appears to be identical to that formed in gen 2, although possibly thicker. A higher electrode potential during the charge pulse (+0.1 *vs.* –0.5 V *vs.* Li/Li^+) was consistent with spectroscopy. A higher electrolyte conductivity appears to provide an explanation for the absence of Li deposition during charge in EC/PC/DMC.

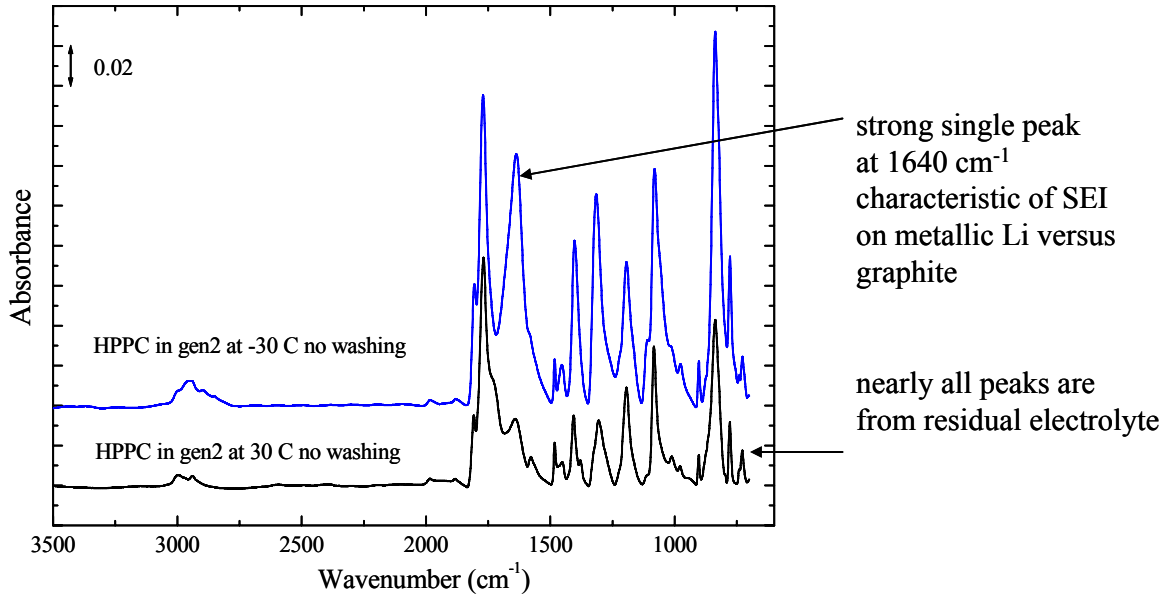

Figure IV-39. FTIR Analysis after HPPC testing

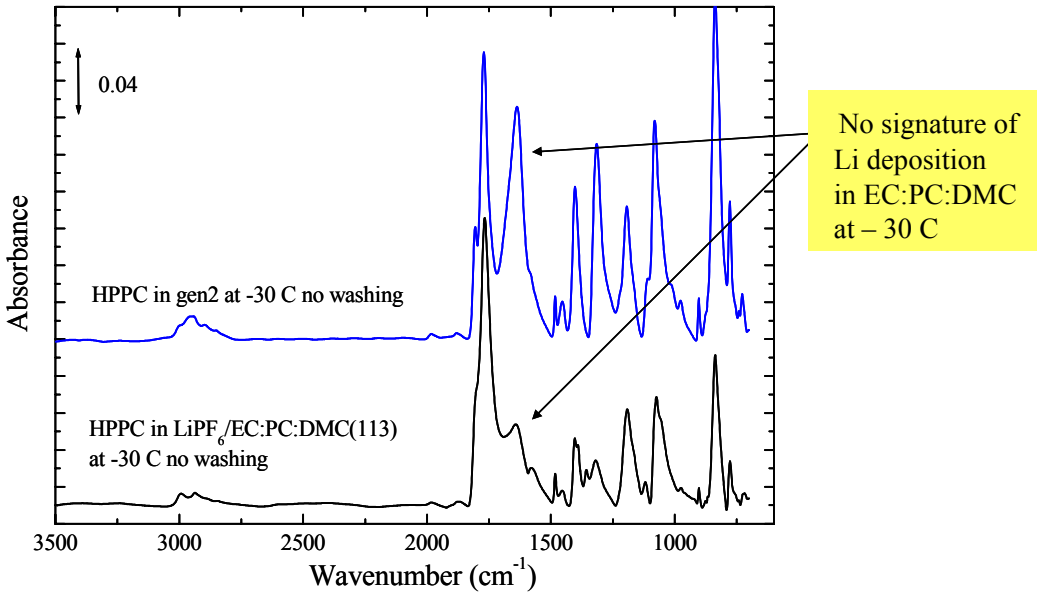

Figure IV-40. gen 2 vs. EC:PC:DMC Electrolyte

This study identified lithium ethylene dicarbonate as the passive film on metallic Li in EC:EMC/$LiPF_6$ electrolyte. It also determined that the SEI layer on graphite is much more complex than on metallic Li and that lithium ethylene dicarbonate is not a primary SEI component. There is a need to establish general applicability of these conclusions, *i.e.*, using other anode materials and electrolytes.

Overcharge Protection – Abuse tolerance in general and overcharge tolerance specifically continue to be major barriers to the commercialization of HEV sized Li-ion batteries. The BATT program has developed a polymer overcharge protection material that is non-conducting at the normal operating voltages of the cell, and becomes conducting at elevated potentials.

Recently, a bilayer conducting polymer composite separator impregnated with poly(9,9-dioctylfluorene) on the cathode side and poly(3-butylthiophene) on the anode side in a Li cell with a spinel-type $Li_{1.05}Mn_{1.95}O_4$ cathode was tested. A cell with polymer protection was overcharged by 20% at 4.3 V. An unprotected cell was charged to 4.3 V at the same current density, and then held at 4.3 V for the same charging time as the protected cell. The protected cell carried constant current during normal charging and overcharging in each cycle, while the current through the unprotected cell decreased during overcharging. Rapid capacity fading occurred in the unprotected cell, while the protected cell maintained its discharge capacity (Figure IV-41). The polymer composites set an upper potential limit of ~4.3 V. Reversible protection was achieved at current densities up to 0.75 mA/cm^2. At higher currents, the potential limit was higher, and gradual capacity fading took place.

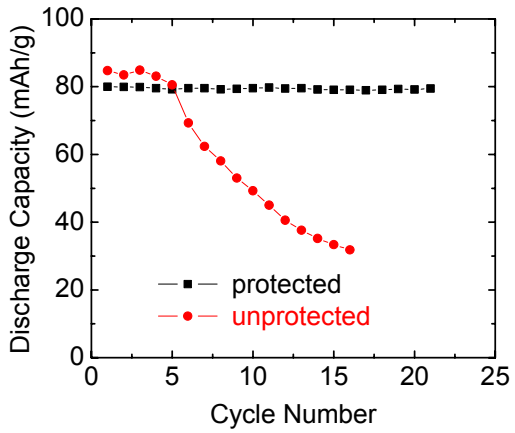

Figure IV-41. Capacity vs cycle number for an unprotect and protected spinel cell

Next, the performance of this composite separator was studied at different charge-discharge rates. Because the resistance across the polymer-impregnated separator varies with current density, the potential at which a cell is shorted increases with the charging rate (Figure IV-42).

After extensive cycling under the above conditions, the cathodes were removed at the end of charge and examined by XRD. The electrode from the protected cell showed no evidence of damage and was in the fully charged state, indicating no self-discharge due to the protection mechanism. On the other hand, the XRD pattern of the cathode from the unprotected cell showed significant peak broadening and a shift to a smaller unit cell, consistent with the BATT program's previous FTIR study, which suggested conversion to a defect spinel by Mn dissolution.

Low temperature overcharge protection is particularly important because cells are more susceptible to overcharging at low temperatures and due to the increased possibility of Li dendrite formation. A low-temperature study of the same cell illustrates the ability of the polymer composite to protect the

cell down to at least -20°C. The electrolyte resistance becomes significant at 10°C, causing the short to appear early, then the short gradually grows less resistant as the polymer is oxidized. Some protection is afforded at -20°C, where the electrolyte (LP40) is beginning to solidify. Note that the conducting polymer shunt protects the cells at risk, and generates heat where needed so that the stack could operate sooner.

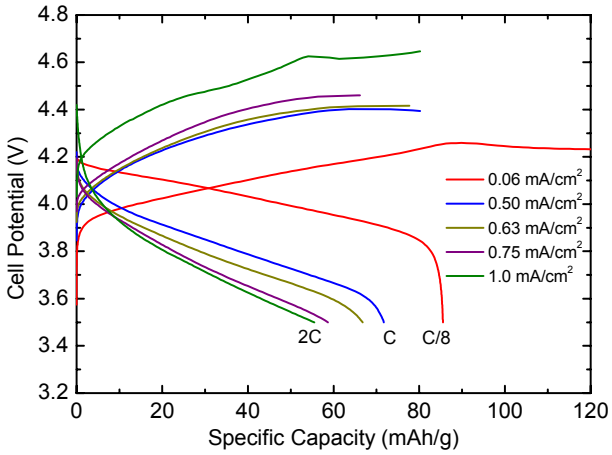

Figure IV-42. Variable rate charge-discharge curves for protected spinel cell

Electrode morphology affects – A strategy has been developed for implementing a combined MD/continuum finite element model for baseline chemistries. The approach uses computational fluid dynamics, mass transport, and reaction rates to determine the response of the system.

This group has also studied the impact of electrode compression. It was recently found that the addition of conductive additives and compression of electrodes in Gen-2 graphite/$LiFePO_4$ is required to increase the cyclability and conductivity. Therefore, compressed and uncompressed graphitic anodes and coated and uncoated $LiFePO_4$ cathodes have been studied. For SL20 (pure graphite), compression does not improve electrochemical performance, but does improve the electrical conductivity. For the GDR series graphite (carbon coated), 14% carbon coating with a compressed mass density (1.4) resulted in the best electrochemical performance and the highest electrical conductivity, and reduced the ICL, as shown in Figure IV-43. Contact resistance decreased as the amount of carbon coating increased, but it varied substantially with compression.

The required force to pack the particles to a prescribed volume fraction during manufacturing can be predicted via simulation. The post "jamming" compression (volume fraction>58%) leads to significant increase in internal pressure. Both the simulation results and the decreased post-packing conductivity in experiments indicate that a pressure over 200 kg/cm^2 (200 MPa) can cause breakage in particle materials in SL-20 electrodes.

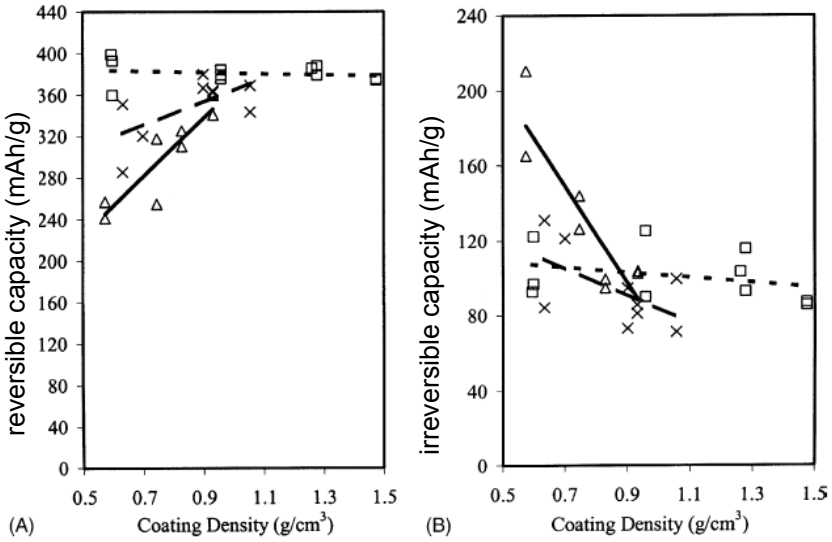

Figure IV-43. Coating density vs reversible and irreversible graphite capacity

Particle Expansion and Fracture – Lithium intercalation materials (*e.g.*, graphite and Mn_2O_4) only expand by ~10% during lithium insertion, but can fracture at high rates. Tensile stress is greatest in the center during lithium insertion, and at the surface during extraction. To investigate this phenomenon, a mathematical model of particle volume expansion has been formulated and used to calculate stress profiles in electrode materials. Results indicate that graphite particles may fracture at high charge rates typical of HEV applications, but are unlikely to fracture at low to moderate rates. It was also found that non-ideal behavior (*i.e.*, diffusivity varies with the lithium content) plays a significant role. Regions of low diffusivity, taking into account non-idealities, halve the acceptable dimensionless current and result in potential fracture in HEV applications, Figure IV-44. Experiments have begun in order to investigate the degradation of graphite at high charge rates.

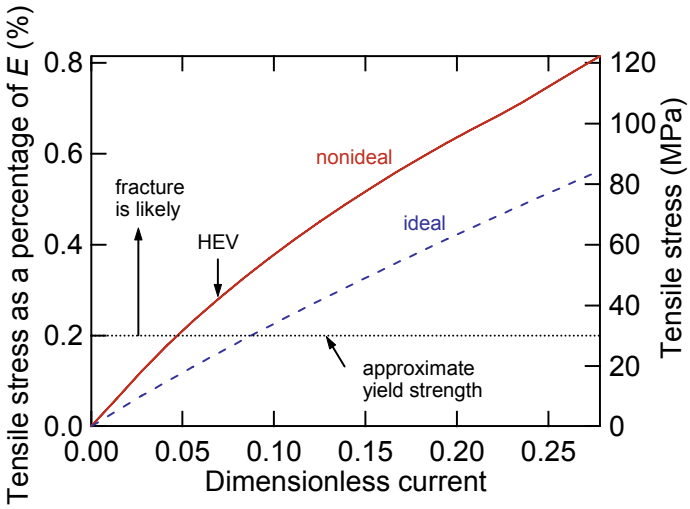

Figure IV-44. Non-ideal solution predicts fragmentation in high-power applications

Dendrite Initiation in Li Polymer cells – A model for dendrite initiation has been formulated that takes into account the plastic deformation of Li metal. This model provides an explanation for the effect of external pressure and indicates that an elastic modulus of 5 x 10^7 Pa for the cross-linked polymer is sufficient to kinetically inhibit dendrite initiation. Experiments to verify the model have been initiated.

Thermodynamic and Transport Property Measurements – One ongoing activity is to improve the accuracy of thermodynamic and transport properties measurements in Li-ion electrolytes. The objective is to characterize transport in single- and multiple-solvent electrolytes. Poor transport properties limit charge and discharge rates and lead to large electrolyte concentration gradients, which promote failure mechanisms. Finally, full-cell models depend on property measurement accuracy.

f_{+-} is found directly with an electroactive polymer electrode (which is reversible to the anion). Side reactions are prevented by using a reference electrode of more positive potential, $Li_4Ti_4O_{12}$ (reversible to Li^+). t_+^0 is measured using a concentration cell. By varying the salt concentration and measuring the equilibrium cell potential, f_{+-} can be determined.

The development of an anion-reversible electrode continues for $LiPF_6$ electrolytes. A reference electrode will be used in electro motive force measurements to independently determine activity coefficients. New methods are being developed to avoid the effects of side reactions in diffusion-coefficient measurements.

Conductivity data has been obtained for $LiPF_6$ based electrolytes, shown in Figure IV-45. It is found that the conductivity increases with DMC concentration; with the maximum shifting to a higher concentration, and, as found by others, that the LiBOB based electrolytes have lower conductivities.

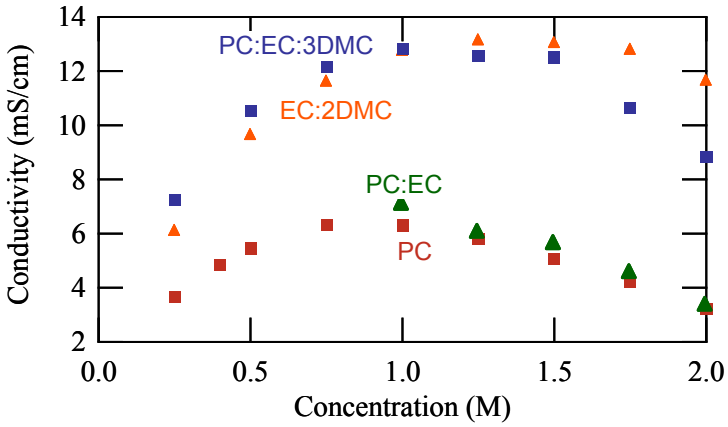

Figure IV-45. Conductivity of $LiPF_6$ based electrolytes

Diagnostics and Highly Conducting Electrodes – The purpose of this work is to understand some of the fundamental causes of impedance and capacity fade in Li-ion cells and to investigate new ways of producing highly conductive electrodes. A large number of diagnostics techniques have been used, including SEM, Raman, IR, and EIS.

It has been determined that improved electrochemical properties of $LiFePO_4$ are associated with a larger ratio of sp^2 coordinated carbon (which exhibits better electronic conductivity) to sp^3-coordinated carbonaceous materials. However, *in situ* carbon coating of $LiFePO_4$ by simple pyrolysis of organic precursors at temperatures below 800°C cannot produce graphite-like conductive carbon.

One approach is to improve the high-rate performance of cathodes by direct *in-situ* microwave-assisted synthesis of graphitic carbon. Note that microwave plasma assisted chemical vapor deposition is now widely used in industrial scale thin-film deposition. The main advantage of using microwave heating is that energy is delivered directly to the material, which reduces treatment time and produces carbons of higher crystallinity and better electronic conductivity.

To test this concept, organic precursors were microwaved in a low-pressure Ar plasma at 300-1000 W for 5 seconds to 3 min. Highly crystalline graphitic carbon with consistent graphene domain size was obtained, Figure IV-46. Thin graphite films consist of densely packed ~50 nm primary particles.

This technique was then used to coat $LiFePO_4$ with conductive carbon. A direct low-pressure microwave induced plasma synthesis of graphitic carbon on $LiFePO_4$ active material was demonstrated. Vaporization of the organic precursor and subsequent rapid pyrolysis leads to the formation of uniform films of nanometer-sized carbon particles. Carbon coatings exhibit high sp^2-graphene structure, and excellent electronic conductivity is expected. Electrochemical performance of carbon-coated $LiFePO_4$ will be investigated.

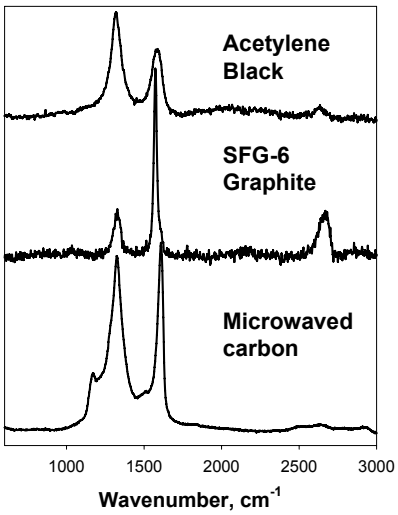

Figure IV-46. Raman data comparing microwaved carbon, acetylene black and graphite

The effect of electrode pre-treatment on the evolution of interfacial impedance of electrodes stored in electrolyte at 45˚C was also investigated. Al/carbon black, gen 2, and 1/3 material composite electrodes were investigated. Three sets of electrodes were dried under vacuum at 120˚C for 6, 12

and 42 hours, respectively. The electrodes were then stored in 1.2 M $LiPF_6$, EC:EMC (3:7 vol.) at open circuit potential and 45˚C in a glove box.

Electrochemical impedance of the electrodes was monitored periodically during storage. *Ex situ* diagnostic analysis was carried out after the test. Findings from this study are:

- The initial impedance of the electrodes is determined by heat treatment time,
- Carbon additive properties contribute to the impedance of the composite electrodes, and
- The electrode heat pre-treatment time determines the rate of the impedance increase upon aging at elevated temperatures.

Al Current Collector Corrosion – Recently, work has focused on determining the mechanism of Al current collector corrosion in Li-ion batteries. Earlier results indicated that corrosion occurred by under deposit corrosion, a type of crevice corrosion. This corrosion is a consequence of the microscopic porosity of the cathodes that cover the Al. While microporous cathodes act as crevice formers of Al, a polyethylene disk with radially oriented grooves was found to not cause crevice corrosion of Al. The inability of polyethylene to act as a crevice former suggested that the battery's cathodes play an active role in crevice corrosion.

However, at the operating voltages during battery charging there is no compelling evidence of either catalytic oxidation of electrolytes on the cathode's surface, or the formation of corrosive oxidation products. Furthermore, this research had found corrosion of Al current collectors independent of cathode material (three were employed).

Recent work was focused on three aspects of the corrosion behavior of aluminum in an electrolyte consisting of LiBOB dissolved in 1:1 EC/DMC.

(1) Corrosion of Al in salt-free organic solvent: Al foil was polarized in 1:1 EC+DMC to 6V vs. Li. Above a critical potential, aluminum sustained significant pitting corrosion. A protective film is not formed on Al in salt-free EC+DMC and the air-formed surface oxide controls cannot prevent pitting corrosion at high potentials.

(2) Passivation of Al in 1M LiBOB/EC+DMC: Even under CV with a maximum potential of 6.5 V, no corrosion was detected on the Al surface. The combined results of CV, EIS, and electrochemical quartz crystal microbalance (EQCM) measurements indicate a passive film is formed on aluminum anodically polarized in 1.0 M LiBOB/EC+DMC and the film's thickness increases with increasing potential.

(3) Passivation of Al in LiBOB + LiTFSI electrolytes: Electrolytes with LiTFSI exhibit severe corrosivity towards aluminum. Corrosion pits formed on the surface of aluminum after 3 cycles from OCP to 5.5V in 1.0 M LiTFSI/EC+DMC. LiBOB was found to either markedly reduce, or, in some instances, completely eliminate the corrosion. Aluminum subjected to 3 CVs (maximum potential of 5.5V) in electrolytes composed of LiTFSI and as little as 2% LiBOB, which was the smallest concentration tested, were free of any detectable corrosion.

A final finding is related to the impact of AlF_3 films on corrosion by LiTFSI, and is that 1 nm AlF_3 increases resistance to corrosion by LiTFSI and does not decrease battery's capacity, see Figure IV-47.

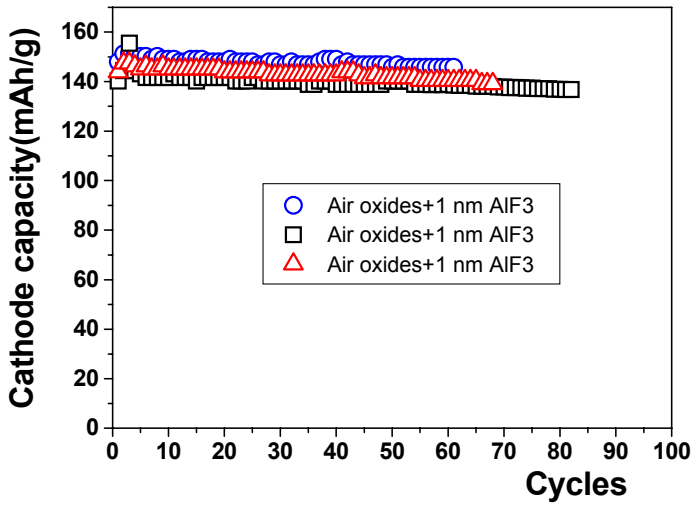

Figure IV-47. Cycling is not affected by AlF_3 film

Cell Construction – The objective of this task is to enable repeatable and high quality lab sized cells to be made and supplied to the various researchers. Towards this end, the team has identified limitations, re-configured their laboratory and purchased and built equipment to address them, assessed reproducibility, identified a technique for identifying the highest quality cells, and begun to iterate through this process, incorporating understanding at each step.

A recommendation from the 2004 merit review was to focus on power limitations. High rate cells are inherently more difficult to make than high capacity cells. As a result of a cell development analysis effort, the electrode components are now combined in a glove box and mixed in an Argon atmosphere. The laminates are dried in one hour as opposed to 24 hours previously. The laminates are calendared, cut, and tabbed in one hour in the open atmosphere before they are vacuum dried at 60°C for 6 hours prior to cell assembly in a glove box. The electrolyte vacuum filling remains to be optimized.

This group has selected the spinel baseline system to demonstrate reproducible cells. An example of improved performance achieved over the past year is shown in Figure IV-48. Coatings of several chemistries including $LiFePO_4$, $LiNi_{1/3}Co_{1/3}Mn_{1/3}O_2$, $LiNi_{0.8}Co_{0.15}Mn_{0.05}O_2$, $LiMn_2O_4$, and GDR-AB11 have been made. Previous results indicated that some of the coatings, especially the $LiFePO_4$, required an initial carbon coating on the current collector to achieve good performance. It has recently been found that this can be circumvented with proper mixing and calendaring.

Four cells with gen 2 cathode material were assembled and formed and then evaluated with EIS. Figure IV-49 and Table IV-1 demonstrates present capabilities. The performance of cells 2 and 3 are nearly identical, exhibiting equivalent ohmic drop and interfacial impedance. Cells 1 and 4

appear to have a different low-frequency impedance and cell 4 also suffers from high ohmic and interfacial impedance.

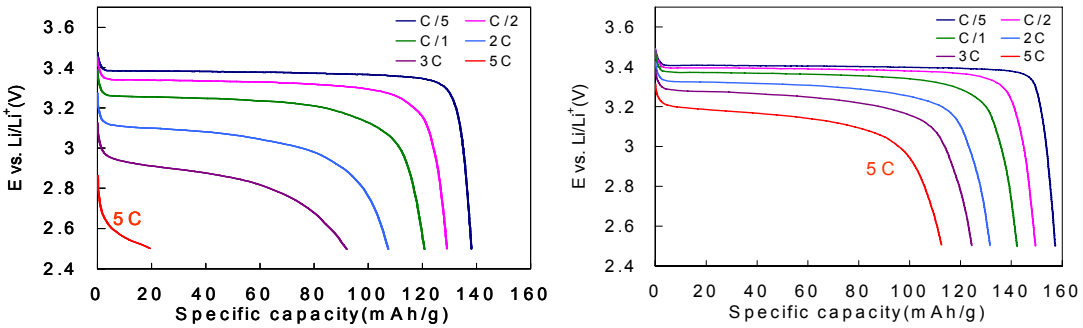

Figure IV-48. Improved performance (right) of $LiFePO_4$ cells.

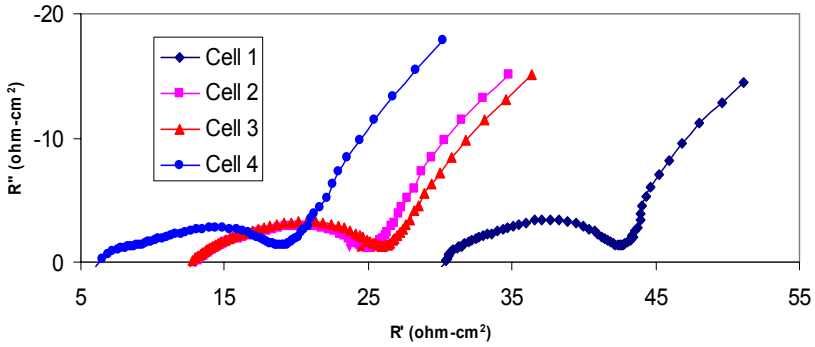

Figure IV-49. EIS spectra of Gen 2 cell

Table IV-1. Gen 2 capacity and specific capacity

Cell No.	Capacity (mAh)	Spec. Cap. (mAh/g)
1	9.69	162.5
2	10.65	162.5
3	10.37	162.4
4	11.09	165.0
Average	10.45	163.1
Standard Dev.	0.6	1.3
%COV	**5.6%**	**0.8%**

Future Plans

Interfacial Chemistry at Low T – Establish general applicability of SEI conclusions, i.e. with other anode materials and electrolytes.

Cell and Component Modeling

- Simulate the $LiMn_2O_4$ system with the finite element model approach
- Experimentally verify finite element model results
- Expand the finite element model to study thermal expansion, induced stresses.

Transport Property Measurements

- Investigate the use of the refractive index technique to measure transport properties.
- Investigate new electroactive polymers for activity-coefficient measurements.
- Differentiate between active material loss and cyclable lithium loss contributions to capacity fade.

Cell Development - To further qualify and improve cell repeatability

- Demonstrate batch-to-batch repeatability and operator-to-operator repeatability
- Age pouch cells with gen 2 chemistry and compare to ATD cell aging data.
- Perform comparison between coin cells, Swagelok cells, and pouch cells.
- Identify a qualified cell builder to provide baseline cell chemistries.
- Finish BET, PSA, SEM, XRD, and TGA of all materials used in baseline cells.

Selected Publications

1. A. Van der Ven, G. Ceder, Electrochemistry Communications **6**, (2004) 1045-1050.
2. F. Hu and M. M. Doeff, JPS[20], **129**, 296 (2004).
3. G. Chen, G. V. Zhuang, T. J. Richardson, G. Liu, and P. N. Ross, "Anodic Polymerization of Vinyl Ethylene Carbonate in Li- Battery Electrolytes," ESSL[21], **8**, A344 (2005).
4. G. V. Zhuang, G. Chen, J. Shim, X. Song, P. N. Ross, and T. J. Richardson, "Li_2CO_3 in $LiNi_{0.8}Co_{0.15}Al_{0.05}O_2$ Cathodes and its Effects on Capacity and Power," JPS, **134**, 293 (2004).
5. H. S. Lee, Z. F. Ma, X.-Q. Yang, X. Sun, and J. McBreen "Synthesis of a series of fluorinated boronate compounds and their use as additives in lithium battery electrolytes" JECS[22], **151**, (2004) A1429.
6. J.-S. Kim, C. S. Johnson, J. T. Vaughey, S. A. Hackney, W.-S. Yoon, C. P. Grey and M. M. Thackeray "Electrochemical and Structural Properties of $xLi_2M'O_3\bullet(1-x)LiMn_{0.5}Ni_{0.5}O_2$ Electrodes for Lithium Batteries (M′=Ti, Mn, Zr; $0\leq x\leq 0.3$)" Chemistry of Materials, **16** (2004) 1996.
7. K. A. Striebel, J. Shim, R. Kostecki, T. J. Richardson, P. N. Ross, X. Song, and G. V. Zhuang, "Characterization of High-power Lithium-ion Cells: Performance and Diagnostic Analysis," Proc. Electrochem. Soc., 2003-24, **88** (2004).
8. K. E. Thomas-Alyea, J. Newman, G. Chen, and T. J. Richardson, "Design Principles for the Use of Electroactive Polymers for Overcharge Protection of Lithium-Ion Batteries," Proc. Electrochem. Soc., 2003-28, **326** (2004).
9. Kerr, J. B., Han, Y.B.Liu, G, Reeder, C.L. Xie,J. and Sun, X., "Interfacial Behavior of Polymer Electrolytes", Electrochimica Acta **50**, 235 (2004).
10. L. Liu, L. Chen, X. Huang, X.-Q. Yang, W.-S. Yoon, H. S. Lee, and J. McBreen "Electrochemical and In Situ Synchrotron XRD Studies on Al_2O_3-Coated $LiCoO_2$ Cathode Material" JECS, Vol. 151, (2004) A1344.
11. M. Dolle, J. Hollingsworth, T. J. Richardson, and M. M. Doeff, "Investigation of Layered Intergrowth $LiMMnO_2$ (M=Ni, Co, Al) Compounds as Positive Electrodes for Li-ion Batteries," Solid State Ionics, **175**, 225 (2004).
12. M. M. Doeff, T. J. Richardson, and K.-T. Hwang, "Electrochemical and Structural Characterization of Titanium-substituted Manganese Oxides based on $Na_{0.44}MnO_2$," JPS, **135**, 240 (2004).
13. M. Ma, N.A. Chernova, P.Y. Zavalij, and M.S. Whittingham, "Structural and Electrochemical Properties of $LiMn_{0.4}Ni_{0.4}Co_{0.2}O_2$," Mater. Res. Soc. Proc., **835**, K11.3 (2005).
14. M.S. Whittingham, Y. Song, S. Lutta, P.Y. Zavalij, and N.A. Chernova, "Some Transition Metal (Oxy)Phosphates and Vanadium Oxides for Lithium Batteries," J. Mater. Chem., **15** (2005).
15. Peter Y. Zavalij, Shoufeng Yang, and M. Stanley Whittingham, Acta Cryst., 2004, B60: 716-724
16. Q. Fan, P. Zavalij, and M. Stanley Whittingham, "Anode Hosts for Lithium Batteries: Revisiting Tin and Aluminum," Mater. Res. Soc. Proc., **835**, K6.16 (2005).
17. Striebel, K.A., Sierra, A., Shim, J., Wang, C.-W. & Sastry, A.M., "The Effect of Compression on Natural Graphite Anode Performance and Matrix Conductivity," JPS, **134**, 241 (2004).

[20] JPS = Journal of Power Sources
[21] ESSL = Electrochemical and Solid State Letters
[22] JECS = Journal of the Electrochemical Society

18. Sun, X, Hou, J; Kerr, J. B. "Comb-shaped single ion conductors based on polyacrylate ethers and lithium alkyl sulfonate," Electrochimica Acta **50**, 1139-1147 (2005).
19. Sun, X; Kerr, J. B.; Reeder, C. L.; Han Yongbong; Liu, Gao. "Network single ion conductors based on comb-branched polyepoxide ethers and lithium bis(allylmalonato)borate," Macromolecules, **37** (2004), 5133
20. Sun, X; Reeder, C. L.; Kerr, J. B., "Synthesis and characterization of network type single ion conductors," Macromolecules, **37** (2004), 2219.
21. Sun,X.; Liu,G.; Xie J.; Han,Y and Kerr, J.B., "New Gel Polyelectrolytes for Rechargeable Lithium Batteries" Solid State Ionics **175**, 713 (2004).
22. T. A. Arunkumar and A. Manthiram, "Influence of Lattice Parameter Differences on the Electrochemical Performance of the 5 V Spinel $LiMn_{1.5-y}Ni_{0.5-z}M_{y+z}O_4$ (M=Li, Mg, Fe, Co, and Zn)", ESSL **8**, A403 (2005)
23. W.-S. Yoon, M. Balasubramanian, X.-Q Yang, J. McBreen, and J. Hanson "Time Resolved XRD Study on the Thermal Decomposition of $Li_{1-x}Ni_{0.8}Co_{0.15}Al_{0.05}O_2$ Cathode Materials for Li-ion Batteries" ESSL, **8**, A83 (2005).
24. Wang, C.-W., Sastry, A.M., Striebel, K.A. and Zaghib, K., "Extraction of Layerwise Conductivities in Carbon-Enhanced, Multilayered $LiFePO_4$ Cathodes," JECS, **152**, A1001 (2005).
25. Wang, C.-W., Yi, Y.-B., Sastry, A.M., Shim, J. and Striebel, K.A., 2004,"Particle Compression and Conductivity in Li-ion Anodes with Graphite Additives," JECS, **151,** 1489 (2004).
26. Y. Song, P.Y. Zavalij, M.S. Whittingham, "ε-$VOPO_4$: Electrochemical Synthesis and Enhanced Cathode Behavior," JECS, **152**, A721-A728 (2005).
27. Y. Song, P.Y. Zavalij, N.A. Chernova, and M.S. Whittingham, "Synthesis, Crystal Structure, Electrochemical and Magnetic Study of New Iron (III) Hydroxyl-Phosphates, Isostructural with Lipscombite," Chem. Mater., **17**, 1139-1147 (2005).

Appendix A

Contributors

Battery Technology Development	
J. Barnes	Naval Surface Warfare Center West Bethesda, MD 20817-5700
A. Pesaran	National Renewable Energy Laboratory 1617 Cole Boulevard Golden, CO 80401-3393
I. Weinstock	Sentech Corp 7475 Wisconsin Ave. Bethesda, MD 20814

Applied Battery Research	
DOE Program Manager	**David Howell** U.S. Department of Energy Office of FreedomCar & Vehicle Technologies 1000 Independence Avenue, SW Washington, DC 20585
National Laboratory Program Manager	**Gary Henriksen** Argonne National Laboratory Chemical Engineering Division, Bldg 205 9700 South Cass Avenue Argonne, IL 60439
Low Temperature	
D. Abraham, K. Amine, D. Dees, A. Jansen, J. Liu, A. Kahaian, W. Lu, P. Schultz, J. Vaughey, Q. Wang	Argonne National Laboratory Argonne, IL 60439-4837
M. Ding, R. Jow	Army Research Laboratory 2800 Powder Mill Rd Adelphi, MD 20783-1197
C. Ashton, J. Christophersen, G. Cole, K. Gering, C. Ho, C. Motloch, T. Murphy	Idaho National Engineering and Environmental Laboratory Idaho Falls, ID 83415-3830
V. Battaglia, P. Ross, V. Zhuang	Lawrence Berkeley National Laboratory Berkeley CA 94720-8168
Calendar and Cycle Life	
D. Abraham, D. Andrekus, K. Amine, J. Basco, I. Bloom, Z. Chen, D. Dees, G. Henriksen, A. Jansen, S-H. Kang, J. Liu, P. Nelson, B. Potter, G. Reynolds	Argonne National Laboratory Argonne, IL 60439-4837
J. Christophersen, K. Gering, C. Ho, G. Hunt, C. Motloch	Idaho National Engineering and Environmental Laboratory Idaho Falls, ID 83415-3830
V. Battaglia, E. Cairns, S. K Jeong, M. Kerlau, J. Kerr, R. Kostecki, M. Marcinek, K. McCarthy, F. McLarnon, J. Newman, J. Reimer, T. Richardson, P. Ross, A. Sierra-VanDyke, X. Song, V. Srinivasan, S. Wilcke, H. Yang, V. Zhuang	Lawrence Berkeley National Laboratory Berkeley CA 94720-8168
E. Thomas	Sandia National Laboratories Albuquerque, NM 87185-0613
Abuse Tolerance	

Applied Battery Research	
D. Abraham, K. Amine, I. Belharouak, G. Henriksen A. Jansen, J. Liu, Q. Lu, S. MacLaren, D. Vissers	Argonne National Laboratory Argonne, IL 60439
K. Y. Chung, H. S. Lee, J. McBreen, X. Q. Yang, W. S. Yoon	Brookhaven National Laboratory P.O. Box 5000, MSD Bldg. 555, Upton, NY 11973-5000
J. Prakash	Illinois Institute of Technology Department of Chemical and Environmental Engineering, Chicago, IL 60616
R. Kostecki	Lawrence Berkeley National Laboratory Berkeley CA 94720-8168
H. Case, L. Davis, D. Doughty, C. Durant, B. Hance, D. Johnson, J. Langendorf, G. Nagasubramanian, D. Pile, E. P. Roth, B. Sanchez	Sandia National Laboratory Mail Stop 0613 Albuquerque, NM 87185
R. Spotnitz	Battery Design
Cost Reduction	
K. Amine, I. Belharouak, D. Chaiko, Z. Chen, D. Dees, A. Jansen, G. Henriksen, S. Kang, J. Liu, P. Nelson, A. Newman, G. Nielsen, S. Niyogi, E. Redey, J. Vaughey, D. Vissers, L. Wang	Argonne National Laboratory Argonne, IL 60439
J. Allen, M. Ding, T. R. Jow. K. Xu, S. Zhang	Army Research Laboratory 2800 Powder Mill Rd Adelphi, MD 20783-1197
S. W. Cornell	Plastic Technology Partners Naperville, IL 60540

Long-Term Battery Research	
DOE Program Manager	**David Howell** U.S. Department of Energy Office of FreedomCAR & Vehicle Technologies 1000 Independence Avenue, SW Washington, DC 20585
National Laboratory Program Manager	**Venkat Srinivasan** Lawrence Berkeley National Laboratory MS 70R-0108B One Cyclotron Road Berkeley, CA 94720
New Cathode Systems, Performance and Limitations	
$LiFePO_4$ System	
J. Harb and D. Wheeler	Brigham Young University Chemical Engineering Department, 350 CB Provo, UT 84602
W.S. Yoon	Brookhaven National Laboratory Upton, NY 11973
K. Zaghib	Hydro Quebec Varennes, J3X 1S1 Quebec Canada
V. Battaglia, M. Doeff , R. Fiñones, Y. Hu, J. Kerr, R. Kostecki, G. Liu, F. Mclarnon, X. Song, V. Srinivasan, Kathy Striebel, J. Wilcox	Lawrence Berkeley National Laboratory Berkeley CA 94720-8168
J. Chen, N. Chernova, M. Ma, Whittingham, J. Xiao, P. Zavalij	State University of New York at Binghamton Chemistry and Materials Research Center Binghamton, NY 13902-6000
A.M. Sastry	University of Michigan Dept of Mechanical Engineering and Applied Mechanics Ann Arbor, MI 48109-2125
$LiMn_2O_4$ Spinel System	
X.Q. Yang	Brookhaven National Laboratory Upton, NY 11973
K. Zaghib	Hydro Quebec Varennes, J3X 1S1 Quebec Canada
V. Srinivasan, Doeff, T. J. Richardson, J. Reed, T. Devine	Lawrence Berkeley National Laboratory Berkeley CA 94720-8168

Long-Term Battery Research	
M.S. Whittingham	State University of New York at Binghamton Chemistry and Materials Research Center Binghamton, NY 13902-6000
R. Katiyar	University of Puerto Rico
T. A. Arunkumar, J. Choi, A. Manthiram, W. Choi	Univ of Texas Texas Materials Institute , ETC 9-104 Austin TX 78712-0292
$LiNi_{1/3}Co_{1/3}Mn_{1/3}O_2$ System	
J.S. Kim, M. Thackeray, C. Johnson, J. Vaughey, R. Benedek	Argonne National Laboratory Chemical Technology Division Argonne IL 60439
G. Ceder, Y.S. Meng, A. Van der Ven, Y. Hinuma	Massachusetts Institute of Technology Cambridge, MA 02139-4307
C. P. Grey	State University of New York at Stony Brook, Department of Chemistry Stony Brook, NY
Y. Huang, J. Goodenough, K-S. Park	University of Texas at Austin
New Anode Materials	
R. Benedek, C. Johnson, M. Thackeray, J. Vaughey	Argonne National Laboratory Chemical Technology Division Argonne IL 60439
R. Kostecki	Lawrence Berkeley National Laboratory Berkeley CA 94720-8168
Q. Fan, Whittingham	State University of New York at Binghamton Chemistry and Materials Research Center Binghamton, NY 13902-6000
C. P. Grey	State University of New York at Stony Brook Department of Chemistry Stony Brook, NY
Novel Electrolytes and their Characterization	
S. Creager, D. DesMarteau, P. Hallac, O. Geiculescu, R. Rama	Clemson University Department of Chemistry Clemson, SC 29634-0973.
N. Balsara, Y. Han, J. Kerr, L. Odusanya, C. Reeder, K. Shin, M. Singh, X. G. Sun , K. Striebel	Lawrence Berkeley National Laboratory Berkeley CA 94720-8168

Long-Term Battery Research	
G. L. Baker	Michigan State University Department of Chemistry East Lansing, MI 48824-1322
P. S. Fedkiw, S. A. Khan	North Carolina State University Department of Chemical Engineering Raleigh, NC 27695
O. Borodin, G. D. Smith	University of Utah Department of Materials Science and Engineering Salt Lake City, UT
Li-Ion Modeling, Diagnostics, and Cell Analysis	
T.R. Jow, K. Xu , S.S. Zhang	Army Research Laboratory 2800 Powder Mill Rd Adelphi, MD 20783-1197
K.-Y. Chung, H. S. Lee, J. McBreen, X.-Q. Yang, W.-S. Yoon	Brookhaven National Laboratory P.O. Box 5000, MSD Bldg. 555, Upton, NY 11973-5000
V. Battaglia, E. Cairns, G. Chen, T. M. Devine, M. Doeff, J. Handono, R. Kostecki, M. Kerlau, G. Liu, M. Marcinek, J. Newman, R. Purnawan, T. Richardson, P. Ross, A. Sierra-VanDyke, X. Y. Song, K. Striebel, V. Srinivasan, H. Yang, X. Zhang, V. Zhuang	Lawrence Berkeley National Laboratory Berkeley CA 94720-8168
K. Cook, A. M. Sastry, C-W. Wang, Yun-Bo Yi	University of Michigan Dept of Mechanical Engineering and Applied Mechanics Ann Arbor, MI 48109-2125
C. Monroe	Imperial College London

Appendix B

List of Acronyms

AEM	Advanced electrolyte model
ANL	Argonne National Laboratory
ARC	Accelerated rate calorimetry
ARL	Army Research Laboratory
ASI	Area specific impedance
ATD	Advanced Technology Development
BATT	Batteries for Advanced Transportation Technologies
BC	Button cell
BNL	Brookhaven National Laboratory
CV	Cyclic voltammetry
DEC	Diethyl carbonate
DMC	Dimethylcarbonate
DOD	Depth-of-discharge
DOE	Department of Energy
DSM	Double sigmoid model
DSC	Differential scanning calorimetry
EA	Ethylene acetate
EC	Ethylene carbonate
EDS	Electron dispersive spectroscopy
EDX	Energy dispersive x-ray analysis
EIS	Electrochemical impedance spectroscopy
EMC	Ethyl methyl carbonate
EP	Ethyl proprionate
EPRI	Electric Power Research Institute
EQCM	Electrochemical quartz crystal microbalance
EV	Electric vehicle
EXAFS	Extended x-ray absorption fine structure
FCV	Fuel cell vehicle
FCVT	FreedomCAR and Vehicle Technology
FTP	Federal test procedure
FTIR	Fourier transform infrared
FY	Fluorescence yield
GC	Gas chromatography
γBL	γ-butyrolactone
HEV	Hybrid electric vehicle
HPPC	Hybrid pulse power characterization
HQ	Hydro-Québec
HRTEM	High resolution transmission electron microscopy

ICL	Irreversible capacity loss
IIT	Illinois Institute of Technology
INL	Idaho National Laboratory
IR	Infrared
JPL	Jet Propulsion Laboratory
LBNL	Lawrence Berkeley National Laboratory
LiBETI	$LiN(SO_2C_2F_5)_2$
LiBOB	Lithium bis(oxolato)borate
LiTFSI	Lithium bis(trifluoromethane-sulfonyl)imide
MB	Methyl butyrate
MCM	Multiple sigmoid model
MCMB	Meso carbon micro beads
MD	Molecular dynamics
MPPC	Minimum pulse power characterization
MS	Mass spectrometry
MW	Molecular weight
NMC	$LiNi_{1/3}Co_{1/3}Mn_{1/3}O_2$
NCA	$LiNi_{0.8}Co_{0.15}Al_{0.05}O_2$
NiMH	Nickel metal hydride
NIST	National Institute of Standards and Technology
NMR	Nuclear magnetic resonance
nPA	n-propyl acetate
NREL	National Renewable Energy Laboratory
OCV	Open circuit voltage
PA	Pyromellitic acid
PC	Propylene carbonate
PDF	Pair distribution function
PE	Polyethylene
PEG	Polyethylene glycol
PEO	Poly(ethylene oxide)
PEY	Partial electron yield
PNGV	Partnership for a New Generation of Vehicles
PP	Polypropylene
PPV	Pulse power verification
PPY	Polypyrrole
PS	Polystyrene
PTFE	Polytetrafluoroethylene
PTMO	Poly(trimethylene oxide)
PVdF	Poly(vinylidene fluoride)
RFPI	Request for proposal information
RPT	Reference performance test
RRDE	Rotating ring-disk electrode
SAXS	Small angle X-ray scattering

SBIR	Small Business Innovative Research
SEI	Solid electrolyte interface
SEM	Scanning electron microscopy
SIC	Single ion conductor
SOA	State of the art
SOC	State of charge
SNL	Sandia National Laboratory
SPM	Scanning probe microscopy
SRPT	Special reference performance test
TEM	Transmission electron microscopy
TGA	Thermal gravimetric analysis
TLVT	Technology Life Verification Test
TM	Transition metal
TMO	Trimethylene oxide
TPFPB	tris(pentafluorophenyl) borane
USABC	United States Advanced Battery Consortium
USCAR	United States Council for Automotive Research
VC	Vinylene carbonate
VEC	Vinyl ethylene carbonate
WVTR	Water vapor transmission rate
XAFS	X-ray absorption fine structure
XAS	X-ray absorption spectroscopy
XPS	X-ray photoelectron spectroscopy
XRD	X-ray diffraction
WSB	Water soluble binder

A Strong Energy Portfolio for a Strong America

Energy efficiency and clean, renewable energy will mean a stronger economy, a cleaner environment, and greater energy independence for America. Working with a wide array of state, community, industry, and university partners, the U.S. Department of Energy's Office of Energy Efficiency and Renewable Energy invests in a diverse portfolio of energy technologies.

For more information contact:
EERE Information Center
1-877-EERE-INF (1-877-337-3463)
www.eere.energy.gov